Congenital Complete Atrioventricular Block
Clinical and Experimental Studies

Andreas Christian Blank

Cover image www.123rf.com

Layout Menno van den Bergh

Printed by Proefschriftmaken.nl || Uitgeverij BOXPress

ISBN 978-9-46-295999-6

© 2014 Christian Blank, Utrecht, the Netherlands . All rights reserved. No parts of this publication may be reproduced, stored in a retrieval system or transmitted in any form or by any means without prior written permission by the author.

Congenital Complete Atrioventricular Block
Clinical and Experimental Studies

Congenitaal Compleet Atrioventriculair Blok
Klinische en Experimentele Studies

(met een samenvatting in het Nederlands)

Proefschrift

ter verkrijging van de graad van doctor aan de Universiteit Utrecht op gezag van de rector magnificus, prof. dr. G.J. van der Zwaan, ingevolge het besluit van het college voor promoties in het openbaar te verdedigen op maandag 8 december 2014 des ochtends te 10:30 uur

door

Andreas Christian Blank

geboren op 5 februari 1968
te Potsdam-Babelsberg, Duitsland

Promotoren	Prof. dr. M.A. Vos Prof. dr. F. Haas
Co-promotoren	Dr. A.A.B. van Veen Dr. T. Takken

The studies described in this thesis were supported by a grant from the Dutch Heart Foundation (NHS 2009-2013 to A.A.B. van Veen). Printing of this thesis was kindly supported by Wilhelmina Children's Hospital, University Medical Center Utrecht and St Jude Medical. Financial support by the Dutch Heart Foundation for the publication of this thesis is gratefully acknowledged.

"Wohl aber dem, der seinen Bürgen weiß,..."

Recitative, church cantata, BWV 105
Herr, gehe nicht ins Gericht mit deinem Knecht
Johann Sebastian Bach

TABLE OF CONTENTS

SCOPE AND OUTLINE		**9**
CHAPTER 1	Atrioventricular block Zipes DP, Jalife J, editors. Cardiac Electrophysiology: From Cell to Bedside, 6th edition, Philadelphia, 2012, Saunders Elsevier	**15**
CHAPTER 2		
PART I	Cardiopulmonary exercise testing in congenital heart disease: equipment and test protocols *Neth Heart J* 2009; 17: 339-44	**33**
PART II	Cardiopulmonary exercise testing in congenital heart disease: (contra)indications and interpretation *Neth Heart J* 2009; 17: 385-92	**47**
PART III	Exercise capacity in children with isolated congenital complete atrioventricular block: does pacing make a difference? *Pediatr Cardiol* 2012; 33: 576-85	**63**
CHAPTER 3	Rewiring the heart: stem cell therapy to restore normal cardiac excitability and conduction *Curr Stem Cell Res Ther* 2009; 4: 23-33	**83**
CHAPTER 4	Computer three-dimensional reconstruction of the canine atrioventricular conduction axis under physiologic and pathologic conditions *Manuscript submitted*	**105**
CHAPTER 5	Stem cell therapy to restore conduction in a dog model of complete AV block *Manuscript to be submitted*	**127**
SUMMARY		**157**
SAMENVATTING		**167**
DANKWOORD | CURRICULUM VITAE | PUBLICATIES		**177**

Scope and outline of this thesis

Complete atrioventricular block (CAVB) is a cardiac conduction defect wherein the transmission of the normal electrical impulse from the atria to the ventricle is interrupted due to structural or functional impairment of the atrioventricular (AV) conduction system. If CAVB is diagnosed in utero or during the first month of life, it is named congenital CAVB. This thesis attempts to enhance our knowledge concerning the AV node anatomy, to evaluate current clinical therapies and propose new strategies using experimental data.

Chapter 1 reviews in depth the ECG characteristics and definitions that are applicable to the different types of AV block. It, furthermore, describes congenital CAVB as a distinctive form of AV block, and discusses its pathogenesis and possibilities for therapy.

Chapter 2 is a synergy of three published studies. Two of them review the equipment, test protocols and interpretation of cardiopulmonary exercise testing in children with congenital heart disease. In the third study, the discussed techniques have been used to investigate the exercise capacity in a small cohort of children with congenital CAVB.

The current therapy of congenital CAVB, implantation of an electronic pacemaker, might be a lifesaving intervention, but it can cause considerable morbidity, and even mortality. The need for instrumentation with an electronic pacemaker, with its possible disadvantages, might be circumvented by future application of stem cell-derived techniques with the aim to provide biological pacemaking or restoration of the damaged AV conduction in congenital CAVB. The attemps that, to date, have been made by the scientific community, the different types of cells, modes of administration, successes and pitfalls have been reviewed in depth as expressed in **Chapter 3**.

Understandably, cell therapy of the AV conduction system requires knowledge about the precise 3D structure of the normal and diseased AV conduction system. **Chapter 4** reports the results of a submitted study that provided an extensive description of the 2D and 3D structure of the canine AV conduction system. Formalin-fixed and paraffin embedded tissue sections were derived from: (1) normal AV junction, (2) AV junction in (natural) acquired CAVB, and (3) AV junction of ablation-induced CAVB. The sections were stained with Masson's trichrome-, and van Gieson's stain, and immunolabeled with antibodies against connexin 43, pan-cadherin and neurofilament. Digitalized 2D sections were transformed into interactive 3D models by surface rendering.

Chapter 5 describes the results of a study that aimed to repair CAVB in dogs by transplantation of cardiac progenitor cells (CPCs). In this study, CAVB was induced by radiofrequency ablation. From human and canine heart tissue CPCs were isolated by magnetic cell sorting. Three weeks after ablation CPCs were injected into the damaged AV conduction system. Within the study, several sources and amounts of cells have been tested with respect to their potency to restore AV conduction upon transplantation following different regimens. The chapter also includes a discussion regarding the multiple hurdles that are associated with the tested strategies of stem cell therapy.

Finally, we provide a summary of all mentioned chapters and, based on the acquired knowledge, also some future perspectives.

CHAPTER 1

Atrioventricular block

Atrioventricular block

A.C. Blank, P. Loh, M.A. Vos

Published in Zipes DP, Jalife J, editors: Cardiac Electrophysiology: From Cell to Bedside, 6th edition, Philadelphia, 2012, Saunders Elsevier, pages 1043-49.

Department of Cardiology
University Medical Center Utrecht (UMCU), Utrecht, the Netherlands
P Loh
MA Vos

Department of Paediatric Cardiology, Wilhelmina Children's Hospital, UMCU, Utrecht, the Netherlands
AC Blank

Introduction

On its way from the sinus node to the ventricles, an electrical impulse passes through the atrioventricular (AV) conduction system comprising atrial myocardium, the AV node, the penetrating AV bundle (bundle of His), and the network of Purkinje fibers. Regular cardiac function requires some AV conduction delay to allow the ventricles to relax before the next atrial contraction. AV block is defined as further delay or block of impulse transmission that occurs mostly in the AV node. The AV node forms a heterogeneous and highly complex three-dimensional lattice of distinct cell types with different molecular make-up and therefore different functional behavior (Figure 1). Large atrial cells connect to midsized transitional cells, which, in turn, contact the small, closely packed cells of the compact node. It must be emphasized that the compact part represents one component of the AV node, which comprises all the different cell groups that determine its functional properties. Many morphologic and functional factors like action potential characteristics, cell-to-cell coupling, and autonomic innervation determine impulse transmission and control AV conduction.[1] Numerous pathologic processes, congenital or acquired, can affect this delicate system. First, an overview of the different types of AV block will be provided, followed by congenital and acquired causes. Then, the ventricular consequences of chronic complete AV block obtained in a canine model will be described. Finally, future therapy considerations will be discussed in light of the findings described.

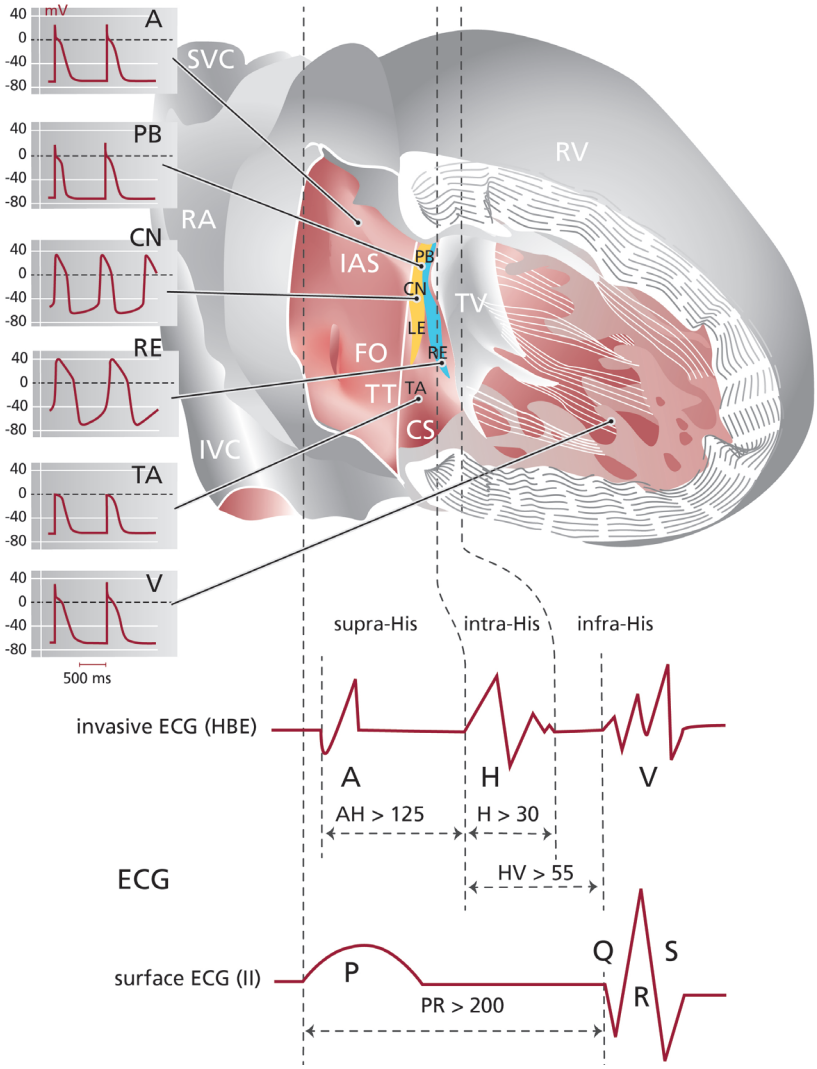

Figure 1: **Diagram illustrating anatomical, histo-molecular, and electrical complexity of the human AV node in relation to AV block.** Anteriorly, the AV node is bordered by the tricuspid valve (TV), and posteriorly by the tendon of Todaro (TT). Histo-morphologically, the AV node is composed of a transitional area (TA), left inferior (LE) and right inferior extensions (RE), and the compact node (CN), which connects to the penetrating bundle of His (PB); yellow region, Cx43-negative; blue region, Cx43-positive. Calculated action potentials (APs) derived by mathematic modeling of mRNA expression data. Supra-His AV block if AH >125 ms; intra-His AV block if H >30 ms; infra-His block if HV >55 ms. CS, Coronary sinus; FO, foramen ovale; IAS, interatrial septum; IVC, inferior vena cava; RA, right atrium; RV, right ventricle; SVC, superior vena cava. Data from Kurian T, Ambrosi C, Hucker W, *et al*. Anatomy and electrophysiology of the human AV node. Pacing Clin Electrophysiol 2010; 33: 754-762. APs reproduced with permission of Dobrzynski H, Monfredi O, Greener ID, *et al*. Molecular basis of the electrical activity of the atrioventricular junction and Purkinje fibres. In Tripathi ON, Ravens U, Sanguinetti M [eds]: Heart Rate and Rhythm. Berlin, Heidelberg, Springer-Verlag, 2011.

Electrocardiographic characteristics and definitions of AV block

AV block can be defined anatomically —supra- (i.e., atrial or AV nodal), intra-, or infra-His (see Figure 1) —or electrocardiographically —first-, second-, and third-degree (complete) AV block. Thorough analysis of the electrocardiogram (ECG) can provide an estimation of the anatomical site of the block. If ventricular depolarization is undisturbed and QRS complexes appear normal, the site of delay or block is usually supra-His (usually AV nodal). Variations of the PR interval point to the AV node as the source of delay and block. When abnormal ventricular depolarization with prolonged QRS duration or left or right bundle branch block is present, the AV node can still be the substrate, but involvement of the His-Purkinje system distal to the AV node is likely. The site of conduction delay can be determined more precisely by endocardial recordings of AH and HV intervals. If impulse transmission is impaired in the atrium or in the AV node, the AH interval will be prolonged (>125 ms) and the HV interval will be normal (Figure 1). A prolonged HV interval (>55 ms) indicates conduction disturbances in the His-Purkinje system (Figure 1). Supra-His AV conduction delay or block usually has a favorable prognosis, whereas intra- or infra-His AV conduction delay or block implies a more serious prognosis.[2,3] In the next section, a description of each specific AV block will be combined with data concerning incidence, prognosis, and treatment.

First-degree AV block

On the surface ECG, the PR interval is measured from the onset of atrial depolarization (P wave) to the beginning of ventricular depolarization (QRS complex) and ranges normally between 0.12 and 0.20 seconds. In first-degree AV block, every non-premature atrial impulse is conducted to the ventricles with a PR interval that exceeds 0.20 seconds. The incidence of first-degree AV block in asymptomatic subjects is low, ranging between 0.5% and 1.6%.[4,5] The prognosis for PR prolongation in the presence of a normal QRS complex until recently was thought to be benign. However, an observation from the Framingham Heart Study showed increased risk of development of atrial fibrillation (hazard ratio [HR], 2.06) and of pacemaker implantation (HR, 2.89) and revealed a moderately increased risk of death with a hazard ratio of 1.4.[5]

Asymptomatic patients with first-degree AV block do not require treatment. Patients should be followed to detect progression to higher-degree AV block. In patients with a marked PR interval increase (>0.3 s) that approaches the preceding RR interval, symptoms can result from impaired ventricular filling and synchronous atrial and ventricular contraction ("cannon waves") that may necessitate pacemaker implantation.

Second-degree AV block

Second-degree AV block is subclassified into type 1 (Wenckebach or Mobitz type I), type 2 (Mobitz type II), or advanced block.

Type 1 second-degree AV block

Electrocardiographically, typical type 1 block is characterized by several features: (1) progressive prolongation of the PR intervals, (2) the greatest increase in PR interval noted in the second beat of a cycle, with the increment being progressively less in subsequent beats, (3) gradual shortening of RR intervals, (4) a P wave not followed by a QRS complex, (5) a pause with an RR interval less than the sum of two PP intervals, and (6) the first conducted atrial impulse after the pause showing a shorter or normal PR interval (Figure 2). Clinically, only a minor part of type 1 second-degree AV block complies with all criteria.[3]

Progressive (beat-to-beat) slowing of conduction velocity during a fast atrial rate, referred to as decremental conduction, can be attributed to the AV node and its atrial nodal extensions.[1] Therefore, in type 1 second-degree AV block with normal QRS complexes, conduction delay and block occur most often within the AV node proximal to the His bundle.

Type 1 block can occur in 1% to 2% of healthy individuals as a result of enhanced efferent discharge of parasympathetic nerve fibers. This vagally mediated block, in combination with slowing of the sinus rate, can occur in normal persons, for instance, as a result of pain or during sleep, or in persons with high vagal tone, like endurance athletes at rest.[6] It is functionally determined and usually benign and disappears with increased sympathetic tone.

Syncope is rare, although it sometimes can lead to serious symptoms in athletes and can necessitate de-training. In asymptomatic individuals without evident infra-nodal conduction disturbances, permanent pacemaker implantation is not recommended (class III).[2] Progression to so-called advanced second-degree AV block or third-degree AV block is uncommon. If patients develop symptomatic bradycardia, permanent pacemaker implantation is indicated.[2]

Type 2 second-degree AV block

In type 2 block, abrupt failure of a non-premature atrial impulse to reach the ventricles is not preceded by lengthening of the PR interval, meaning that the RR interval spanning the pause equals two PP intervals. The site of type 2 block is generally infra-nodal and, if the QRS complex appears normal, can be located within the His bundle. This indicates diffuse disease of the infra-nodal conduction system, especially if associated with a wide QRS. If failure of AV conduction is associated with conduction delay in the Purkinje system and/or bundle branch block, the site of block is distal to the His bundle. If two or more non-premature atrial impulses fail to activate the ventricles, but some QRS complexes are related to preceding P waves, advanced or high-grade AV block is present. In this case, AV conduction is compromised, but some conduction is preserved. Sometimes, 2 : 1 AV block is referred to as high-grade AV block. The incidence of type 2 block is rare in healthy individuals and increases with age and in the presence of structural heart disease. About 2% of people older than 70 years with structural heart disease present with type 2 block. It carries a relatively high risk of progression to high-grade or third-degree AV block and thus is associated with increased risk of mortality. Implantation of a permanent pacemaker is recommended for patients with type 2 second-degree AV

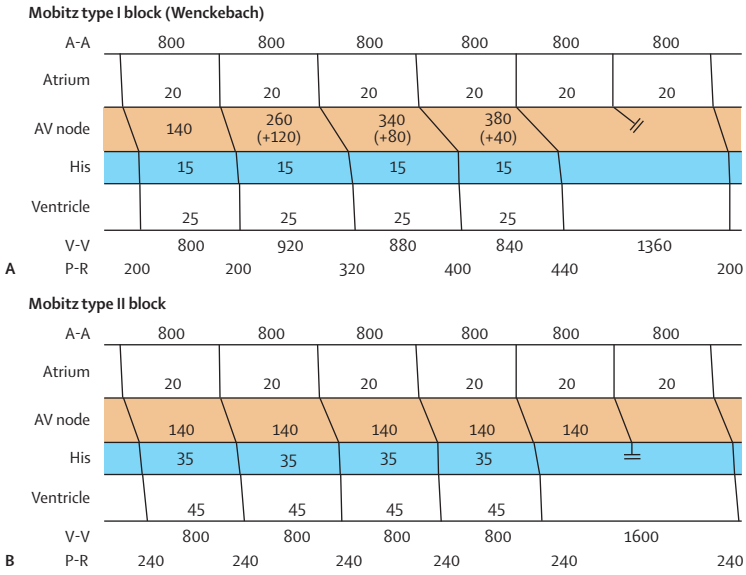

***Figure 2*: ECG recordings from type I and II second-degree AV block.** In Mobitz type I or Wenkebach block (panel A), progressive delay of the artial impulse occurs in the AV node proximal to the His bundle. The greatest increment occurs in the second beat (+120 ms) and becomes less in subsequent beats (+80 ms, +40 ms), leading to gradual shortening of the RR interval (920 ms - 880 ms - 840 ms). The pease measures less than the sum of two PP intervals (1360 ms). Mobitz type II AV block (panel B) is not preceded by PR interval lengthening, and the pause equals two PP intervals. The site of block is usually distal to the AV node. Activation times in the diagrams are given in milliseconds (ms); double bars indicate conduction block. A, atrium; V, ventricle.

block and should be considered also in asymptomatic patients. An electrophysiological study can sometimes be useful for determining intra- or infra-His levels of block. Type 2 second-degree AV block during exercise in the absence of ischemia indicates a diseased His-Purkinje system and should lead to permanent pacemaker implantation.[2]

Third-degree AV block

In third-degree or complete AV block, no conduction from the atrium to the ventricle is possible, and all atrial impulses halt somewhere in the atrioventricular conduction axis. The term AV dissociation is often used to describe third-degree AV block. However, this term can be misleading because several situations can lead to dissociated atrial and ventricular activation in the presence of normal AV conduction. In principle, any junctional or ventricular rhythm with a rate that exceeds the sinus rate and without VA conduction may appear dissociated, especially if only a standard 12-lead ECG is recorded. Sinus bradycardia with a junctional escape rhythm or junctional or ventricular tachycardias with retrograde block can mimic AV dissociation too. Longer ECG recordings and thorough analysis are sometimes required for correct diagnosis of third-degree AV block. The site of block can be the AV node, the His bundle, or the bundle branches. Most often, a pace-

maker distal to the site of block takes over, leading to an "escape" rhythm. If the site of block is located within the AV node, a junctional escape with narrow QRS complexes can occur, whereas a block distal to the AV node generates a wide QRS rhythm from the His-Purkinje system or the ventricular myocardium. Clinically, the site of block dictates the symptoms, which can vary from no symptoms when the site of block is proximal in the AV node with a reasonable escape rhythm, to syncope or cardiac death when the site of block is distal with a slow or no ventricular escape rhythm. In patients with atrial fibrillation, a strictly regular ventricular rhythm around 60 bpm with normal QRS complexes indicates third-degree AV block, often as a result of too high a dose of rate-control drugs. Third-degree block is a rare condition in healthy people and is more frequent in the elderly with structural heart disease. In a large, community-based, cohort study, the incidence of third-degree block was 9 per 100 000 person-years. The presence of first-degree AV block and left bundle branch block increased the risk of progression to third-degree block.[7] The estimated prevalence of congenital third-degree AV block is 1 per 15 000 to 22 000 live births in the general population.[8]
Treatment of reversible causes and withdrawal of eventually causative drugs may resolve AV block. Most patients with third-degree AV block will require permanent pacemaker implantation, even if they are asymptomatic. This will be further discussed later.

Congenital atrioventricular block

A modern definition of congenital AV block (CAVB) requires its diagnosis in utero or during the first month of life.[9] About one-third of cases have concomitant complex structural heart defects (i.e., congenitally corrected transposition of the great arteries or left isomerism). Two-thirds of cases have no or only minor structural defects.[8] In most of these cases (90% to 99%), AV block is associated with the presence of maternal autoantibodies against intracellular ribonucleoproteins SS-A/Ro (especially Ro52) and SS-B/La. These autoantibodies are frequently found in mothers with overt autoimmune disease, as well as in apparently healthy mothers (although less frequently). The exact mechanism by which commonly found autoantibodies can cause a rare disease such as congenital AV block is not yet fully elucidated. Figure 3 depicts a recent pathophysiological model from Ambrosi and Wahren-Herlenius[9]: maternal autoantibodies cross the placenta and are deposited in various fetal tissues, producing a syndrome called neonatal lupus. In the heart, a subgroup of antibodies against Ro52 bind to cross-reactive molecules on the surface of the fetal cardiomyocytes.

Accumulating evidence suggests that among these cross-reactive molecules are the pore-forming protein alpha$_1$-subunits of the two L-type calcium channels Cav1.2 and Cav1.3.[10] Subsequent inactivation of these channels leads to calcium dysregulation and apoptosis. After apoptosis, intracellular Ro and La proteins are translocated to the cell surface and become the target for maternal anti-Ro/La autoantibodies. Binding of the autoantibodies attracts macrophages that will clear the apoptotic cells and secrete proinflammatory and profibrotic factors, finally leading to fibrosis and calcification.

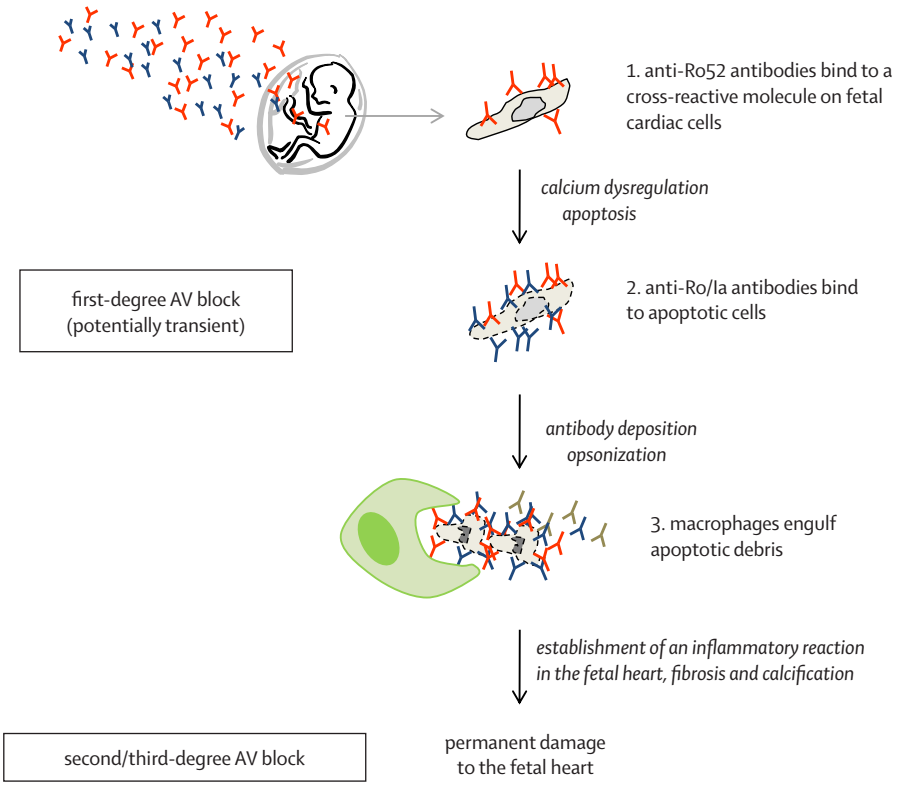

***Figure 3*: Pathophysiological model for the development of congenital AV block**. Reproduced with permission from Ambrosi A, Wahren-Herlenius M: Congenital heart block: Evidence for a pathogenic role of maternal autoantibodies. Arthritis Res Ther 2012; 14: 208-218.

The inflammatory reaction causes a wide spectrum of cardiac abnormalities (Table 1).[11,12] Involvement of the AV conduction system produces different stages of AV block. First-degree AV block, seen in 3% to 25% of antibody-positive pregnancies, is transient and resolves in most cases without treatment. Second-degree AV block reverses only very rarely, whereas complete AV block is always irreversible. Unfortunately, to date, no "golden bullet" is available that could prevent or treat complete AV block and its complications. The key therapeutic concept is to treat mothers with single or multiple immunomodulatory agent(s) as soon as second- or third-degree AV block is detected in the fetus, or "prophylactic" as a previous pregnancy was affected. Case reports and small cohort studies suggest that the following agents might revert or prevent AV block: fluorinated steroids, intravenous immunoglobulin (IVIG), and hydroxychloroquine. However, a recent multicenter prospective study has shown that the fluorinated steroid dexamethasone could not prevent progression from second-degree to complete AV block.[13]

Cardiac defect	Mortality rate
Electrophysiological	
• Children with isolated congenital AV block	4-6%
• Infants with isolated congenital AV block	4-8%
• Adults with isolated congenital AV block who were previously asymptomatic	5%
• First-, second-, and third-degree AV block	
• Atrial and ventricular ectopic beats	
• Atrial flutter	
• Ventricular and junctional ectopic tachycardia	
• Sinus node dysfunction	
• Long QT interval	
Myocardial/Functional	80%
• Myocarditis	
• Cardiomyopathy	
• Can develop before birth, after infancy, or in adults	
• Can occur with or without conduction abnormalities	
• Endocardial fibroelastosis	
• Pericarditis/pericardial effusion	
Structural	
• Infants with congenital AV block and structural disease	29%
• Children with congeniteal AV block and structural disease	10%
• Semilunar and AV valve dysplasia, stenosis, regurgitation	
• Patent ductus arteriosus	
• Atrial septal defects	
• Ventricular septal defects	

***Table 1*: Spectrum of cardiac abnormalities in neonatal lupus and associated mortality rates**. Reproduced with permission from Capone C, Buyon JP, Friedman DM, Frishman WH: Cardiac manifestations of neonatal lupus: A review of antibody associated congenital heart block and its impact in an adult population. Cardiol Rev 2012; 20: 72-76; and Hornberger LK, Al Rajaa N: Spectrum of cardiac involvement in neonatal lupus. Scand J Immunol 2010; 72: 189-197.

Moreover, once complete AV block was observed, dexamethasone could not cause it to revert. Two recent multicenter prospective studies (one in Europe and one in the United States) demonstrated that IVIG given to mothers with a previous child with congenital AV block could not prevent recurrence of CAVB.[14,15] Most recently, a multicenter case-control study found that hydroxychloroquine, given to mothers with a previous child with cardiac neonatal lupus, reduced the recurrence rate by 64.6% (odds ratio [OR], 0.23).[16] After birth, pacing becomes the most important treatment option.

Genetic factors in atrioventricular block

AV block can occur as the result of mutations in genes that play an important role in the normal development of the cardiac conduction system, as, for example, the genes TBX5 and NKX2-5, which encode major transcription factors.

Another gene associated with AV block is SCN5A, which encodes the major cardiac sodium channel. Loss-of-function mutations in SCN5A have been linked with hereditary Lev-Lenègre disease, characterized by progressive fibrosis of the His-Purkinje system, leading to bundle branch block and eventually to complete AV block.[17]

Acquired AV block including AV block in the setting of acute myocardial infarction

Causes of acquired AV block include ischemic heart disease and degenerative processes resulting in cardiac (replacement) fibrosis. Other causes include the following:

- *Infiltrative processes*: amyloidosis, sarcoidosis, carcinoma, Hodgkin's disease, multiple myeloma
- *Infection*: myocarditis, rheumatic fever, Lyme borreliosis, Chagas' disease, Aspergillus myocarditis
- *Rheumatic diseases*: ankylosing spondylitis, Reiter's disease, polychondritis, rheumatoid arthritis, scleroderma
- *Neuromuscular disorders*: myotonic muscular dystrophy, benign pseudohypertrophic muscular dystrophy (Becker), Erb's dystrophy, Kearns-Sayre syndrome, Charcot-Marie-Tooth disease (peroneal muscular atrophy)
- Other causes, such as calcification of the aortic or mitral valve annuli, surgical trauma, unintended damage during catheter ablation, and electrolyte disturbances.

AV block may also be an adverse effect related to the use of drugs such as ß-blockers, calcium channel blockers, class I and class III antiarrhythmic drugs, or digitalis.
In acute myocardial infarction, incidence and site of AV block depend on the affected vessel and the anatomical location of the infarction. In inferior myocardial infarction, the AV nodal artery may be involved with subsequent necrotic changes in the AV node and its approaches. The His-Purkinje system is usually spared. In anterior and anteroseptal infarction, necrotic changes are seen most often in the distal His bundle and in the bundle branches. In extensive infarction, the AV node and the penetrating AV bundle may also be involved.

Second- or third-degree AV block occurs in 2% to 13% of patients with acute myocardial infarction. In inferior myocardial infarction, the incidence of high-degree AV block can be two- to fourfold higher compared with anterior myocardial infarction.[18,19] The development of AV block in acute myocardial infarction is associated with higher in-hospital and long-term mortality.[20] Late occurring high-degree AV block up to 3 weeks after myocardial infarction may be associated with increased risk of heart failure and life-threatening ventricular arrhythmias.[21]

Primary percutaneous coronary intervention, where available, has become the treatment of choice for most patients with acute myocardial infarction, and the overall incidence of second- or third-degree AV block seems to be decreasing significantly. However, development of AV block within the first 30 days after infarction is still associated with a poor prognosis.[19] Occlusion of the right coronary artery, age >65 years, female sex, hypertension, and diabetes have been shown to be independent predictors of high-degree AV block.[19]

Animal models of AV block and its consequences

Cellular and molecular bases of ventricular remodeling in CAVB dogs

Creation of complete AV block in dogs at adult ages (≥1 year) initiates numerous cardiac adaptations that in the end (6 to 10 weeks) result in compensated biventricular hypertrophy in the large majority (>95%) of animals.[22] Associated with these "benign" remodeling processes is enhanced susceptibility to repolarization-related arrhythmias, especially with the use of drugs that block the rapid component of the delayed rectifier current (I_{Kr}) and further reduce repolarization strength. In this part of the chapter, various aspects of the ventricular remodeling process will be highlighted.

Electrical remodeling

The drop in heart rate from 100 to 120 to 50 to 60 bpm will slightly increase repolarization times (QT time and duration of [monophasic] action potentials [APDs]) on the basis of QT-APD/frequency dependency. A further increase in these repolarization parameters is seen with ventricular remodeling. The latter is more severe (+35%) and encompasses alterations in both ionic currents and different ion pumps (Table 2) involved in the shift of ion gradients over the sarcolemma and within the cytoplasm during each heart cycle. As has been observed recently, electrical remodeling not only is dependent on the bradycardia- induced volume overload but is determined by altered ventricular activation caused by the new idioventricular pacemaker.[23]

The molecular correlates of the altered functions of ion channels are often nicely noted in the corresponding downregulation or upregulation of the alpha-subunits of important pore-forming proteins. Their individual protein function seems intact, as can be seen in their response to modulating factors, such as stimuli representing the ß-adrenergic system. It is therefore the expression levels of the available numbers of ion channel proteins that determine their exact contribution to the shape and duration of the ventricular action potential. The emphasis of electrical remodeling seems to be on the repolarizing currents (see Table 2), of which I_{Kr} and I_{Ks} are downregulated. It is clear that electrical remodeling is a fast process that is fully completed within 2 weeks, with the first signs of protein alterations already evident after 3 days.

Contractile remodeling

In the acute moments after AV block, the drop in stroke volume and/or the increase in ventricular preload induces neurohumoral activation to compensate for the reduction in cardiac output. This temporarily increased neurohumoral activity involves (nor)epi-

nephrine, angiotensin II, and aldosterone, and it considerably improves stroke volume. This process is relatively fast and consists of changes in intracellular calcium handling, as well as increased sarcoplasmic calcium storage and subcytoplasmic sodium concentrations (see Table 2), allowing for a larger calcium transient, which provides a stronger contraction and leads to pumping of more blood out of the heart per beat.

Structural remodeling

The slower adaptation pathway consists of the development of biventricular hypertrophy. Over weeks, this eccentric growth of cardiomyocytes becomes visible. As compared with the normal heart, the capillary/myocyte ratio is normal with similar expression of the gap junction Connexin 43 and no increase in fibrosis. Conduction velocity therefore is not impaired at all.[24]

Arrhythmia consequence

Ventricular remodeling that occurs in the CAVB dog considerably enhances susceptibility to drug-induced torsade de pointes (TdP) arrhythmias. In a series of experiments, anesthetized dogs in sinus rhythm (normal) or after creation of acute AV block (bradycardia) did not respond with TdP (0%) after infusion of the drug dofetilide, but in the presence of ventricular remodeling (CAVB dog), this incidence reproducibly increased to 75% TdP. Numerous TdP occurred not only within a single experiment but also over a testing period of weeks. In isolated cardiomyocytes of CAVB dogs, infusion of dofetilide induces early afterdepolarizations (EADs)—the presumed trigger for TdP in the intact heart.

Channel/ionic current	Left ventricle	Right ventricle
Peak and late sodium: I_{Na}	↓	=
Delayed rectifier I_{Kr}	=/↓	↓
Delayed rectifier I_{Ks}	↓	↓↓
L-type Ca window	↑	?
Na/Ca exchange: NCX		
Forward (Ca-efflux)	↑↑	↑
Reverse (Ca-influx)	↑↑	↑
$[Ca]_i$ transient	↑↑	↑
$[Na]_i$ subsarcolemma	↑	?
Na/H exchanger	↑	↑
Cx43 heterogeneity	↑	↑↑

***Table 2*: Molecular and ionic remodeling in the CAVB dog.**

Differences between left and right ventricular remodeling

Contractile adaptations are similar in cases where increases in stroke volume are involved. The way this is achieved differs: The right ventricle (RV) demonstrates increased hypertrophy and less action potential (AP) lengthening, whereas the left ventricle (LV) shows the opposite.

Other animal models of complete AV block

Whereas dogs seem well suited to overcome (acute) bradycardia and decreased cardiac output, smaller animals experience greater difficulty or even are unable to cope. This holds true for rabbits[25] and mice, which need pacemaker assistance to overcome the drop in rate over the long term.

Therapy on the long run

Treatment for AV block is divided into acute and chronic phases. Acute therapy depends on the presence of bradycardia-related symptoms and is aimed at the prevention of acute heart failure and/or asystole. Intravenous drug therapy (atropine, isoprenaline, or epinephrine) and/or transcutaneous or transvenous temporary pacing can be used during this phase.

The decision to proceed from temporary to permanent pacing (chronic therapy) is determined by the type, cause, and prognosis of AV block. A detailed overview on pacing indications in congenital and acquired AV block can be found in current guidelines.[2] Timing is of crucial importance because not all procedures are effective and not all are devoid of adverse effects. As indicated in the chronic AV block dog model, these animals are able to overcome the reduction in heart rate. Whether young children with congenital AV block have the same ability to delay pacemaker implantation and to what time point is unknown, but it remains a point of discussion when problems with chronic (RV) pacing are considered.[26]

Some important points need to be considered: (1) which pacemaker system should be used, (2) how it should be implanted, and (3) which chamber should be paced. Children with congenital complete heart block are especially challenging to treat because of their size, growth, and need for lifelong pacing, often combined with the concomitant presence of structural congenital heart disease. Transvenous lead implantation might be impossible because of the tiny vessel size in neonates and infants or closed vascular access to the heart due to palliation of complex congenital heart disease. In these patients, epicardial pacemaker lead implantation represents an alternative with excellent long-term performance and durability.[27] Traditionally, chronic RV pacing has been performed by placing an epicardial lead on the RV free wall or an endocardial transvenous lead in the apex of the RV. Experimental animal studies and clinical studies in children and adults demonstrated that chronic RV pacing might result in electromechanical dyssynchrony, leading to adverse LV remodeling with LV dilatation and asymmetric hypertrophy.[28-30]

Up to 30% of patients develop dilated cardiomyopathy,[29] and 5% to 10% develop heart failure.[30] These unfavorable consequences have produced considerable interest in alternative pacing sites. Very recently, Salameh *et al.* described the effects of LV apical pacing as opposed to RV free wall pacing on ventricular synchrony, function, and ultrastructure in a mini-pig model mimicking chronic pacing for complete AV block started during early childhood.[28] After 1 year of pacing, the RV free wall–paced animals showed the poorest LV performance. Biventricular pacing using cardiac resynchronization therapy (CRT) is another treatment modality that is not associated with adverse LV effects and can even alleviate the effects of RV pacing in a young patient.[31]

Future perspectives

Pacing may be a lifesaving intervention, but it can cause considerable morbidity (see earlier). In the future, stem cell–based pacemakers might replace current instruments, or stem cell–derived techniques may be used to rewire the conduction over the AV node.[32]

References

1. Hwang HJ, Ng FS, Efimov IR: Mechanisms of AV nodal excitability and propagation. In Zipes DP, Jalife J, editors: Cardiac Electrophysiology: From Cell to Bedside, ed 6, Philadelphia, 2012, Saunders Elsevier.
2. Epstein AE, DiMarco JP, Ellenbogen KA, et al. ACC/AHA/HRS 2008 guidelines for device-based therapy of cardiac rhythm abnormalities. J Am Coll Cardiol 2008; 51: e1–e62.
3. Atrioventricular conduction abnormalities. In Issa Z, Miller JM, Zipes DP, editors: Clinical Arrhyth- mology and Electrophysiology: A Companion to Braunwald's Heart Disease, ed 1, Philadelphia, 2008, Saunders Elsevier, pp 127–142.
4. Averill KH, Lamb LE: Electrocardiographic findings in 67,375 asymptomatic subjects. I. Incidence of abnormalities. Am J Cardiol 1960; 6: 76–8.
5. Cheng S, Keyes MJ, Larson MG, et al. Long-term outcomes in individuals with prolonged PR interval or first-degree atrioventricular block. J Am Med Assoc 2009; 301: 2571–2577.
6. Josephson ME: Atrioventricular conduction. In Clinical Cardiac Electrophysiology: Techniques and Interpretations. Philadelphia, 2008, Lippincott Williams & Wilkins, pp 93–113.
7. Watanabe H, Makita N, Tanabe N, et al. Electrocardiographic abnormalities and risk of complete atrioventricular block. Int J Cardiol 2012; 155: 462–464.
8. Al-Ahdab M: Complete heart block-third-degree heart block. In Macdonald D, editor: Clinical Cardiac Electrophysiology in the Young, New York, 2006, Springer Science+Business Media, pp 173–181.
9. Ambrosi A, Wahren-Herlenius M. Congenital heart block: Evidence for a pathogenic role of maternal autoantibodies. Arthritis Res Ther 2012; 14:208–218.
10. Karnabi E, Qu Y, Mancarella S, et al. Rescue and worsening of congenital heart block–associated electrocardiographic abnormalities in two trans- genic mice. J Cardiovasc Electr 2011; 22: 922–930.
11. Capone C, Buyon JP, Friedman DM, et al. Cardiac manifestations of neonatal lupus: A review of antibody associated congenital heart block and its impact in an adult population. Cardiol Rev 2012; 20: 72–76.
12. Hornberger LK, Al Rajaa. Spectrum of cardiac involvement in neonatal lupus. Scand J Immunol 2012; 72: 189–197.
13. Friedman DM, Kim MY, Copel JA, et al. Prospective evaluation of fetuses with autoimmune-associated congenital heart block followed in the PR interval and dexamethasone evaluation (PRIDE) study. Am J Cardiol 2009; 103: 1102–1106.
14. Friedman DM, Llanos C, Izmirly PM, et al. Evaluation of fetuses in a study of intravenous immunoglobulin as preventive therapy for congenital heart block: Results of a multicenter, prospective, open- label clinical trial. Arthritis Rheum 2010; 62: 1138–1146.
15. Pisoni CN, Brucato A, Ruffatti A, et al. Failure of intravenous immunoglobulin to prevent congenital heart block: Findings of a multicenter, prospective, observational study. Arthritis Rheum 2010; 62: 1147–1152.
16. Izmirly PM, Costeodat-Chalumeau N, Pisoni CN, et al. Maternal use of hydroxychloroquine is associ- ated with a reduced risk of recurrent anti-SSA/ Ro-antibody-associated cardiac manifestations of neonatal lupus. Circulation 2012; 126: 76–82.
17. Park DS, Fishman GI: The cardiac conduction system. Circulation 2011; 123: 904–915.
18. Meine TJ, Al-Khatib SM, Alexander JH, et al. Incidence, predictors, and outcomes of high-degree atrioventricular block complicating acute myocardial infarction treated with thrombolytic therapy. Am Heart J 200; 149: 670–674.
19. Gang UJO, Hvelplund A, Pedersen S, et al. High-degree atrioventricular block complicating ST-segment elevation myocardial infarction in the era of primary percutaneous coronary intervention. Europace 2012; 14: 1639–1645.
20. Nguyen HL, Lessard D, Spencer FA, et al. Thirty- year trends (1975-2005) in the magnitude and hos- pital death rates associated with complete heart block in patients with acute myocardial infarction: A population-based perspective. Am Heart J 2008; 156: 227–233.
21. Gang UJ, Jons C, Jorgensen RM, et al. Clinical significance of late high-degree atrioventricular block in patients with left ventricular dysfunction after an acute myocardial infarction—A Cardiac Arrhythmias and Risk Stratification After Acute Myocardial Infarction (CARISMA) substudy. Am Heart J 2011; 162: 542–547.
22. Oros A, Beekman JDM, Vos MA. The canine model with chronic, complete atrioventricular block. Pharmacol Ther 2008; 119: 168–178.
23. Winckels SKG, Thomsen MB, Oosterhoff P, et al. High-septal pacing reduces ventricular electrical remodeling and proarrhythmia in chronic atrioventricular block dogs. J Am Coll Cardiol 2007; 50: 908–913.
24. Boulaksil M, Jungschleger JG, Antoons G, et al: Drug induced torsade de pointes arrhythmias in the chronic AV-block dog are perpetuated by focal activity. Circ Arrhythm Electrophysiol 2011; 4: 566–576.
25. Tsuji Y, Hojo M, Voigt N, et al. Calcium related signaling and protein phosphorylation abnormalities play central roles in a new experimental model of electrical storm. Circulation 2011; 123: 2192–2203.
26. Blank AC, Hakim S, Strengers JL, et al. Exercise capacity in children with isolated congenital heart block: Does pacing make a difference? Pediatr Cardiol 2012; 33: 576–585.

27. Odim J, Suckow B, Saedi B, et al. Equivalent performance of epicardial versus endocardial permanent pacing in children: A single institution and manufacturer experience. Ann Thorac Surg 2008; 85: 1412–1416.
28. Salameh A, Dhein S, Blanke K, et al. Right or left ventricular pacing in young minipigs with chronic atrioventricular block: Long-term in-vivo cardiac performance, morphology, electrophysiology and cellular biology. Circulation 2012; 125: 2578–2587.
29. Silvetti MS, Drago F, Ravà L. Determinants of early dilated cardiomyopathy in neonates with congenital complete atrioventricular block. Europace 2010; 12: 1316–1321.
30. van Geldorp IE, Delhaas T, Gebauer RA, et al. Impact of the permanent ventricular pacing site on left ventricular function in children: A retrospective multicentre survey. Heart 2011; 97: 2051–2055.
31. Janousek J. Cardiac resynchronization in congenital heart disease. Heart 2009; 95: 940–947.
32. Blank AC, van Veen TAB, Jonsson MKB, et al. Rewiring the heart: Stem cell therapy to restore normal cardiac excitability and conduction. Curr Stem Cell Res 2009; 4: 23–33.

CHAPTER 2

PART I

Cardiopulmonary exercise testing in congenital heart disease: equipment and test protocols

Cardiopulmonary exercise testing in congenital heart disease: equipment and test protocols

T. Takken, A.C. Blank, E.H. Hulzebos, M. van Brussel, W.G. Groen, P.J. Helders

***Neth Heart J** 2009; 17: 339-44*

Child Development and Exercise Center, Wilhelmina Children's Hospital, University Medical Center Utrecht (UMCU), Utrecht, the Netherlands
T Takken
EH Hulzebos
M van Brussel
WG Groen
PJ Helders

Department of Paediatric Cardiology, Wilhelmina Children's Hospital, UMCU, Utrecht, the Netherlands
AC Blank

Abstract

Cardiopulmonary exercise testing (CPET) in paediatric cardiology differs in many aspects from the tests as performed in adult cardiology. Children's cardiovascular responses during exercise testing present different characteristics, particularly oxygen uptake, heart rate and blood pressure response, which are essential in interpreting haemodynamic data. Diseases that are associated with myocardial ischaemia are very rare in children. The main indications for CPET in children are evaluation of exercise capacity and the identification of exercise-induced arrhythmias. In this article we will review exercise equipment and test protocols for CPET in children with congenital heart disease.

Children with congenital or acquired heart disease often have impairment of their functional capacity. This occurs in the preoperative, postoperative, as well as in the long-term setting and may be the result of the primary cardiac problem, treatment of that problem or hypoactivity leading to detraining.[1,2] Lunt *et al.*[3] found that adolescents with congenital heart disease (CHD) were less likely to reach minimum exercise requirements and perform vigorous exercises than were healthy adolescents.

Measurement of exercise capacity and other physiological responses provides objective information about the functional status of heart, lungs and peripheral muscle. This information can be of value in making clinical decisions resulting in a reduced use of hospital facilities, and improved functional capacity and quality of life.[4]

The aim of this article is to review the equipment, the main indications for CPET in children with congenital heart disease, the contraindications for exercise testing and the indications for terminating an exercise test. Moreover, we will address the interpretation of gas-exchange data from CPET in children with congenital heart disease.

Equipment for exercise testing

Laboratory and personnel

The exercise laboratory needs a special fitting. Exercise testing should be performed in a well-ventilated room with a temperature of ≈22°C and a relative humidity of ≈50%. Furthermore, it is recommended that the exercise lab is at least 23 m^2 in size and when several ergometers, computers and other medical equipment are accommodated preferably 45 to 65 m^2.[5]

Persons who are conducting the CPET (physicians, exercise physiologist or lab technicians) should have experience in paediatric exercise testing, especially in conducting CPET in children. When performing CPET, 50 supervised exercise tests and performing at least 25 tests per year are recommended to retain the skills of CPET.[5]

Although emergencies are rare in paediatric exercise testing, staff should be familiar with emergency manoeuvres and equipment should be available in case of exercise-induced problems. This equipment includes a cardiac defibrillator and a fully stocked crash cart. Furthermore, the lab should have medication readily available to treat exercise-induced asthma. A treatment table should be available for resuscitation or whenever the patient feels dizzy and needs to lie down following exercise. This table can also be used to record a standard supine ECG before CPET. In addition, having an emergency physician or paediatric cardiologist on site is recommended when performing a CPET in children with CHD.

Clinical laboratory testing

The basic premise for treadmill or cycle testing of young persons is not different from that for adults to assess symptoms, tolerance, and cardiopulmonary response to high-intensity exercise in a controlled setting. In general, satisfactory testing of children can be conducted equally well as in adults, even in subjects as young as four years. However, a number of particular features need to be appreciated when dealing with this age group.[6] Most importantly, children are emotionally immature and need encouragement and positive support by an experienced testing staff to achieve an adequate exercise effort.

Ergometers

Both cycle and treadmill protocols have been used for exercise testing of children. However, the use of the treadmill is more appropriate when testing very young children, because this modality requires that the subject maintain the pace of the belt rather than provide the volitional effort to maintain a cycle cadence with increased workloads. Electronically braked cycle ergometers reduce the dependence on a specific cadence by allowing a range of cadence to achieve the same workload. However, appropriate small-sized ergometers are not available in most laboratories. To accommodate children, seat height, handlebar height and position, and pedal crank length may have to be modified for cycle ergometer testing. Most children who are ≥125 cm tall can be tested on a standard cycle ergometer. The greater potential for accidental falls on the treadmill requires greater attention by the testing staff. Regardless of the mode or protocol, children most be familiarised with all testing procedures to ensure the opportunity for a successful evaluation. It is advised to use an ergometer to get objective and reproduceable information. In table 1 we summarise several considerations regarding when to choose the treadmill or the cycle ergometer.

Treadmill

The treadmill is useful for a wide range of patient sizes and ages. Treadmill exercise testing yields a 5 to 10% higher VO_{2peak} than cycle ergometry due to recruitment of more muscle groups. The amount of work performed depends on body weight rather than machine set resistances. Fatigue of the leg muscles is less likely to be the cause of test termination than would be the case on a cycle ergometer. This increases the likelihood of the cardiorespiratory system being the limiting factor.[1]

Cycle ergometer

The patient must be tall enough to reach the pedals. The cycling motion might be difficult for young children to perform. Workload on a cycle ergometer is not dependent on patients' weight and can be used with a continuous ramp protocol allowing the workload to be precisely determined. The upper body is more stable on a cycle ergometer than on a treadmill, so ECG and blood pressure measurements are more reliable.[1]
Sometimes semi-recumbent ergometers are used in combination with echocardiographic measurements. However, one must take into account the different cardiopulmonary response to exercise compared with upright cycling exercise.

Other equipment

An electrocardiographic (ECG) monitoring system, blood pressure monitor, metabolic cart and a pulse oximeter are also needed for exercise testing. An exercise ECG monitoring system is necessary to monitor cardiac rhythm and rate. Moreover, it can be used to detect cardiac ischaemia during the exercise test, although this is observed far less in paediatric patients than in adult populations. In addition, an exercise ECG system is valuable for detecting prolongation of the QT interval during exercise, as seen in patients with long-QT syndrome.

Condition or question	Preferred ergometer	Rationale
Aortic stenosis/insufficiency (unrepaired/repaired)	Cycle	Ischaemia detection on ECG easier because there is less motion artifact
Repaired transposition of great arteries	Cycle	Ischaemia detection on ECG easier
Repaired tetralogy of Fallot	Cycle	Arrhythmia assessment during exercise essential
Coronary artery anomaly (repaired/unrepaired)	Cycle	Ischaemia detection on ECG easier
(Functional) single ventricle	Cycle/treadmill	Ischaemia and arrhythmia detection on ECG easier
Coarctation of the aorta (unrepaired/repaired)	Cycle	Blood pressure assessment more accurate
Exercise-induced asthma bronchospasm/chest pain	Treadmill	Running more likely to induce symptoms than cycling
Aerobic capacity	Cycle/treadmill	Higher VO_{2max} with treadmill than with cycle
Arrhythmia assessment Long QT syndrome	Cycle	Arrhythmia detection and measurement of QT interval on ECG easier
Assessment of rate responsive pacemakers	Treadmill	Better activation of accelerometer-based sensors

***Table 1*: Matching the ergometer with the desired information**. Modified from Stephens *et al.*[7]

To minimise artifacts on the ECG, the recording system should have a muscle artifact filter system. It is also imperative to pay meticulous attention to the electrode placement. The skin should be prepared by cleaning with alcohol followed by scrubbing with an abrasive paper. We use disposable adhesive electrodes made from a breathable material to minimise skin transpiration. The connecting cables should be fixed to the skin with tape. The cable connector should hang above or behind the patient. This can be achieved by using a rack.

A metabolic cart is used to determine peak oxygen uptake (VO_{2peak}), carbon dioxide production and ventilatory threshold. There is a variety of commercially available metabolic carts, which can be used for measuring ventilatory gas exchange.[8] Moreover, several portable metabolic carts are available to measure VO_2 during activities in the field.[8]
A pulse oximeter provides information about arterial oxygen saturation at rest and during exercise. It is important to consider that oximeters may have difficulty tracking the signal at peak exercise because they are motion-sensitive.[1]

Although blood pressure is sometimes difficult to measure reliably during exercise,[9] especially during treadmill running, its measurement is important in children with aortic coarctation, aortic stenosis, cardiomyopathy and syncope, for instance. The laboratory should always have a variety of blood pressure cuffs available of appropriate sizes for the entire range of patients tested.
There are only a few automatic systems that can measure blood pressure during exercise. It is our experience that the Suntech Tango® system (SunTech Medical Instruments, Morrisville, North Carolina, USA) is a valid and reliable system to measure blood pressure during cycling exercise in children (Figure 1).[10] All equipment should, of course, be calibrated before use following the specifications of the manufacturer.

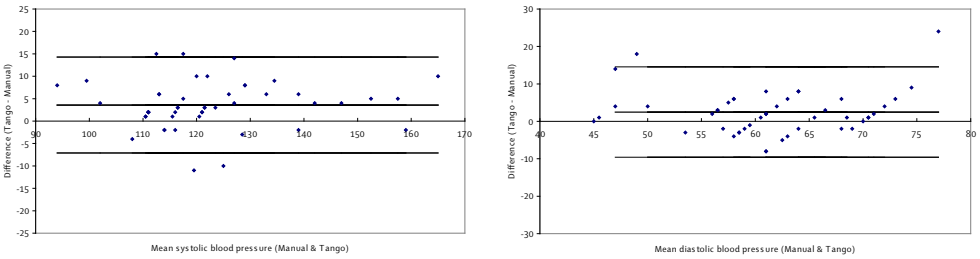

Figure 1: Bland-Altman plot of systolic (left) and diastolic (right) blood pressure (in mmHg) during exercise as measured with the Suntech Tango® system compared with auscultatory blood pressure measurement (Takken *et al.*, unpublished observations).

Testing protocols

Because of the wide ranges of ages and testing indications, there is no single standard testing protocol for children. There are a number of established treadmill exercise testing protocols, of which the Bruce protocol is the most commonly used.[11] This protocol is appropriate for most young, physically active patients; however, the incremental increases in workloads may be too great for others. Treadmill testing protocols that may be more appropriate for less-fit patients include Cornell, McNaughton, and Balke,[12,13] which have a slower increase in workload.
When a cycle ergometer is available, the most commonly used protocols are McMaster protocol,[14] James protocol,[15] Godfrey protocol,[16] and recently a continuous ramp protocol.[17] Increments in workload can be increased by 5, 10, 15 or 20 Watt per unit of time depending on height, weight or body surface area.[1,16] The aim is to reach a maximum of 6 to 10 minutes of exercise for young children[18] and 8 to 12 minutes for adolescents.[19]
In the early days of exercise physiology, it was quite common to use a discontinuous protocol.[20,21] In such protocols, exercise stages were performed on consecutive days until a subject reached his VO_2 plateau. These protocols were very impractical in clinical and occupational settings because of the time constraints of both the subject and the lab personnel. Therefore, exercise protocols were designed with a much shorter time between

exercise stages (several minutes). The intervals between the exercise stages allowed physiologists to perform several measurements such as blood sampling, and other invasive measurements such as muscle biopsies. Currently, most laboratories use continuous exercise protocols while many different exercise protocols are available. Exercise stages vary from a couple of seconds in the so-called ramp protocols to three to five minutes if a steady state for most physiological functions (heart rate and oxygen uptake) is required. The use of computerised treadmills allows smaller work increments at a higher frequency. These ramp protocols provide better haemodynamic and gas exchange responses during exercise than the protocols with longer exercise stages (i.e. three to five minutes).[22,23] Determination of the ventilatory threshold, for instance, is easier in protocols with a shorter stage duration.[23,24] Since Nobel laureate A.V. Hill described the concept of VO_{2max} in 1924,[25] many different test protocols have been designed for testing or predicting VO_{2max}. In the following section we will describe several exercise testing protocols including maximal and submaximal exercise tests.

Maximal exercise tests

Treadmill tests

A large number of treadmill protocols have been developed for measuring VO_{2max}, of which the Bruce and the Balke protocol are the most popular ones. The Bruce protocol is the most widely used treadmill protocol in clinical exercise testing.[11,26,27] This test was originally developed for cardiac patients by Robert A. Bruce in the 1960s.[28] The test involves a change of speed and elevation every three minutes, so that the incremental increases for each stage are relatively large (2-3 METS). Oxygen uptake values expressed in METS were derived from tests of normal subjects and were established for each minute of testing for the Bruce treadmill protocol.[29] In the modified version of the Bruce treadmill protocol, the speed stays constant for the first three stages, starting at 2.7 km/h at 0% incline. After the third stage, both the speed and grade increase every three minutes. McInnis *et al.* compared the modified Bruce and the Bruce protocol in patients with documented coronary artery disease and found that the physiological responses at matched submaximal rates were similar.[30]

Disadvantages of the Bruce test are: (1) large interstage increments in work that can make estimation of VO_{2max} less accurate and (2) a fourth stage that can be either run or walked, resulting in different oxygen costs.[31]

The Bruce protocol can be performed by small children whose legs may be too short to reach the pedals of a cycle ergometer. Treadmill protocols are useful in the evaluation of motion-sensitive, rateresponsive pacemakers because the upper torso is in constant motion.[32]

In the 1950s, Bruno Balke described a treadmill protocol which he used in exercise tests on Air Force personnel. In this protocol the workload is increased by increasing the angle of the treadmill while the walking speed remains unchanged during the test. Originally Balke used a speed of 5.3 km/h and a horizontal angle of the treadmill, with a 1° increase in angle of every minute.[33,34] Based on the endurance time or the final angle of the treadmill an estimation of the VO_{2max} could be made using the following formula:[34]

VO_{2max} = walking speed (metres/min) x body mass (kg) x (0.73 x angle/100) x 1.8

In this formula, the given fraction of the angle in degrees is needed, and 1.8 is the factor of the oxygen uptake for generating 1 m/kg of work. Since Balke's original study, many modifications have been made.[35] These modifications were made to limit the exercise time during the treadmill test. The optimal time for an aerobic capacity test is between 8 to 12 minutes on average.[36] In table 2, modifications of the Balke protocol are provided.

Bicycle ergometry testing

Cycle ergometry is one of the oldest methods to measure the exercise capacity of a subject. The first cycle ergometer was developed in 1896 by the French medical student Elisée Bouny. Later, several other mechanical braked and electromagnetically braked cycle ergometers were developed in both the United States[37] and Europe.[38]

Patient	Speed (km/h)	Angle % (start)	Angle % (increase/min)
Original	5.3	0	1
Poor condition	4.8	6	2
Inactive	5.2	6	2
Active	8	0	2.5
Athlete	8.5	0	2.5

***Table 2*: Modified Balke protocol**. From Rowland.[35]

Maximal cycle ergometer protocols

In Europe most maximal exercise tests are performed on the cycle ergometer, while in North America the treadmill is more commonly used. This probably reflects the use of the bicycle as a mode of transportation in daily life in Europe. Cycle ergometry has some advantages over treadmill exercise testing. The advantage of bicycle testing is that it is portable and less expensive than treadmill testing. Because the body is more stable during cycling and the bicycle is less noisy, blood pressure can be determined more easily and fewer motion artifacts are observed in electrocardiograms during exercise. Moreover, during cycle ergometry the workload and work efficiency can be precisely determined, while in treadmill exercise only an estimate can be made.

In addition, the VO_{2max} can be easily predicted from the peak workload (W_{peak}). As a rule of the thumb, every Watt costs about 10.3 ml O_2/min. W_{peak} can be computed as follows when a non-ramped protocol has been used:[39]

$$W_{peak} = POf + (t/T \times D)$$

where POf is the power output (W) of the last com- pleted workload, t is the time (in s) the last uncompleted workload was maintained, T is the duration (in s) of each completed workload, and D is the power-output difference (Watt) between consecutive workloads.
The disadvantage of bicycle protocols is that many (North American) subjects may not be accustomed to cycling and muscular fatigue may occur prematurely, preventing subjects from reaching their maximal capacity. VO_{2max} is 10 to 15% lower in cycle versus treadmill testing in those not accustomed to cycling.[40] With computerised ergometers it is possible to bypass the conventional protocols in which the workload is increased every one to five minutes. Using this ramp approach, there is a smaller increase in workload per time unit, providing a more linear increase of workload, which facilitates the determination of the ventilatory threshold.[41] Usually, the ventilatory threshold occurs at an exercise intensity between 40 to 60% of VO_{2max}. As mentioned previously, the best quality and quantity of data during clinical exercise tests are collected when the exercise time is between eight to 12 minutes in adults and adolescents and six to ten minutes in children.[18,19] This implies that a ramp protocol should be individualised, based on the subject's fitness status. For children the following method is used.[17] First, an estimation of basal VO_2 is made using the formula:

$$\text{Basal } VO_2 \text{ (ml/min)} = \text{height (in cm)} \times 2 - 100$$

The increase in workload per minute (RAMP) is calculated as follows:

$$(VO_{2peak} \text{ predicted} - VO_{2basal})/82.5$$

This will lead to exhaustion in approximately 8 minutes.
Another approach has been proposed by Tanner *et al*. They standardised the ramp protocol using a constant load in children of 0.25 W/kg/min.[42] In healthy children they found no difference in VO_{2peak} between the ramp protocol and a conventional James protocol. In children with exercise intolerance, the ramp protocol was preferable.[43]

Test termination

During a CPET, a patient can develop several exercise-induced physiological signs or complaints that warrant a termination of the test. Criteria for terminating a CPET are listed in table 3.

1. **Clinical**
   a. Symptoms — chest pain, severe headache, dizziness, chills, sustained nausea, inappropriate dyspnoea
   b. Signs — sustained pallor, clammy skin, disorientation, inappropriate affect
   c. Patient requests termination of study
2. **ECG**
   a. Failure of heart rate to increase with exercise, and extreme fatigue, dizziness, or other symptoms suggestive for insufficient cardiac output
   b. Premature ventricular contractions (PVCs) with increasing frequency
   c. Ventricular tachycardia (run of >3 PVCs)
   d. Supraventricular tachycardia
   e. ST segmental depression, or elevation, of more than 3 mm
   f. Triggering of atrioventricular (AV) block (2nd degree AV-block type Mobitz or 3rd degree AV block) by exercise
   g. Triggering of QTc lengthening >500 ms
3. **Blood pressure**
   a. Excessive levels (age-dependent) — systolic blood pressure 250 mmHg, diastolic blood pressure 125 mmHg
   b. Progressive fall in systolic blood pressure with increasing workload
4. **Progressive fall in oxygen saturation**
   <90% or a 10-point drop from resting saturation in a symptomatic patient

***Table* 3: Criteria for terminating a CPET in children**. Modified from Paridon *et al* and Bar-Or.[27,44]

Conclusion

Cardiopulmonary exercise testing in children with congenital heart disease differs in many ways from adult cardiological exercise testing. In this article we have reviewed exercise equipment and protocols, the main indications for cardiopulmonary exercise testing in children with congenital heart disease, the contraindications for exercise testing and the indications for terminating an exercise test. Moreover, we have addressed the interpretation of gas-exchange data from cardiopulmonary exercise testing in children with congenital heart disease.

Acknowledgement

We thank Professor Emeritus David A. de Wolf for his valuable comments on our manuscript.

References

1. Connuck DM. The role of exercise stress testing in pediatric patients with heart disease. Prog Pediatr Cardiol 2005; 20: 45-52.
2. Bar-Or O. Pathophysiological factors which limit the exercise capacity of the sick child. Med Sci Sports Exerc 1986; 18: 276-82.
3. Lunt D, Briffa T, Briffa NK, et al. Physical activity levels of adolescents with congenital heart disease. Aust J Physiother 2003; 49: 43-50.
4. Rich MW. Heart failure disease management: a critical review. J Card Fail 1999; 5: 64-75.
5. James FW, Blomqvist CG, Freed MD, et al. Standards for exercise testing in the pediatric age group. American Heart Association Council on Cardiovascu- lar Disease in the Young. Ad hoc committee on exercise testing. Circulation 1982; 66: 1377A-97A.
6. Rowland TW. Aerobic exercise testing protocols. In: Rowland TW, editor. Pediatric Laboratory Exercise Testing: Clinical Guidelines. Champaign, Ill: Human Kinetics; 1993. p. 19-41.
7. Stephens P Jr, Paridon SM. Exercise testing in pediatrics. Pediatr Clin North Am 2004; 51: 1569-87, viii.
8. Macfarlane DJ. Automated metabolic gas analysis systems: a review. Sports Med 2001;31:841-61.
9. Lightfoot JT. Can blood pressure be measured during exercise? A review. Sports Med 1991; 12: 290-301.
10. Cameron JD, Stevenson I, Reed E, et al. Accuracy of automated auscultatory blood pressure measurement during supine exercise and treadmill stress electro- cardiogram-testing. Blood Press Monit 2004; 9: 269-75.
11. Chang RK, Gurvitz M, Rodriguez S, et al. Current practice of exercise stress testing among pediatric car- diology and pulmonology centers in the United States. Pediatr Cardiol 2006; 27: 110-6.
12. Balke B, Ware RW. An experimental study of "physical fitness" of air force personnel. U S Armed Forces Med J 1959; 10: 675-88.
13. Ellestad M. Stress Testing. Oxford: Oxford University Press; 2003.
14. Bar-Or O, Rowland TW. Pediatric Exercise Medicine. From Physiologic principles to healthcare Application. Champaign, IL: Human Kinetics; 2004.
15. James FW, Kaplan S, Glueck CJ, Tsay JY, Knight MJ, Sarwar CJ. Responses of normal children and young adults to controlled bicycle exercise. Circulation. 1980;61:902-12.
16. Godfrey S. Exercise testing in children. London: W.B. Saunders Company Ltd; 1974.
17. Karila C, de Blic J, Waernessyckle S, et al. Cardiopulmonary exercise testing in children: an individualized protocol for workload increase. Chest 2001; 120: 81-7.
18. Hebestreit H. Exercise testing in children —What works, what doesn't, and where to go to? Paediatr Respir Rev 2004; 5: S11-S4.
19. Buchfuhrer MJ, Hansen JE, Robinson TE, et al. Optimizing the exercise protocol for cardiopulmonary assessment. J Appl Physiol 1983; 55: 1558-64.
20. Taylor HL, Buskirk E, Henschel A. Maximal oxygen intake as an objective measure of cardiorespiratory performance. J Appl Physiol 1955; 8: 73-80.
21. Mitchell JH, Blomqvist G. Maximal oxygen uptake. N Engl J Med 1971; 284: 1018-22.
22. Will PM, Walter JD. Exercise testing: improving performance with a ramped Bruce protocol. Am Heart J 1999; 138: 1033-7.
23. Myers J, Buchanan N, Walsh D, et al. Comparison of the ramp versus standard exercise protocols. J Am Coll Cardiol 1991; 17: 1334-42.
24. Whipp BJ, Davis JA, Torres F, Wasserman K. A test to determine parameters of aerobic function during exercise. J Appl Physiol 1981; 50: 217-21.
25. Hill AV, Long CNH, Lupton H. Muscular exercise, lactic acid and the supply and use of oxygen. Parts I-III. Proc R Soc Biol 1924; 96: 438-75.
26. Bruce RA. Exercise testing for evaluation of ventricular function. New Engl J Med 1977; 296: 671-5.
27. Paridon SM, Alpert BS, Boas SR, et al. Clinical stress testing in the pediatric age group: a statement from the American Heart Association Council on Cardiovascular Disease in the Young, Committee on Atherosclerosis, Hypertension, and Obesity in Youth. Circulation 2006; 113: 1905-20.
28. Bruce RA, Blackmon JR, Jones JW, Strait G. Exercise testing in adult normal subjects and cardiac patients. Pediatrics 1963; 32: Suppl-56.
29. American College of Sports M. Guidelines for exercise testing and prescription. Philadelphia: Lea and Febiger; 1991.
30. McInnis K, Balady G, Weiner D, Ryan T. Comparison of ischaemic and physiologic responses during exercise tests in men using the standard and modified Bruce protocols. Am J Cardiol 1992; 69: 84-9.
31. Fletcher GF, Balady GJ, Amsterdam EA, et al. Exercise standards for testing and training: a statement for healthcare professionals from the American Heart Association. Circulation 2001; 104: 1694-740.
32. Barber G. Pediatric exercise testing: methodology, equipment and normal values. Prog Pediatr Cardiol 1993; 2: 4-10.
33. Balke B. [Optimum physical working capacity, its measurement and change as a result of the working fatigue]. Arbeitsphysiologie 1954; 15: 311-23.
34. Balke B, Ware RW. An experimental study of physical fitness of Air Force personnel. U S Armed Forces Med J 1959; 10: 675-88.
35. Rowland TW. Crusading for the Balke protocol. Pediatr Exer Sci 1999; 11: 189-92.
36. Buchfuhrer M, Hansen J, Robinson T, et al. Optimizing the exercise protocol for cardiopulmonary assessment. J Appl Physiol 1983; 55: 1558-64.

37. Benedict FG, Cady WG. A bicycle ergometer with an electric brake. Washington DC: Carnegie Institute of Washington; 1912. Report No: Publication no. 167.
38. Krogh A. A bicycle ergometer and respiration apparatus for the experimental study of muscular work. Scand Arch Physiol 1913; 33: 375-80.
39. Kuipers H, Verstappen FT, Keizer HA, et al. Variability of aerobic performance in the laboratory and its physiologic correlates. Int J Sports Med 1985; 6: 197-201.
40. Astrand P, Rodahl K. Textbook of work physiology, physiological bases of exercise. New York: McGraw-Hill Book Company; 1986.
41. Wasserman K, Hansen JE, Sue DY, et al. Principles of Exercise Testing and Interpretation. Baltimore, MD: Lippincott, Williams and Wilkins; 1999.
42. Tanner CS, Heise CT, Barber G. Correlation of the physiologic parameters of a continuous ramp versus an incremental James exercise protocol in normal children. Am J Cardiol 1991; 67: 309-12.
43. Barber G. Pediatric exercise testing: methodology, equipment and normal values. Progr Pediatr Cardiol 1993; 2: 4-10.
44. Bar-Or O. Pediatric sports medicine for the practitioner. New York: Springer-Verlag; 1983.

CHAPTER 2

PART II
Cardiopulmonary exercise testing
in congenital heart disease:
(contra)indications and interpretation

Cardiopulmonary exercise testing in congenital heart disease: (contra)indications and interpretation

T. Takken, A.C. Blank, E.H. Hulzebos, M. van Brussel, W.G. Groen, P.J. Helders

Neth Heart J *2009 ; 17: 385-92*

Child Development and Exercise Center, Wilhelmina Children's Hospital, University Medical Center Utrecht (UMCU), Utrecht, the Netherlands
T Takken
EH Hulzebos
M van Brussel
WG Groen
PJ Helders

Department of Paediatric Cardiology, Wilhelmina Children's Hospital, UMCU, Utrecht, the Netherlands
AC Blank

Abstract

Cardiopulmonary exercise testing (CPET) in paediatric cardiology differs in many aspects from the tests performed in adult cardiology. Children's cardiovascular responses during exercise testing present different characteristics, particularly oxygen uptake, heart rate and blood pressure response, which are essential in interpreting haemodynamic data. Diseases that are associated with myocardial ischaemia are rare in children. The main indications for CPET in children are evaluation of exercise capacity and the identification of exercise-induced arrhythmias. In this article we will review the main indications for CPET in children with congenital heart disease, the contraindications for exercise testing and the indications for terminating an exercise test. Moreover, we will address the interpretation of gas exchange data from CPET in children with congenital heart disease.

Children with congenital or acquired heart disease often have impairment of their functional capacity. This occurs in the preoperative, postoperative, as well as in the long-term setting and may be the result of the primary cardiac problem, treatment of that problem[1] or hypoactivity leading to detraining.[2] Lunt *et al*. found that adolescents with congenital heart disease (CHD) were less likely to reach minimum exercise requirements and perform vigorous exercises than were healthy adolescents.[3]

Cardiopulmonary exercise testing (CPET) provides objective information about the functional status of heart, lungs and peripheral muscle. This information can be of value in making clinical decisions resulting in a reduced use of hospital facilities, and improved quality of life and functional capacity.[4]

The aim of this article is to review the main indi- cations for CPET in children with CHD, the contra-indications for exercise testing and the indications for terminating an exercise test. Moreover, we will address the interpretation of gas-exchange data from CPET in children with CHD.

Contraindications for exercise testing

The risk of CPET in the paediatric population is believed to be low.[5,6] In adults the risk of 1 myocardial infarction or death per 2500 exercise tests has been reported.[7] Because ischaemic heart disease is rare in children with CHD, the risk in children is lower than in adults.[6] Several absolute and relative contraindications can be distinguished for performing CPET (table 1).

Absolute contraindications
Active inflammatory heart disease
Active hepatitis
Acute myocardial infarction
Active pneumonia
Severe systemic hypertension for age
Acute orthopaedic injury to an exercise muscle group
Relative contraindications
Severe left ventricular outflow obstruction
Severe right ventricular outflow obstruction
Congestive heart disease
Pulmonary vascular obstructive disease
Severe aortic stenosis
Severe mitral stenosis
Ischaemic coronary artery disease
Cardiomyopathy
Certain inherited arrhythmia syndromes: LQTS, CPVT
Complex acquired ventricular arrhythmias

***Table 1*: Contraindications for exercise testing**. LQTS, long-QT syndromes; CPVT, catecholaminergic polymorphic ventricular tachycardia. Modified from Stephens and Paridon.[6]

Before testing, all patients with a CHD must have undergone a complete medical evaluation by a paediatric cardiologist. Several conditions are described in the literature that warrant special consideration including severe aortic/pulmonary stenosis, unrepaired arterial abnormalities, bleeding diatheses, pulmonary hypertension and acute disease processes involving any vital organ.[6] If a test can be highly life-threatening, CPET is strongly discouraged.

Indications for CPET in children with CHD

CPET in children with CHD has several indications (table 2). The first is to assess the physical capacity or aerobic capacity of a child with a CHD. This can be used to provide recommendations for physical activity in sports, occupation or rehabilitation. Recommendations for sports participation are available elsewhere.[8] Moreover, a CPET can determine whether a patient's complaints of fatigue have a physical aetiology.

The second indication for exercise testing in CHD is to provide indications for surgery (e.g. pacemaker implantation, valve replacement), therapy (medication or rehabilitation) or additional more invasive/demanding tests (e.g. cardiac CT/MRI, nuclear imaging or heart catheterisation).

Assesses physical capacity for recreational, athletic and occupational recommendations
Evaluates specific pathophysiological characteristics
- Provides indications for surgery, therapy, or additional tests
- Evaluates functional postoperative success
- Diagnoses disease

Assesses adequacy of therapy
Assesses risk for future complications in existing disease Instils confidence in child and parents
Motivates child for further exercise or weight loss

***Table 2*: Indications for exercise testing in children**. Modified from Bar-Or.[11]

Moreover, the stress of the CPET can be used to evaluate the success of interventions such as pacemaker implantation, closure of shunt (normalising in exercise SaO_2%), or ablation of arrhythmogenic substrates. In addition, CPET can be used to diagnose inherited arrhythmia syndromes (e.g. LQTS and CPVT) or chronotropic incompetence.

The third indication for CPET is to evaluate the adequacy of medication, for instance ß-blockers, angiotensin-converting enzyme inhibitors and digoxin in heart failure.

The fourth indication is to assess the risk for future disease complications, for instance complex Premature Ventricular Contractions (PVCs) during exercise in hypertrophic cardiomyopathy; and the fifth indication for CPET is to instil confidence in children and parents. Parents of children with a CHD are often overprotective of their child, even though the underlying disorder is only small and might not be restrictive for performing physical activities including competitive sports (e.g. children with a small ventricular

septum defect or atrial septum defects). It usually provides confidence in their child's ability to perform physical exercise when parents see their child running on a treadmill or cycling on an ergometer with high heart rates till exhaustion without any complications. In adult cardiac patients after myocardial infarction (MI), it has been shown that the confidence of the patient and their spouse can be significantly improved when a CPET is performed three weeks after the MI.[9]
Lastly, CPET (as well as field tests, such as the 6- minute walk test[10]) can be used to show improvement of physical rehabilitation in children with CHD. Furthermore, a fitness assessment including CPET can be helpful in motivating children with CHD to maintain a healthy body weight or to combat overweight/obesity.

Interpretation of exercise test results

The use of CPET depends on obtaining a maximal exercise effort from the patient, although several important parameters can also be obtained during submaximal exercise (e.g. ventilatory threshold).

Maximal oxygen uptake

Maximal oxygen uptake (VO_{2max} or VO_{2peak}) is widely recognised as the best single indicator of cardio- pulmonary function in children and adults.[12] VO_{2peak} is the highest possible oxygen consumption a patient can attain for a specific type of exercise.[12] The VO_2 plateau theory originates from A.V. Hill and coworkers.[13] This theory proposes that oxygen uptake reaches a finite value during exhaustive aerobic exercise: a point at which, despite further increases in exercise intensity, there is no further increase in oxygen uptake. This levelling-off in oxygen uptake can be graphically defined by an asymptotic curve, thus giving exercise physiologists a clear indication of maximal cardiopulmonary exertion, a plateau in oxygen uptake.[14] However, with up to 50% of children not reaching a levelling-off in oxygen uptake, the use of a plateau in oxygen uptake as a marker of maximal exertion is not supported in children and the term peak oxygen uptake (VO_{2peak}) is thought to be more appropriate.[15,16]
Many factors influence VO_{2peak}. The VO_{2peak} can be described using the Fick equation[17] in which the oxygen uptake of exercising muscle reflects the product of oxygen delivery by cardiac output and its cellular extraction as indicated by the difference in arterial and venous content:

$$VO_{2peak} = SV_{max} \times HR_{max} \times (CaO_2 - CvO_2)$$

in which the cardiac output is a product of heart rate (HR) and stroke volume (SV), and the arterial-venous oxygen difference is the difference in oxygen content of arterial (CaO_2) and mixed-venous blood (CvO_2). Dynamic changes in one of these parameters related to exercise, therefore, might influence the maximal amount of oxygen uptake during exercise.

Measuring aerobic capacity

VO_{2peak} is the reflection of the maximal oxygen flux through the lungs, transported by the circulation to the mitochondria of the exercising muscle. Based on the Fick principle (as

described above), VO_{2peak} is the product of cardiac output and the mixed arterio-venous oxygen difference.[17] Thus VO_{2peak} is dependent on cardiac function and the ability of the muscles to extract (utilise) oxygen from the circulation. In healthy subjects, the cardiac output increases linearly with oxygen uptake, such that for every 1 L/min increase in oxygen uptake, cardiac output increases by about 5 to 6 L/min.[19] In order to increase the VO_2, and therefore also VO_{2peak}, either the cardiac output or the arterial- venous oxygen difference must rise.

The gold standard for determining absolute VO_{2peak} in an individual is by metabolic measurement system analysis of O_2 and CO_2 concentrations in expired air at regular intervals and attainment of a plateau of VO_2 during increasing workloads.[20] However, in many subjects, including children, a plateau in VO_2 is not observed.[15] Several secondary parameters have therefore been established to determine VO_{2peak} without a VO_2 plateau. These parameters include:[21]

a. *subjective criteria*: Signs of intense effort (unsteady walking, running or biking; sweating; facial flushing; clear unwillingness to continue despite encouragement) and
b. *objective criteria*: HR_{peak} >180/minute and/or RER_{peak} >0.99.[22]

Reported values of VO_{2peak} are approximately 38±7 ml/min/kg for 6- to 11-year-old healthy girls and 34±4 ml/kg/min for healthy girls >11 years. In healthy boys, a value of 42±6 ml/kg/min is found before the age of 13, and 50±8 ml/kg/min thereafter.[23]

Because VO_{2peak} is strongly biased by body weight, it is usually expressed as VO_{2peak} per millilitre per minute per kilogram body mass.[20,24] This procedure, however, underestimates the fitness of overweight and obese subjects.[25] Moreover, VO_{2peak}/kg body mass also underestimates the VO_{2peak} of taller subjects.[26] Therefore, several other fractional-power relationships have been suggested such as per kg 0.66, kg 0.75 or kg 0.87.[27,28] Adjusting bodyweight according to these formulas allows a more accurate estimation of an individual's VO_{2peak} than when expressed as VO_{2peak}/kg; however, the optimal scaling power for children is unclear.

The mode of exercise testing and the age and gender of the subject determine oxygen uptake with exercise testing. In general, the highest oxygen uptake is achieved with the type of exercise that uses the greatest amount of muscle mass. In normal subjects, the highest VO_{2peak} is obtained with treadmill testing due to the quantity of the muscle mass involved, followed by bicycle testing. VO_{2peak} achieved by bicycle testing is reported to be 5 to 15% lower than with treadmill testing in normal subjects.[29,30] Predicted VO_{2peak} in ml/kg/min estimated from arm exercise testing is 60 to 70% of leg exercise in normal subjects. The intra-arterial blood pressure during arm exercise is higher than in leg exercise at given oxygen uptake or cardiac output and the submaximal HR is also higher. The consequence is a heavier load on the heart.[31] For completely untrained subjects, older subjects, or those whose cardiac status is unclear, this mode of exercise testing is not recommended. Normal females reach 65 to 75% of male VO_{2peak}.[24] The lower oxygen uptake capacity in women may be connected with their lower haemoglobin concentration and higher body fat content. Per kilogram lean body mass, VO_{2peak} is not significantly different between men and women.

Heart rate

HR is mainly determined by both cardiac autonomic nervous activity and sinus nodal function. Dynamic change to some extent reflects the state of the cardiac autonomic nervous system.[32]

HR_{peak} normally increases with exercise, varying according to age and sex. Highly conditioned athletes may have a delayed increase in HR, while decondi- tioned persons or patients with cardiac dysfunction may have a more rapid than normal HR response.[1]

The HR at rest and both submaximal and maximal exercise are higher in young subjects compared with adults. Although the HR at rest and the HR at a given workload progressively decreases as a child grows, HR_{peak} does not change. HR at exhaustion in a progressive test remains stable for both boys and girls during the growing years, and does not begin to decline until about the age of 16 years. Consequently, formulae for estimating HR_{peak} (e.g. 220 – age) are inappropriate for children and young adolescents. The maximal achievable HR during exhaustive exercise has been used extensively as a marker of exertion in normal children,[33] and depends on testing modality and protocol. During treadmill running the HR_{peak} is typically 200 beats/min, whereas walking or cycling protocols usually elicit a HR_{peak} of approximately 195 beats/min. However, it should be recognised that wide inter-individual variability exists in such values, and HR_{peak} of 185 to 225 beats/min are consistent with exhaustive exercise efforts in individual subjects, making adherence to rigorous criterion values unadvisable. The potential difficulties of using HR_{peak} as an indicator of maximum exertion are made more acute in children with CHD. The HR response in this population varies considerably, depending on the particular defect, largely as a result of chronotropic incompetence.[33]

Recently the use of HR recovery after maximal exercise has emerged. It has been described that attenuated HR recovery is a risk factor for cardio- vascular disease in adults.[34] One-minute HR recovery after exercise is attenuated with age in children. It was found that children with higher BMI, particularly those who are overweight, and those with lower endurance capacity, have slower HR recovery.[34] Moreover, Singh *et al*. reported a significant improvement in HR recovery after maximal exercise in children with CHD following a 12-week cardiac rehabilitation programme.[35]

Cardiac output

Cardiac output is the product of HR and stroke volume (SV). Since maximal HR during childhood is independent of age and gender, maximal HR can be dismissed as a defining determinant of the increase of cardiac output with age in healthy children. The increase of cardiac output in healthy children is entirely due to maximal SV, which increases in parallel with growth of the left ventricle.[11] The maximal SV during exercise shows a clear difference between children and adults; children show a smaller SV during maximal exercise.[36] It is known that stroke volume rises progressively in the initial phase of upright exercise up to moderate submaximal intensities (± 40-50% of VO_{2peak}) and then plateaus as exercise intensity increases.[31] The further increase in cardiac output with increasing exercise intensity is regulated by the HR. In children with a CHD, the cardiac output might be reduced by a reduction in HRpeak and/or a reduction in SV (e.g. children with a Fontan type circulation or tetralogy of Fallot).

There are several acceptable noninvasive methods to measure cardiac output and SV in children: indirect Fick, acetylene rebreathing, electrical bioimpedance, and Doppler ultrasound.[37]

Oxygen (O_2/HR) pulse

The O_2 pulse is the amount of oxygen consumed per heartbeat (O_2/HR). A reduced submaximal oxygen pulse may indicate reduced oxygen extraction at the cellular level (reduced arteriovenous difference) or simply a lower SV (O_2/HR= SV x (CaO_2 – CvO_2). Oxygen pulse has been used as an indicator for cardiac output assessment when testing children with CHD.[33] The O_2 pulse has a decreased rise during exercise in conditions that reduce SV or that decrease arterial oxygen content, such as anaemia or hypoxaemia.[1]

Oxygen uptake efficiency slope

The oxygen uptake efficiency slope (OUES) represents the rate of increase of VO_2 in response to a given VE during incremental exercise, indicating how effectively oxygen is extracted and taken into the body.[38] OUES was originally developed by Baba *et al*. for children with CHD.[39] OUES is determined from the linear relation of VO2 (y-axis) *vs*. the logarithm of minute ventilation (VE) (x-axis) during exercise, i.e. VO_2 = a $\log^{10}$ VE + b, where a is the OUES and b is the intercept.[38] The logarithmic transformation of VE is aimed at linearising the otherwise curvilinear relation of VO_2 vs. VE, so making the OUES theoretically independent of the patient-achieved effort level.

OUES is influenced by both the metabolic acidosis and the physiological pulmonary dead space.[39] The OUES is a variable that indicates the status of both systemic and pulmonary perfusion, and which explains the high correlation with VO_{2peak}. The advantage of the OUES is that it can be calculated from submaximal exercise test data and is therefore effort-independent.[39] In healthy children the OUES increases from 1132±149 ml/min/logL in 7-year-old subjects to 2726±602 ml/min/logL in 18-year-old subjects, which shows that the results are influenced by development in children.[40]

Work efficiency

Work efficiency ($\Delta VO_2/\Delta WR$) is a measure of the metabolic cost of performing external work. $\Delta VO_2/\Delta WR$ is calculated using the slope of the relationship between oxygen uptake and work rate during incremental exercise. The $\Delta VO_2/\Delta WR$ slope has remarkable linearity and is explained by the rigid physiological coupling of these parameters, especially below the ventilatory threshold (VT). In healthy subjects the relationship remains linear above the VT, while in children with CHD the relationship can be lowered above the VT, due to reduced oxygen delivery to working muscle.[41] Paradoxically, a lower slope might be taken to indicate better work efficiency; however a shallow slope is considered abnormal.

In adults the $\Delta VO_2/\Delta WR$ is frequently reported,[42] and a normal value of 10.3±1 ml O_2/Watt is reported for healthy subjects.[43] In children, however, less data are available. In children with a coarctation of the aorta, a significantly reduced value is reported compared with healthy subjects.[44]

Blood oxygen saturation

An important parameter to measure in children with CHD during exercise is arterial blood oxygen saturation (SaO_2%). Using a transcutaneous saturation measurement, SaO_2% can be estimated noninvasively. This value gives an estimate of the arterial and venous blood mixing in the heart. CHD with a right-to-left shunt in the heart (e.g. tetralogy of Fallot) are causing reduced SaO_2% at rest but sometimes further decreasing during maximal exercise. Usually a drop in SaO_2% of >4% during exercise is considered abnormal.[45]

Blood pressure response

Blood pressures at rest and during exercise are lower in children compared with adults.[46] At maximal exercise, a child with a body surface area (BSA) of 1.25 m^2 demonstrates a systolic blood pressure of about 140 mmHg, whereas 160 mmHg is expected in a subject with a BSA of 1.75 m^2.

Maintaining proper perfusion pressure is a crucial and major role of the circulation. Several mechanisms are needed during exercise, or in the setting of the failing heart, to maintain adequate pressures of perfusion.[32] Systolic blood pressure should show a progressive increase during exercise and a progressive decline after exercise. A decrease in systolic pressure or a failure to increase systolic pressure is abnormal and may indicate clinically significant left ventricular dysfunction.[1] Diastolic blood pressure should remain stable or decrease with exercise.[1] The level of pressure maintained by arterial baroreflex mechanisms is set at a higher level during exercise. The rapid increase in HR following withdrawal of parasympathetic nervous activity is a major means of attaining adequate cardiac output to achieve the initial target for arterial blood pressure at the beginning of exercise, while metabolic reflexes from working muscle and vasoconstrictive mechanisms are additional stimuli involved in achieving higher arterial blood pressure during moderate to severe exercise.[47] An impaired response in terms of the level of blood pressure, therefore, indicates an abnormal function of these regulators.

Ventilatory indexes

Respiratory exchange ratio

The respiratory exchange ratio (RER) is a useful variable, both as a marker of effort and as an indicator of the contribution of anaerobic metabolism.[33] RER is the ratio of CO_2 exhaled to the O_2 uptake per unit time. It is usually around 0.7-0.8 at rest. RER reflects both tissue level exchange of gasses (measured by the respiratory quotient or RQ) and transient changes in O_2 and CO_2.[1] For normal children, RER values at VO_{2peak} reported during cycle ergometry generally range from 1.0 to 1.10.[48]

Ventilatory threshold

The ventilatory threshold (VT) has traditionally been considered to be the point at which oxygen supply no longer meets the oxygen demands of the working muscle and the increasing contribution from anaerobic metabolism is reflected by a rapidly rising blood lactate level.[33] The VT is the level of oxygen uptake above which anaerobic metabolism supplements aerobic energy consumption.

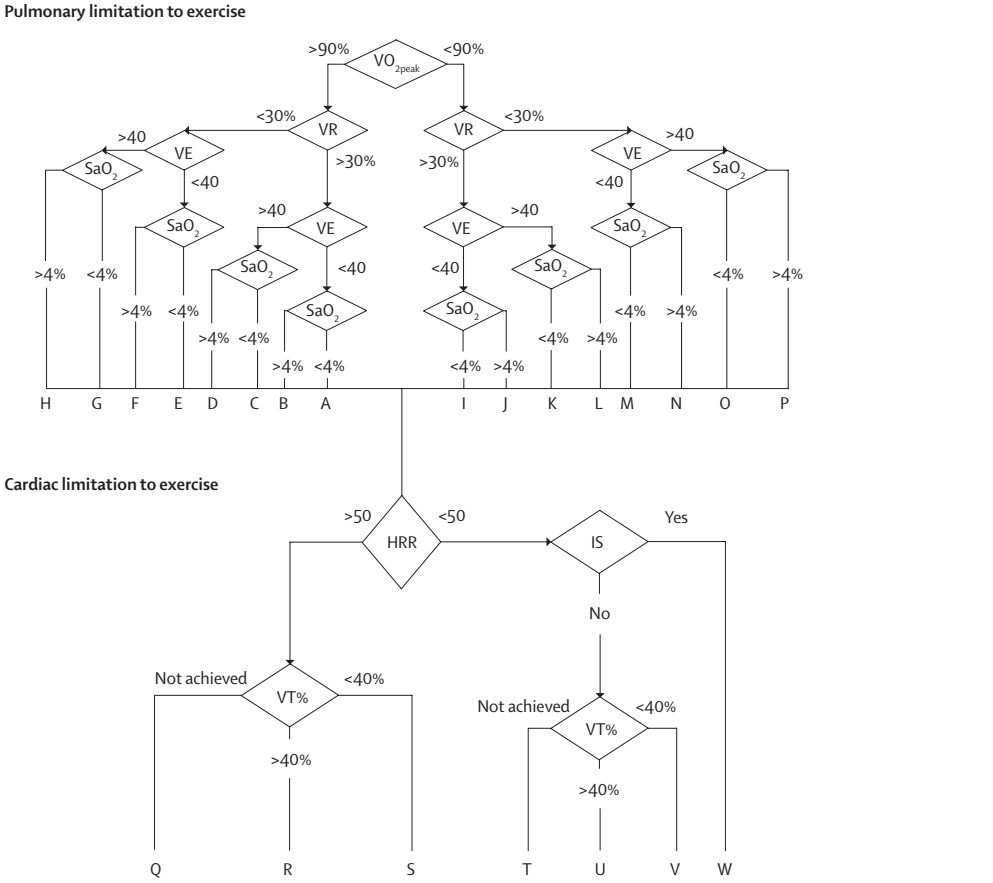

***Figure 1*: Algorithm for interpretation of CPET data in adults.** For an explanation of the interpretation see tables 3 and 4. Modified from Eschenbacher and Mannina.[45] VE, Ventilator equivalent for carbon dioxide; SaO_2, change in arterial saturation; IS, Ischemic Symptoms; HRR, Heart Rate Response; VT%, Ratio of VT to predicted VO_{2peak}.

This is characterised by an increase in CO_2 production above that of aerobic metabolism. Graphically this appears as an abrupt increase in the slope of CO_2 production during exercise.[1] Usually, the VT occurs at an exercise intensity between 40 and 70% of VO_{2peak} in healthy children.[23] A variety of gas-exchange criteria have been used, including an abrupt increase in ventilation (VE), in ventilatory equivalent for oxygen (VE/VO_2), in the RER or the end-tidal pressure of oxygen ($P_{ET}O_2$). These increases must be accompanied by a lack of increase in the ventilatory equivalent for carbon dioxide (VE/VCO_2) or the end-tidal pressure of carbon dioxide ($P_{ET}CO_2$).[33] Reybrouck *et al.* found that, irrespective of the type of heart defect, the VT was always below the normal value in children with CHD.[49] The lowest values were recorded in patients after the Fontan operation (62±10% of the normal value).[49]

Pulmonary limitation to exercise

A. No pulmonary limitation or decreased effort or cardiac limitation
B. Mild diffusion type limitation
C. Mild gas exchange abnormality
D. Mild gas exchange abnormality and diffusion-type limitation
E. Mild ventilatory mechanical limitation
F. Mild ventilatory mechanical limitation and diffusion-type limitation
G. Mild ventilatory mechanical limitation and gas exchange abnormality
H. Mild ventilatory mechanical limitation and gas exchange abnormality and diffusion-type limitation
I. Decreased effort or cardiac limitation
J. Moderate or severe diffusion-type limitation
K. Moderate or severe gas exchange abnormality
L. Moderate or severe gas exchange abnormality and diffusion-type limitation
M. Moderate or severe ventilatory mechanical limitation
N. Moderate or severe ventilatory mechanical limitation and diffusion-type limitation
O. Moderate or severe ventilatory mechanical limitation and gas exchange abnormality
P. Moderate or severe ventilatory mechanical limitation and gas exchange abnormality and diffusion type limitation

Cardiac or circulatory limitation to exercise

Q. Moderate or severe cardiac 'pump' limitation (cardiomyopathy, deconditioning)
R. Cardiac pump limitation (cardiomyopathy, deconditioning)
S. Cardiac pump limitation and circulatory limitation (pulmonary vascular or peripheral vascular disease, or pump limitation
T. Moderate or severe pulmonary limitation (see J through P) or poor effort
U. No obvious cardiac or circulatory limitation
V. Circulatory limitation (pulmonary vascular or peripheral vascular disease or pump limitation
W. Ischaemic heart disease

***Table 3*: Interpretive results using the algorithm**. Modified from Eschenbacher and Maninna.[45]

Ventilatory equivalents

The ventilatory equivalent for oxygen (VE/VO_2) is the amount of ventilation needed for the uptake of a given amount of oxygen. It is an index of ventilatory efficiency and is increased in patients with congestive heart failure due to an increase in physiological dead space (large ventilation/perfusion mismatch).

The ventilatory equivalent for carbon dioxide (VE/VCO_2) is the amount of ventilation needed for the elimination of a given amount of carbon dioxide produced by the metabolising tissues. It reflects dead space ventilation, CO_2 production, and PCO_2, and is higher than normal in heart failure.[1]

Parameter	Cut-off point
VO_{2max} (%)	<90% of predicted VO_{2peak}
VE/VCO_{2peak}	>36
HR response	>(-6.25 x age) + 150
VT (%)	<44 % of predicted VO_{2peak}

***Table 4*: Cut-off points in Eschenbacher and Maninna's algorithm[45] modified for healthy children.** Values for children from De Groot *et al*.[50]

Algorithm for interpretation

A tool facilitating the interpretation of the CPET data is the algorithm as described by Eschenbacher and Mannina.[45] This algorithm uses cut-off points regarding standard outcomes from exercise testing to make a distinction between cardiac, pulmonary or 'other' limitations such as deconditioning or musculoskeletal limitations to explain maximal exercise capacity. The following parameters are used in the algorithm: VO_{2peak}, VCO_{2peak}, VE_{peak}, VE_{peak}/VO_{2peak}, VE_{peak}/VCO_{2peak}, HR response (HRR; = $(HR_{peak} - HR_{rest})/VO_{2peak} - VO_{2rest}$), and ventilatory threshold (VT) as percentage of predicted VO_{2peak}. The interpretation of the algorithm can be found in figure 1 and in table 3.

We have modified the cut-off values for adults with values for healthy children.[50] These results are displayed in table 4. Although the algorithm needs further validation in children, it can be helpful for the interpretation of CPET data in children with CHD.

Conclusion

In this article we have reviewed the main indications for cardiopulmonary exercise testing in children with congenital heart disease, the contraindications for exercise testing and the indications for terminating an exercise test. Moreover, we have addressed the interpretation of gas exchange data from cardiopulmonary exercise testing in children with congenital heart disease. The growing body of research information surrounding these issues has identified a number of biological responses to exercise that are unique to physically immature individuals. These have provided evidence that, physiologically, children are not simply small adults. It is important that these features be considered when performing clinical exercise testing in children as well as while designing exercise programmes for young subjects.

Acknowledgement

We thank Professor Emeritus David A. de Wolf for his valuable comments on our manuscript.

References

1. Connuck DM. The role of exercise stress testing in pediatric patients with heart disease. Pediatr Cardiol 2005; 20: 45-52.
2. Bar-Or O. Pathophysiological factors which limit the exercise capacity of the sick child. Med Sci Sports Exerc 1986; 18: 276-82.
3. Lunt D, Briffa T, Briffa NK, Ramsay J. Physical activity levels of adolescents with congenital heart disease. Aust J Physiother 2003; 49: 43-50.
4. Rich MW. Heart failure disease management: a critical review. J Card Fail 1999; 5: 64-75.
5. Alpert BS, Verrill DE, Flood NL, Boineau JP, Strong WB. Com- plications of ergometer exercise in children. Pediatr Cardiol 1983; 4: 91-6.
6. Stephens P Jr, Paridon SM. Exercise testing in pediatrics. Pediatr Clin North Am 2004; 51: 1569-87, viii.
7. Rodgers GP, Ayanian JZ, Balady G, et al. American College of Cardiology/American Heart Association Clinical Competence Statement on Stress Testing. A Report of the American College of Cardiology/American Heart Association/American College of Physicians-American Society of Internal Medicine Task Force on Clinical Competence. Circulation 2000; 102: 1726-38.
8. Pelliccia A, Fagard R, Bjornstad HH, et al. Recommendations for competitive sports participation in athletes with cardiovascular disease: a consensus docu- ment from the Study Group of Sports Cardiology of the Working Group of Cardiac Rehabilitation and Exercise Physiology and the Working Group of Myocardial and Pericardial Diseases of the European Society of Cardiology. Eur Heart J 2005; 26: 1422-45.
9. Taylor CB, Bandura A, Ewart CK, et al. Exercise testing to enhance wives' confidence in their husbands' cardiac capability soon after clinically uncomplicated acute myocardial infarction. Am J Cardiol 1985; 55: 635-8.
10. Moalla W, Gauthier R, Maingourd Y, Ahmaidi S. Six-minute walking test to assess exercise tolerance and cardiorespiratory responses during training program in children with congenital heart disease. Int J Sports Med 2005; 26: 756-62.
11. Bar-Or O. Pediatric sports medicine for the practitioner. New York: Springer-Verlag; 1983.
12. Shephard RJ, Allen C, Benade AJ, et al. The maximum oxygen intake. An international reference standard of cardiorespiratory fitness. Bull World Health Organ 1968; 38: 757-64.
13. Hill AV, Lupton H. Muscular exercise, lactic acid and the supply and utilization of oxygen. Q J Med 1923; 16: 135-71.
14. Howley ET, Bassett DRJ, Welch HG. Criteria for maximal oxygen uptake: review and commentary. Med Sci Sports Exerc 1995; 27: 1292-301.
15. Rowland TW. Does peak VO_2 reflect VO_{2max} in children? Evidence from supramaximal testing. Med Sci Sports Exerc 1993; 25: 689-93.
16. Armstrong N, Welsman J, Winsley R. Is peak VO_2 a maximal index of children's aerobic fitness? Int J Sports Med 1996; 17: 356-9.
17. Fick A. Ueber die Messung des Blutquantums in den Herzventrikeln. Sitx Physik-Med Ges Wurzburg 1870; 2: 16.
18. Shephard RJ, Allen C, Benade AJ, et al. The maximum oxygen intake. An international reference standard of cardiorespiratory fitness. Bull World Health Organ 1968; 38: 757-64.
19. Haller RG, Lewis SF, Cook JD, Blomqvist CG. Hyperkinetic circulation during exercise in neuromuscular disease. Neurology 1983; 33: 1283-7.
20. Taylor HL, Buskirk E, Henschel A. Maximal oxygen intake as an objective measure of cardiorespiratory performance. J Appl Physiol 1955; 8: 73-80.
21. Franklin BA. Abnormal cardiorespiratory responses to acute aerobic exercise. In: Roitman JL, editor. ACSM's resource manual for guidelines for exercise testing and prescription. Third edition. Baltimore: Williams and Wilkins; 1998. p. 146-55.
22. Rowland TW. Aerobic exercise testing protocols. In: Rowland TW, editor. Pediatric Laboratory Exercise Testing: Clinical Guidelines. Champaign,Ill: Human Kinetics;1993. p. 19-41.
23. Cooper DM, Weiler-Ravell D, Whipp BJ, Wasserman K. Aerobic parameters of exercise as a function of body size during growth in children. J Appl Physiol 1984; 56: 628-34.
24. Astrand PO. Experimental studies of physical work capacity in relation to sex and age: Copenhagen, Munkgaard; 1952.
25. Owens S, Gutin B. Exercise testing of the child with obesity. Pediatr Cardiol 1999; 20: 79-83.
26. Tanner JM. Fallacy of per weight and per surface area standards and their relation to spurius correlation. J Appl Physiol 1949; 2: 1-15.
27. Schmidt-Nielsen K. Scaling: Why is animal size so important? Cambridge: Cambridge University Press; 1984.
28. Weibel ER, Hoppeler H. Exercise-induced maximal metabolic rate scales with muscle aerobic capacity. J Exp Biol 2005; 208: 1635-44.
29. Hermansen L, Ekblom B, Saltin B. Cardiac output during sub-maximal and maximal treadmill and bicycle exercise. J Appl Physiol 1970; 29: 82-6.
30. Hermansen L, Saltin B. Oxygen uptake during maximal treadmill and bicycle exercise. J Appl Physiol 1969; 26: 31-7.
31. Astrand P, Rodahl K, Astrand PRK. Textbook of work physiology, physiological bases of exercise. New York: McGraw-Hill Book Company; 1986.
32. Ohuchi H. Cardiopulmonary response to exercise in patients with the Fontan circulation. Cardiol Young 2005; 15 Suppl 3: 39-44.

33. McManus A, Leung M. Maximising the clinical use of exercise gaseous exchange testing in children with repaired cyanotic congenital heart defects: the development of an appropriate test strategy. Sports Med 2000; 29: 229-44.
34. Singh TP, Rhodes J, Gauvreau K. Determinants of heart rate recovery following exercise in children. Med Sci Sports Exerc 2008; 40: 601-5.
35. Singh TP, Curran TJ, Rhodes J. Cardiac rehabilitation improves heart rate recovery following peak exercise in children with repaired congenital heart disease. Pediatr Cardiol 2007; 28: 276-9.
36. Godfrey S. Exercise testing in children. London: W.B. Saunders Company Ltd.; 1974.
37. Driscoll DJ, Staats BA, Beck KC. Measurement of Cardiac Output in Children During Exercise: A Review. Pediatr Exerc Sci 1989; 1: 102-15.
38. Baba R, Nagashima M, Nagano Y, et al. Role of the oxygen uptake efficiency slope in evaluating exercise tolerance. Arch Dis Child 1999; 81: 73-5.
39. Baba R, Nagashima M, Goto M, et al. Oxygen uptake efficiency slope: a new index of cardio-respiratory functional reserve derived from the relation between oxygen uptake and minute ventilation during incremental exercise. J Am Coll Cardiol 1996; 28: 1567-72.
40. Marinov B, Mandadzhieva S, Kostianev S. Oxygen-uptake efficiency slope in healthy 7- to 18-year-old children. Pediatr Exerc Sci 2007; 19: 159-70.
41. Groen WG, Hulzebos EH, Helders PJ, Takken T. Oxygen uptake to work rate relationship during exercise in children with lung, heart or muscle Disease. Med Sci Sports Exerc 2009; 41: S5, Abstract 1658.
42. Hansen JE, Sue DY, Oren A, Wasserman K. Relation of oxygen uptake to work rate in normal men and men with circulatory disorders. Am J Cardiol 1987; 59: 669-74.
43. Wasserman K, Hansen JE, Sue DY, Casaburi R, Whipp BJ. Principles of Exercise Testing and Interpretation. Baltimore, MD: Lippincott, Williams and Wilkins; 1999.
44. Rhodes J, Geggel RL, Marx GR, et al. Excessive anaerobic metabolism during exercise after repair of aortic coarctation. J Pediatr 1997;131:210-4.
45. Eschenbacher WL, Mannina A. An algorithm for the interpretation of cardiopulmonary exercise tests. Chest 1990; 97: 263-7.
46. Riopel DA, Taylor AB, Hohn AR. Blood pressure, heart rate, pressure-rate product and electrocardiographic changes in healthy children during treadmill exercise. Am J Cardiol 1979; 44: 697- 704.
47. Rowell LB, O'Leary DS. Reflex control of the circulation during exercise: chemoreflexes and mechanoreflexes. J Appl Physiol 1990; 69:407-18.
48. Turley KR, Wilmore JH. Cardiovascular responses to treadmill and cycle ergometer exercise in children and adults. J Appl Physiol 1997; 83: 948-57.
49. Reybrouck T, Rogers R, Weymans M, et al. Serial cardiorespiratory exercise testing in patients with congenital heart disease. Eur J Pediatr 1995; 154: 801-6.
50. De Groot JF, Takken T, Schoenmakers MA, et al. Limiting factors in peak oxygen uptake and the relationship with functional ambulation in ambulating children with Spina Bifida. Eur J Appl Physiol 2008; 104: 657-65.

CHAPTER 2

PART III

Exercise capacity in children with isolated congenital complete atrioventricular block: does pacing make a difference?

Exercise capacity in children with isolated congenital complete atrioventricular block: does pacing make a difference?

A.C. Blank, S Hakim, J.L. Strengers, R.B. Tanke, T.A. van Veen, M.A. Vos, T. Takken

***Pediatr Cardiol** 2012 ; 33: 576-85*

Department of Paediatric Cardiology, Wilhelmina Children's Hospital, University Medical Center Utrecht (UMCU), Utrecht, the Netherlands
AC Blank
JL Strengers

Division of Heart and Lungs, Department of Medical Physiology, UMCU, Utrecht, the Netherlands
S Hakim
TA van Veen
MA Vos

Department of Paediatric Cardiology, Radboud University Medical Center, Nijmegen, the Netherlands
RB Tanke

Child Development and Exercise Center, Wilhelmina Children's Hospital, UMCU, Utrecht, the Netherlands
T Takken

Abstract

The management of patients with isolated congenital complete atrioventricular block (CCAVB) has changed during the last decades. The current policy is to pace the majority of patients based on a variety of criteria, among which is limited exercise capacity. Data regarding exercise capacity in this population stems from previous publications reporting small case series of unpaced patients. Therefore, we have investigated the exercise capacity of a group of contemporary children with CCAVB. Sixteen children (mean age 11.5 ± 4; seven boys, nine girls) with CCAVB were tested. In 13 patients, a median number of three pacemakers were implanted, whereas in three patients no pacemaker was given. All patients had an echocardiogram and completed a cardiopulmonary cycle exercise test. Exercise parameters were determined and compared with reference values obtained from healthy Dutch peers. The peak oxygen uptake/body mass was reduced to 34.4 ± 9.5 ml kg^{-1} min^{-1} (79 ± 24% of predicted) and the ventilatory threshold was reduced to 52 ± 17% of peak oxygen uptake (78 ± 21% of predicted), whereas the peak work load/body mass was 2.8 ± 0.6 W/kg (91 ± 24% of predicted), which was similar to controls. Importantly, 25% of the paced patients showed upper rate restriction by the pacemaker. In conclusion, children with CCAVB show a reduced peak oxygen uptake and ventilatory threshold, whereas they show normal peak work rates. This indicates that they generate more energy during exercise from anaerobic energy sources. Paced children with CCAVB do not perform better than unpaced children.

Introduction

Isolated congenital complete atrioventricular block (CCAVB) is a rare cardiac disorder with an estimated incidence of 1/15,000–20,000 live births.[27] In most cases it occurs after damage of a normally structured fetal heart by maternal autoantibodies against ribonucleoproteins (anti-Ro/SSA, anti-La/SSB).[24] Along with the congenital antibody-associated AV block, a variety of congenital forms of AV block occur secondary to other congenital cardiac defects.[25]

Management of patients with CCAVB has changed during the last decennia. In the past, a minority of patients received a pacemaker whereas the current policy is to pace the majority of patients based on a variety of criteria, among which is limited exercise capacity.[10] Exercise capacity provides relevant information about the health status and the ability to perform age-appropriate activities. Furthermore, it is a known predictor of mortality in both healthy and diseased individuals, including patients with congenital heart disease.[8,9,14,15] Data regarding exercise capacity in CCAVB stems from decades-old publications reporting small case series of unpaced patients.[31,32] Although the current policy is to pace patients, it is unknown whether exercise capacity benefits from this approach. Therefore, the aim of this cross-sectional study was to investigate the cardiopulmonary exercise capacity of a group of contemporary children with CCAVB with and without pacemaker.

Methods

Study population

The databases of the two participating departments of pediatric cardiology (Utrecht and Nijmegen) were screened to identify all patients [>5 years old with isolated CCAVB, which was classified as congenital if (1) CAVB was diagnosed in utero, at birth, or within the neonatal period (0 to 27 days after birth) as proposed by Brucato *et al.*[6] or (2) CAVB was diagnosed in early childhood without signs and findings of a specific etiology (as described by Yater *et al.*[46]). The diagnosis ''isolated CCAVB'' required the absence of major structural heart defects. Eighteen patients were identified, and 16 of them consented to participate in the study. The medical records of those participating patients were reviewed. Data collected included patient age at diagnosis, maternal antibody status, patient age at first pacemaker implantation, all pacemaker-related interventions, and patient status at follow-up.

Fitness questionnaire

To obtain information on self-perceived fitness and health, physical activity in daily life, including sports, participation at school, and leisure, a questionnaire[4,11] from the Department of Integrative Physiology, St. Radboud University Nijmegen Medical Centre, Nijmegen, The Netherlands, was used. The results were compared with those from healthy control subjects.[11]

Anthropometry

Before the cardiopulmonary exercise test (CPET), anthropometric measurements were completed in all patients, including body mass (BM [kg]) and body height (m) using

an electronic scale (Seca, Hamburg, Germany) and a stadiometer (Ulmer Stadiometer, Ulm, Germany), respectively. Body mass index (BMI [kg m^{-2}]) was calculated as BM in kg divided by the square of the body height in meters. SD scores were calculated for BM for age, body height for age and BMI for age using reference values from the 1997 Dutch Growth Study.[12,13] To estimate body surface area (BSA [m^2]), the equation of Haycock *et al.* was used[19], which has been validated in infants, children, and adults.

Echocardiography

Before CPET all patients underwent transthoracic echocardiography, which was performed by the same pediatric cardiologist (A. C. B.) with the patient at rest in supine position using a Vivid 7 machine (GE Vingmed Ultrasound AS, Horten, Norway). Images were obtained using a 3.5- or 5.0-MHz transducer in the suprasternal, parasternal, and apical views. Cine-loops, including three cardiac cycles, were stored digitally and analyzed off-line using EchoPac version 7.0.0 software (GE Healthcare, Horten, Norway). After a brief assessment of the cardiac anatomy, the following measurements were performed: M-mode; pulsed-wave (PW) Doppler of the aortic, pulmonic, mitral, and tricuspid valves and descending aorta; PW tissue Doppler imaging (TDI) of the interventricular septum and left free wall; and color-coded TDI of the left ventricle.

Assessment of left-ventricular size and function

Parasternal M-mode images were used to measure left- ventricular (LV) end-diastolic (LVEDD) and end-systolic diameters (LVESD). The LVEDD was compared with the normal values of body weight-matched children[26] and expressed as percentage of normal. LV dilatation was defined as LVEDD ≥120% of normal. Color-coded TDI of the left ventricle in the apical four- chamber view was used to measure the peak systolic and diastolic tissue velocity of the septal and lateral mitral valve (MV) annulus. The velocities were compared with values obtained in a group of healthy young individuals.[17] Abnormal LV function was defined as measured systolic and/or diastolic velocities <1 SD of the mean velocities of healthy young individuals.[17]

Assessment of dyssynchrony

Two types of dyssynchrony were assessed: interventricular dyssynchrony and intraventricular dyssynchrony of the left ventricle. Interventricular dyssynchrony was examined by calculating the interventricular mechanical delay (IVMD) using PW Doppler measurements in the left-ventricular (LVOT) and right-ventricular outflow tracts (RVOT) according to the following formula: (time from the onset of QRS to the onset of PW curve in the LVOT)—(time from the onset of QRS to the onset of PW curve in the RVOT). Interventricular dyssynchrony was defined as being present if IVMD >40 ms. Intraventricular dyssynchrony of the left ventricle was assessed by analyzing color-coded TDI of the left ventricle in the apical four-chamber view according to the recommendations of the American Society of Echocardiography Dyssynchrony Writing Group.[18] Intraventricular dyssynchrony was defined as being present if the septal-to-lateral wall delay of the left ventricle was >65 ms.

CPET

Subjects performed a CPET using an electronically braked cycle ergometer (Ergoline 9000; Ergoline GmbH, Bitz, Germany) as recently described.[5] In short, patients performed a CPET according to the Godfrey protocol.[16] The end of the CPET was marked by symptom limitation. A 12-lead electrocardiogram (ECG) and pulse oximetry (Nellcor 200E; Nellcor, Breda, The Netherlands) were recorded continuously throughout the entire test. Blood pressure was measured every 2 min (SunTech Tango+; SunTech Medical, Morrisville, NC, USA).[36] The CPET featured a breath-by- breath gas-exchange analysis using a calibrated expiratory gas analysis system (Oxycon Pro; Cardinal, Houten, The Netherlands). Peak values were defined as the highest mean value of any 30 s time interval during exercise. Predicted values were obtained from established values from age- and sex-matched Dutch controls.[38]

Ventilatory threshold (VT)

The VT was determined using the criteria of an increase in both the ventilatory equivalent of oxygen (VE/VO_2) and end-tidal pressure of oxygen ($P_{ET}O_2$) with no increase in the ventilatory equivalent of carbon dioxide (VE/VCO_2).[7,44] $P_{ET}O_2$ and $P_{ET}CO_2$ were taken into account to differentiate lactate buffering from hyperventilation. This method has been validated in pediatric patients.[30] VT was expressed as a percentage of predicted VO_{2peak}.[35] Predicted values were obtained from established values from age- and sex-matched Dutch controls.[38]

VE/VCO_2-slope and oxygen uptake efficiency slope (OUES)

The VE/VCO_2-slope was calculated by linear least-squares regression of the relation between VE and VCO2, respectively, during the entire CPET.[38] The OUES was calculated by a linear least-squares regression of the VO_2 on the common logarithm of the VE, by using the following equation:

$$VO_2 = a \log VE + b.^1$$

In this equation, the constant ''a'' stands for the regression coefficient (called the OUES), and ''b'' represents the intercept. Predicted VE/VCO_2-slope and OUES values were obtained from established values of age- and sex- matched Dutch controls.[38]

Analysis of CPET ECG

During CPET, an electrocardiogram (ECG) was recorded at a speed of 25 mm/s, a gain of 10 mm/mV, and muscle filter +50 Hz. Each minute, a 12-lead trace of several consecutive heartbeats was printed on paper. The traces were analyzed by the same pediatric cardiologist (A. C. B.), who measured the following parameters: rhythm, QRS morphology, QRS duration, and corrected QT interval (QTc) (in normal QRS duration) or corrected JT interval (JTc) (if QRS duration >+2SD). In addition, the presence of arrhythmic events, including pacemaker upper rate behavior (2:1 block or pseudo-Wenckebach), was assessed during exercise.

Statistical analysis

Continuous variables are presented as mean ± SD with minimum and maximum. Nominal data are summarized as frequencies and percentages. Differences between patients and reference values were tested using one-sample Student t test. Differences between the paced and unpaced group were analyzed using independent-samples Student t test, and $p < 0.05$ was considered statistically significant. Statistical analysis was performed with IBM SPSS Statistics 18 for Mac (IBM SPSS, Chicago, IL, USA).

Results

Patient characteristics

The characteristics of the 16 studied patients are listed in Table 1. Patients were diagnosed with CCAVB at a mean age of 0.2 ± 0.6 years. Maternal antibodies were detected at diagnosis in 12 patients (75%). Thirteen patients (81%) had a pacemaker implanted with a median number of three implanted pacemakers. Their first pacemaker was implanted at a mean age of 2.2 ± 4.1 years. Five patients (31%) had minor associated congenital heart defects, such as patent arterial duct (PDA = 2 patients [13%]), PDA and atrial septal defect (PDA + ASD = 1 patient [6%]), ventricular septal defect (VSD = 1 patient [6%]), or ASD and VSD (one patient [6%]). Two patients (13%) were on cardiac medication: one patient used an angiotensin-converting enzyme (ACE) inhibitor, and one patient used a combination of an ACE-inhibitor and a beta-blocker.

Self-rated fitness, health, and physical activity

The results of the questionnaire, as listed in Table 2, identified no significant difference in the self-rated fitness and health of paced and unpaced patients. The majority of CCAVB patients were always able to perform physical activities without or with minor difficulties. Most of the CCAVB patients judged their physical condition to be equal to the average of their peers.

Analysis of LV size, function, and dyssynchrony

The echocardiographic results are listed in Table 3. LVEDD of the studied patients was 110 ± 10% of normal. Three patients (19% [two paced and one unpaced]) had LV dilatation. Two patients (13% [both paced]) showed systolic and diastolic LV dysfunction. MV E velocity (0.99 ± 0.15 vs. 1.39 ± 0.08 m/s, $p = 0.001$), aortic valve (AoV) velocity (1.17 ± 0.13 vs. 1.60 ± 0.03 m/s, $p < 0.0005$), and color-coded TDI lateral MV E' velocity (-7.8 ± 1.2 vs. -10.7 ± 0.7 cm/s, $p = 0.002$) were significantly higher in unpaced patients. Eight patients (50% [all paced]) showed interventricular dyssynchrony and one patient (6% [paced]) showed intraventricular dyssynchrony.

Variable	CCAVB group N = 16	Paced group N = 13	Unpaced group N = 3
Male (%)	7 (44)		
Female (%)	9 (56)		
Age at diagnosis (year)	0.2 ± 0.6[a]		
PM (%)			
No PM	3 (19)		
PM	13 (81)		
1st		3 (23)	
2nd		4 (31)	
3rd		1 (8)	
4th		3 (23)	
5th		2 (15)	
Type of pacemaker (%)			
VVIR		3 (23)	
DDD		5 (38)	
DDDR		3 (23)	
CRT		2 (15)	
Programmed upper rate (bpm)		182 ± 11[a]	
Age at first PM implantation (year)		2.2 ± 4.1[a]	
Maternal antibodies (%)			
Negative	3 (20)		
Positive	12 (75)		
Minor associated CHD (%)			
No	11 (69)		
Yes	5 (31)		
ASD/SD	1 (6)		
VSD	1 (6)		
PDA	2 (13)		
PDA/ASD	1 (6)		

***Table 1*: Patient characteristics**. ACE-I, angiotensin-converting enzyme inhibitor; CHD, congenital heart disease; BB, beta blocker; BM, body mass; BMI, body mass index; BSA, body surface area; PM, pacemaker. [a] Data expressed as mean ± SD —*table continues on next page.*

Variable	CCAVB group N = 16	Paced group N = 13	Unpaced group N = 3
Medication (%)			
No	14 (88)		
Yes	2 (13)		
ACE-I	1 (6)		
ACE-I + BB	1 (6)		
BM (kg)	40.2 ± 16.3[a]	43.9 ± 15.6[a]	23.9 ± 6.2[a]
BM for age (SD)	-0.3 ± 0.9[a]	-0.1 ± 0.9[a]	-1.0 ± 0.4[a]
Body height (m)	1.47 ± 0.21[a]	1.52 ± 0.19[a]	1.24 ± 0.12[a]
Body height for age (SD)	-0.4 ± 0.9[a]	-0.2 ± 0.9[a]	-1.0 ± 0.7[a]
BMI (kg/m^2)	17.8 ± 3.0[a]	18.4 ± 3.0[a]	15.3 ± 0.9[a]
BMI for age (SD)	-0.1 ± 1.0[a]	0.0 ± 1.1[a]	-0.5 ± 0.1[a]
BSA (m^2)	1.26 ± 0.34[a]	1.35 ± 0.32[a]	0.90 ± 0.16[a]

***Table 1*: Patient characteristics** *—continued from previous page.*

CPET ECG

Table 3 lists the ECG results. QRS duration during the rest phase of CPET (145 ± 13 vs. 97 ± 6 ms, p <0.0005) was significantly shorter in unpaced patients. Eleven of the (RV) paced patients showed an LBBB-like QRS morphology. Two of the (cardiac resynchronization therapy [CRT]) paced patients had an indifferent QRS morphology. The JTc in paced patients was 311 ± 24 ms (normal value <350 ms). The QTc in unpaced patients was 420 ± 18 ms (normal value <440 ms). Despite of an average programmed pacemaker upper rate of 182 ± 11 bpm, four patients (25% [three DDDR (dual [atrial/ventricular] paced, dual [atrial/ventricular] sensed, dual [inhibited/triggered], rate-responsive) paced and one CRT paced]) showed upper rate behavior of their pacemaker (one pseudo-Wenckebach and three 2:1 block). No patient displayed premature ventricular beats.

CPET

Table 4 lists the CPET data. Peak HR (135 ± 37 bpm), VO_{2peak} (1.31 ± 0.50 l min^{-1} [79 ± 24% of predicted]), VO_{2peak} kg^{-1} (34.4 ± 9.5 ml kg^{-1} min^{-1} [79 ± 24% of predicted]), peak minute ventilation (50.2 ± 22.9 l min^{-1} [76 ± 26% of predicted]), and VT (52 ± 17% of VO_{2peak} [78 ± 21% of predicted]) were all significantly lower than those of healthy peers. Peak work load corrected for body mass (2.8 ± 0.6 W kg^{-1} [91 ± 24% of predicted]), peak oxygen pulse (10.4 ± 5.1 ml beat^{-1} [111 ± 56% of predicted]), peak systolic blood pressure (131 ± 24 mmHg [99 ± 12% of predicted]), VE/VCO_2-slope (33.3 ± 6.6 [108 ± 17% of predicted]), OUES (1424 ± 510 [92 ± 39% of predicted]), percentage of predicted FEV_1 (92 ± 11%), percentage of predicted forced expiratory vital capacity (FVC) (87 ± 15%), and peak SpO_2% (96 ± 2%) differed nonsignificantly from healthy peers.

Variable	CCAVB group N = 16	Paced group N = 13	Unpaced group N = 3
Self-rated health (scale 1–10)	8.3 ± 1.1[a]	8.2 ± 1.1[a]	9.0 ± 0.0[a]
Self-rated fitness (scale 1–10)	7.5 ± 1.6[a]	7.3 ± 1.6[a]	8.3 ± 1.5[a]
Participation in sports possible? (%)			
Yes, always, without problems	5 (31)	3 (23)	2 (67)
Yes, always, with some problems	7 (44)	6 (46)	1 (33)
Yes, but not always motivated	3 (19)	3 (23)	
No	1 (6)	1 (8)	
All activities possible in physical education class? (%)			
Yes	9 (56)	6 (46)	3 (100)
No	6 (38)	6 (46)	
Self-rated condition compared with class mates (%)			
Equal to mean of class	14 (88)	11 (85)	3 (100)
Less than mean of class	1 (6)	1 (8)	
Would your call yourself a sportsmen? (%)			
Yes, I'm a real sportsmen	1 (6)	1 (8)	1 (33)
Yes, I do a lot of sports	3 (19)	2 (15)	2 (67)
A bit	9 (56)	7 (540	
No, not really	1 (6)	1 (8)	
No, absolutely not	2 (13)	2 (15)	
Way to school (%)			
Walking	4 (25)	3 (23)	1 (33)
Bicycle	10 (63)	8 (62)	2 (67)
Car	2 (13)	2 (15)	

***Table 2*: Physical fitness questionnaire**. [a] Data expressed as mean ± SD

Paced CCAVB patients showed a significantly higher HR at rest (77 ± 10 vs. 53 ± 2 bpm), lower VE/VCO_2-slope (31.8 ± 6.3 vs. 40.0 ± 1.8) and higher OUES (1513 ± 528 vs. 1034 ± 57) compared with unpaced patients. There were no significant differences in all other CPET variables between paced and unpaced patients. There were no significant differences in VO_{2peak} kg^{-1} between paced and unpaced patients (Fig. 1) and between the various pacemaker types (Fig. 2).

Variable	CCAVB group N = 16	Comparison paced *vs.* unpaced	
		Paced group N = 13	Unpaced group N = 3
LVEDD % norm	110 ± 10[a]	108 ± 10[a]	117 ± 11[a]
LV dilatation (LVEDD C 120 %norm) (%)	3 (19)	2	1
MV E velocity (m/s)	1.07 ± 0.21[a]	0.99 ± 0.15[a]	1.39 ± 0.08[*,a]
AoV velocity (m/s)	1.25 ± 0.21[a]	1.17 ± 0.13[a]	1.60 ± 0.03[*,a]
Color-coded TDI septal MV S (cm/s)	4.6 ± 0.8[a]	4.5 ± 0.9[a]	5.2 ± 0.1[a]
Color-coded TDI septal MV E' (cm/s)	-8.4 ± 1.6[a]	-7.8 ± 1.2[a]	-10.7 ± 0.7[*,a]
Color-coded TDI lateral MV S (cm/s)	5.9 ± 1.8[a]	5.6 ± 1.9[a]	7.0 ± 0.3[a]
Color-coded TDI lateral MV E' (cm/s)	-12.2 ± 3.2[a]	-11.9 ± 3.4[a]	-13.7 ± 0.8[a]
LV systolic dysfunction (%)	2 (13)	2	0
LV diastolic dysfunction (%)	2 (13)	2	0
IVMD (ms)	31 ± 38[a]	42 ± 34[a]	16 ± 2[a]
Interventricular dyssynchrony (%)	8 (50)	8	0
Color TVI septal-lateral delay (ms)	18 ± 23[a]	18 ± 26[a]	20 ± 10[a]
Intraventricular dyssynchrony (%)	1 (6)	1	0
Rest QRS duration (ms)	136 ± 23[a]	145 ± 13[a]	97 ± 6[*,a]
QRS morphology (%)			
LBBB-like	11 (69)	11	3
IRBBB	3 (19)		
Indifferent	2 (13)	2	
Rest QTc (unpaced subjects) (ms)	420 ± 18[a]	NA	420 ± 18[a]
Rest JTc (paced subjects) (ms)	311 ± 24[a]	311 ± 24[a]	NA
PVBs (%)	0 (0)	0	0
Upper rate behavior (paced subjects) (%)	4 (25)	4	NA

***Table 3*: Echocardiographic and ECG data.** IRBBB, incomplete right bundle branch block; LBBB, left bundle branch block. * $p < 0.05$. [a] Data presented as mean ± SD

Peak HR of the paced patients differed between the various pacemaker types. DDD (dual [atrial/ventricular] paced, dual [atrial ventricular] sensed, dual [inhibited/triggered])-paced patients had the highest peak HR (171 ± 8 bpm), followed by CRT (161 ± 8 bpm), VVIR (ventricular paced, ventricular sensed, inhibited, rate responsive) (114 ± 25 bpm), and DDDR-paced (98 ± 6 bpm) patients.

Variable	Comparison CCAVB *vs.* healthy peers[38] (p < 0.05)* CCAVB group N = 16	Comparison paced *vs.* unpaced	
		Paced group N = 13	Unpaced group N = 3
Rest HR (bpm)	73 ± 13[a]	77 ± 10[a]	53 ± 2[*,a]
Peak HR (bpm) (% predicted)	135 ± 37[a] (70 ± 19)[*,a]	139 ± 35[a] (72 ± 18)[a]	117 ± 48[a] (60 ± 25)[a]
VVIR		114 ± 25[a]	
DDD		171 ± 8[a]	
DDDR		98 ± 6[a]	
CRT		161 ± 8[a]	
Rest VO2 (l min-1)	0.28 ± 0.07[a]	0.29 ± 0.08[a]	0.23 ± 0.04[a]
Peak RER	1.13 ± 0.11[a]	1.15 ± 0.12[a]	1.06 ± 0.01[a]
Peak workload/BM (W kg^{-1}) (% predicted)	2.8 ± 0.6[a] (91 ± 24)[a]	2.8 ± 0.6[a] (87 ± 23)[a]	3.3 ± 0.2[a] (112 ± 11)[a]
Peak VO_2 (l min^{-1}) (% predicted)	1.31 ± 0.50[a] (79 ± 24)[*,a]	0.95 ± 0.12[a] (68 ± 23)[a]	1.39 ± 0.51[a] (112 ± 39)[a]
Peak VO_2/BM (in ml kg^{-1} min^{-1}) (% predicted)	34.4 ± 9.5[a] (79 ± 24)[*,a]	33.0 ± 9.5[a] (75 ± 24)[a]	40.5 ± 8.3[a] (93 ± 22)[a]
Peak VE (l) (% predicted)	50.2 ± 22.9[a] (76 ± 26)[*,a]	52.4 ± 24.8[a] (72 ± 27)[a]	40.7 ± 8.1[a] (92 ± 19)[a]
VT% peak VO_2 (% predicted)	52 ± 17[a] (78 ± 21)[*,a]	51 ± 18[a] (79 ± 22)[a]	53 ± 14[a] (73 ± 15)[a]
VO_2/BM at VAT (ml kg^{-1} min^{-1})	22.9 ± 6.2[a]	22.0 ± 6.0[a]	26.9 ± 6.6[a]
O_2 pulse (ml $beat^{-1}$) (% predicted)	10.4 ± 5.1[a] (111 ± 56)[a]	10.8 ± 5.6[a] (98 ± 31)[a]	8.6 ± 1.7[a] (170 ± 106)[a]
Peak systolic BP (mmHg) (% predicted)	131 ± 24[a] (99 ± 12)[a]	130 ± 26[a] (84 ± 11)[a]	137 ± 15[a] (98 ± 6)[a]
VE/VCO_2 slope (% predicted)	33.3 ± 6.6[a] (108 ± 17)[a]	31.8 ± 6.3[a] (105 ± 18)[a]	40.0 ± 1.8[*,a] (121 ± 2)[a]
OUES (% predicted)	1424 ± 510[a] (92 ± 39)[a]	1513 ± 528[a] (81 ± 23)[a]	1034 ± 57[*,a] (141 ± 60)[*,a]
FEV_1% predicted	92 ± 11[a]	92 ± 12[a]	89 ± 5[a]
FVC% predicted	87 ± 15[a]	87 ± 16[a]	87 ± 13[a]
Peak oxygen saturation (%)	96 ± 2[a]	96 ± 3[a]	97 ± 1[a]

***Table 4*: CPET data.** RER, respiratory exchange ratio; O_2 pulse, peak VO_2/peak HR; BP, blood pressure.
* $p < 0.05$. [a] Data presented as mean ± SD

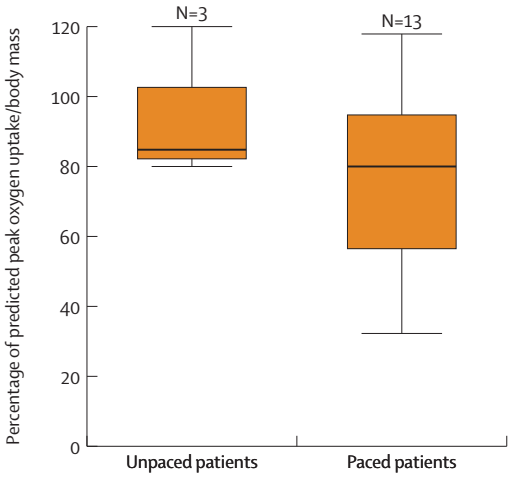

***Figure 1*: Percentage of predicted peak oxygen uptake / body mass (VO_{2peak} kg^{-1}) of unpaced and paced CCAVB patients.** Box-and-whisker diagram: horizontal line in the box depicts median value; the box includes 50% of the values; the upper whisker represents the top 25% of the values; and the lower whisker represents the bottom 25% of the values.

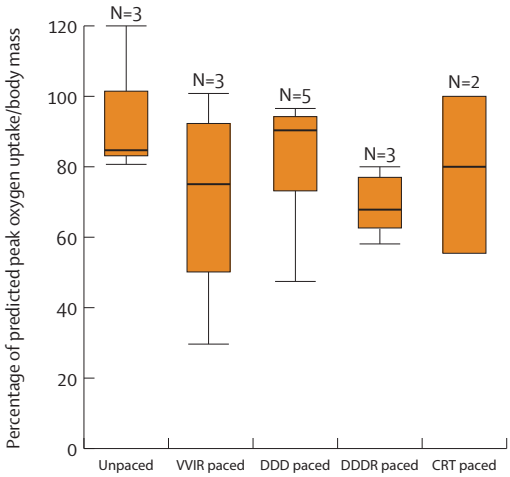

***Figure 2*: Percentage of predicted peak oxygen uptake / body mass (VO_{2peak} kg^{-1}) of unpaced and paced CCAVB patients.** The paced patients are subdivided according to their pacemaker type. Box-and-whisker diagram: horizontal line in the box depicts median value; the box includes 50% of the values; the upper whisker represents the top 25% of the values; and the lower whisker represents the bottom 25% of the values.

Discussion

The aim of this cross-sectional study was to investigate the cardiopulmonary exercise capacity of contemporary children with CCAVB with and without pacemaker. Our study showed that VO_{2peak} kg^{-1} is significantly decreased in children with CCAVB. The VO_{2peak} kg^{-1} values (34.4 ± 9.5 ml kg^{-1} min^{-1}) are comparable with those observed approximately 30 years ago in unpaced children with CCAVB.[29,40,43] These studies reported an average VO_{2peak} kg^{-1} of 36 ± 2, 37, and 31 ml kg^{-1} min^{-1}, respectively.

Furthermore, the VO_2 at VT was significantly decreased compared with healthy peers. The observed VO_2 at VT (22.9 ± 6.2 ml kg^{-1} min^{-1}) was comparable with the VT observed in unpaced children with CCAVB as reported [20 years ago by Reybrouck *et al.* (22.8 ± 5.5 ml kg^{-1} min^{-1}).[32]

It is of interest to note that the peak workload corrected for body mass was not significantly decreased in children with CCAVB. This implies that children with CCAVB are generating more energy from anaerobic sources during exercise, compared with healthy peers, as a compensatory mechanism for their decreased cardiac output. Furthermore, this explains why children with CCAVB do not frequently report exercise intolerance.[2] Based on these figures, the question arises whether pacemaker therapy globally improves exercise capacity in children with CCAVB. Unexpectedly, our current results suggest that the VO_{2peak} and VT values of our paced patients do not differ from those obtained in unpaced patients from 20 to 30 years ago. Moreover, VO_{2peak} values between the paced and unpaced patients of our study population were not significantly different.

Our hypothesis is that by employing the current indications for pacing in CCAVB, as reviewed by Villain,[41] only the ''best'' patients in terms of exercise capacity stay unpaced. Apparently, the exercise capacity of these ''best'' unpaced patients can compete with the paced patients. Thus, perhaps there are factors that prevent normalization of exercise capacity after insertion of a pacemaker.

VO_{2peak} is regarded as the single best parameter to describe exercise capacity.[34] According to the Fick equation, VO_{2peak} is the product of three parameters: peak heart rate (HR_{peak}), peak stroke volume (SV_{peak}), and peak arterial-venous oxygen difference (CaO_2 - CvO_2); ($VO_{2peak} = HR_{peak} \times SV_{peak} \times (CaO_2 - CvO_2)$). Dynamic changes in one of these parameters related to exercise, therefore, might influence the oxygen transport during exercise.

Peak heart rate

Unpaced children with CCAVB mostly have an AV junctional escape rhythm with a lower frequency than healthy individuals at rest (average 46[32] to 59[37] bpm [in this study 53 bpm]). In these patients, this frequency approximately doubles (range 1.6[37] to 2.3[40]) during (peak) exercise to an average frequency of 94[37] to 117 [in this study]). A pacemaker will restore the frequencies at rest as well as during exercise. The extent of frequency restoration depends on the pacemaker mode (e.g., single chamber [VVI] vs. dual chamber (DDD), use of rate response) and the pacemaker programming. Our study showed that the average peak HR of paced CCAVB patients is still lower than in healthy individuals. There are two reasons for that finding.

First, approximately half of the paced patients had a rate-responsive pacemaker (i.e., VVIR or DDDR). They showed a lower average peak HR compared with DDD- or CRT-paced patients. This means that the sensor sensitivity was not appropriate for the type of exercise (cycling). All rate-responsive pacemakers in our study used an accelerometer as activity sensor. Theoretically, an accelerometer should be sensitive to bicycling because it detects horizontal movement.[42] However, it is designed for use in adult patients with the pacemaker implanted in the pectoral region.[3] The majority of patients with a rate-responsive pacemaker in our study had their device implanted in the abdominal region, which blunted the response of their accelerometer during bicycling. Our results underscore the necessity to use the treadmill instead of the bicycle for the exercise testing of pediatric patients with a rate-responsive pacemaker.

Second, despite an average programmed pacemaker upper rate (maximum tracking rate [MTR]) 182 ± 11 bpm, 25% of the paced patients showed upper rate behavior of the pacemaker during the CPET, which limited their exercise capacity significantly. These results show that pediatric CCAVB patients would benefit from MTRs >180 bpm. Unfortunately, not all pacemaker models and manufacturers support MTRs in that range. Finally, another factor that might influence peak HR is the occurrence of premature ventricular beats (PVBs). Earlier studies showed a high incidence (27%[22] to 70%[45]) of PVBs in unpaced CCAVB patients. However, no patient in our study displayed PVBs.

Peak stroke volume

The stroke volume is influenced by cardiac preload, myocardial contractility, and cardiac afterload. There is a difference in these parameters between unpaced and paced CCAVB patients. In unpaced patients, according to Scarpelli and Rudolph,[33] the long diastolic filling in bradycardia causes an increased end-diastolic volume with stretching of the myocardial fibres, augmenting myocardial contractility. Indeed, Kertesz *et al*.[23] demonstrated that moderate LV dilatation is common in these patients and is associated with a normal LV geometry, normal wall stress, and enhanced systolic function during the first two decades of life. The data of this study support the findings of Scarpelli and Rudolph and Kertesz *et al*. The LV end diastolic diameter was greater (although not significantly) in unpaced patients, and one patient had LV dilatation. The MV Doppler inflow velocity was significantly greater in unpaced patients, suggesting an unfavorable relaxation of the stretched left ventricle. All unpaced CCAVB patients had normal LV function.

Paced CCAVB patients had a lower LVEDD and MV Doppler inflow velocity, suggesting less stretching and better relaxation of the left ventricle. However, two of 13 paced patients (15%) showed LV dysfunction (with LV dilatation in one patient). This might be a result of chronic pacing. Earlier studies have shown that chronic (right) ventricular pacing causes an abnormal electrical activation that may lead to mechanical dyssynchrony (seen in 62% of the paced patients in this study), LV remodeling, LV dilatation, LV dysfunction, and low exercise capacity.[28,39] The majority of our patients (87%) had normal LV function at rest. Yet, stroke volume can increase as well as decrease during exercise in the presence of normal LV function at rest.[20,21,37] Therefore, future studies should include exercise echocardiography with (noninvasive) measurement of stroke volume.

Arterial–venous oxygen difference

Although our study does not include (invasive) measurement of the oxygen content of the arterial and venous blood, earlier studies showed a normal (13.8[43] to 14.5[29] ml/100 ml) or increased[21] average arterial–venous oxygen difference during (peak) exercise in patients with CCAVB. It is therefore unclear whether children with CCAVB have an increased arterial–venous oxygen difference during exercise as a compensatory mechanism for their decreased cardiac output.

Study limitations

A limitation of this study was that our data were obtained cross-sectionally from a rather small group of patients in two University Children's Hospitals. In contrast, all patients were tested by the same experienced staff using the same equipment to avoid interobserver or technical variability. Future additional studies should be performed in a larger patient population and should preferably include more unpaced CCAVB patients (although lack of availability is a limitation in itself). In addition, longitudinal exercise data are desirable for investigating the effects of pacemaker therapy on exercise capacity in this population. In conclusion, children with CCAVB show a decreased peak oxygen uptake and VT, whereas they show normal peak work rates. This indicates that they generate more energy from anaerobic energy sources during exercise. Paced children with CCAVB do not perform better than unpaced children. Possible explanations for that finding might be: (1) a selection bias imposed by the current pacemaker criteria (only the clinically ''best'' CCAVB patients stay unpaced), (2) chronic RV pacing–induced LV dysfunction in some CCAVB patients, and (3) suboptimal pacemaker programming.

Future exercise studies, including a greater number of patients and longitudinal follow-up, are warranted to investigate the influence of myocardial properties (LV dysfunction), pacing mode, and optimal pacemaker programming on exercise capacity.

Acknowledgement

We thank A.P. van Dijk and H.B.C. Cornet for their assistance during this study, B. Bongers for calculating the CPET slopes, and M.L. Zonderland and D.A. de Wolf for careful reading and discussion of the manuscript. This study was supported by the Netherlands Heart Foundation (NHS-JUMP [Grant Number 2008T039]).

References

1. Baba R, Nagashima M, Goto M, et al. Oxygen uptake efficiency slope: a new index of cardiorespiratory functional reserve derived from the relation between oxygen uptake and minute ventilation during incre- mental exercise. J Am Coll Cardiol 1996; 28: 1567–1572.
2. Beaufort-Krol GCM, Schasfoort-van Leeuwen MJM, Stienstra Y, Bink-Boelkens MTE. Longitudinal echocardiographic follow-up in children with congenital complete atrioventricular block. Pacing Clin Electrophysiol 2007; 30: 1339–1343
3. Berul CI, Barrett KS. Unique aspects of pacemaker implantation in pediatric patients. In: Walsh EP, Saul JP, Triedman JK (eds) Cardiac arrhythmias in children and young adults with congenital heart disease. Lippincott Williams & Wilkins, Philadelphia, pp 301–317, 2001.
4. Binkhorst M, van de Belt T, de Hoog M, et al. Exercise capacity and participation of children with a ventricular septal defect. Am J Cardiol 2008; 102: 1079–1084.
5. Bongers B, Hulzebos H, Blank A, et al. The oxygen uptake efficiency slope in children with congenital heart disease: construct and group validity. Eur J Cardiovasc Prev Rehabil 2011; 18: 384–92.
6. Brucato A, Jonzon A, Friedman D, et al. Proposal for a new definition of congenital complete atrioventricular block. Lupus 2003; 12: 427–435.
7. Caiozzo VJ, Davis JA, Ellis JF, et al. A comparison of gas exchange indices used to detect the anaerobic threshold. J Appl Physiol 1982; 53: 1184–1189.
8. Diller G-P, Dimopoulos K, Okonko D, et al. Exercise intolerance in adult congenital heart disease: comparative severity, correlates, and prognostic implication. Circulation 2005; 112: 828–835.
9. Diller G-P, Giardini A, Dimopoulos K, et al. Predictors of morbidity and mortality in contemporary Fontan patients: results from a multicenter study including cardiopulmonary exercise testing in 321 patients. Eur Heart J 2010; 31: 3073–83.
10. Dolara A, Favilli S. Controversies in the therapy of isolated congenital complete heart block. J Cardiovasc Med 2010; 11: 426–430
11. van Beek, Binkhorst M, Hoog M, et al. Exercise performance and activity level in children with transposition of the great arteries treated by the arterial switch operation. Am J Cardiol 2010; 105: 398–403.
12. Fredriks AM, van Buuren S, Burgmeijer RJ, et al. Continuing positive secular growth change in The Netherlands 1955–1997. Pediatr Res 2000; 47: 316–332.
13. Fredriks AM, van Buuren S, van Heel WJM, et al. Nationwide age references for sitting height, leg length, and sitting height/height ratio, and their diagnostic value for disproportionate growth disorders. Arch Dis Child 2005; 90: 807–812.
14. Giardini A, Specchia S, Tacy TA, et al. Usefulness of cardiopulmonary exercise to predict long-term prognosis in adults with repaired tetralogy of Fallot. Am J Cardiol 2007; 99: 1462–1467.
15. Giardini A, Hager A, Lammers AE, et al. Ventilatory efficiency and aerobic capacity predict event-free survival in adults with atrial repair for complete transposition of the great arteries. J Am Coll Cardiol 2009; 53: 1548–1555.
16. Godfrey S. Exercise testing in children. Saunders, Philadelphia. 1974.
17. Goebel B, Arnold R, Koletzki E, et al. Exercise tissue Doppler echocardiography with strain rate imaging in healthy young individuals: feasibility, normal values and reproducibility. Int J Cardiovasc Imaging 2007; 23: 149–155.
18. Gorcsan J, Abraham T, Agler DA, et al. Echocardiography for cardiac resynchronization therapy: recommendations for performance and reporting—a report from the American Society of Echocardiography Dyssynchrony writing group endorsed by the heart rhythm society. J Am Soc Echocardiogr 2008; 21: 191–213.
19. Haycock GB, Schwartz GJ, Wisotsky DH. Geometric method for measuring body surface area: a height-weight formula validated in infants, children, and adults. J Pediatr 1978; 93: 62–66.
20. Holmgren A, Karlberg P, Pernow B. Circulatory adaptation at rest and during muscular work in patients with complete heart block. Acta Med Scand 1959; 164: 119–130.
21. Ikkos D, Hanson JS. Response to exercise in congenital complete atrioventricular block. Circulation 1960; 22: 583–590.
22. Karpawich PP, Gillette PC, Garson A, et al. Congenital complete atrioventricular block: clinical and electrophysiological predictors of need for pacemaker insertion. Am J Cardiol 1981; 48: 1098–1102
23. Kertesz NJ, Friedman RA, Colan SD, et al. Left ventricular mechanics and geometry in patients with congenital complete atrioventricular block. Circulation 1997; 96: 3430–3435.
24. Lazzerini PE, Capecchi PL, Guideri F, et al. Autoantibody-mediated cardiac arrhythmias: mechanisms and clinical implications. Basic Res Cardiol 2008; 103: 1–11.
25. Lev M. Anatomic basis for atrioventricular block. Am J Med 1964; 37: 742–748.
26. Marek J. Echokardiografie. Dêtská kardiologie, Czech Republic, 2006.
27. Michaelsson M. Congential complete atrioventricular block. Prog Ped Card 1995; 4: 1–10.
28. Moak JP, Hasbani K, Ramwell C, et al. Dilated cardiomyopathy following right ventricular pacing for AV block in young patients: resolution after upgrading to biventricular pacing systems. J Cardiovasc Electrophysiol 2006; 17: 1068–1071.

29. Mocellin R, Bastanier C. Functional studies in children and adolescents with congenital complete heart block (author's translation). Z Kardiol 1977; 66: 298–302.
30. Ohuchi H, Nakajima T, Kawade M, et al. Measurement and validity of the ventilatory threshold in patients with congenital heart disease. Pediatr Cardiol 1997; 17: 7–14.
31. Paul MH, Rudolph AM, Nadas AS. Congenital complete atrioventricular block: problems of clinical assessment. Circulation 1958; 18: 183–190.
32. Reybrouck T, van den Eynde B, Dumoulin M, van der Hauwaert LG. Cardiorespiratory response to exercise in congenital complete atrioventricular block. Am J Cardiol 1989; 64: 896–899.
33. Scarpelli EM, Rudolph AM. The hemodynamics of congenital heart block. Progr Cardiovasc Dis 1964; 6: 327–342.
34. Shephard RJ, Allen C, Benade AJ, et al. The maximum oxygen intake. An international reference standard of cardiorespiratory fitness. Bull World Health Org 1968; 38: 757–764.
35. Takken T, van der Net J, Engelbert RHH, et al. Responsiveness of exercise parameters in children with inflammatory myositis. Arthritis Rheum 2008; 59: 59–64.
36. Takken T, Blank AC, Hulzebos EH, et al. Cardiopulmonary exercise testing in congenital heart disease: equipment and test protocols. Neth Heart J 2009; 17: 339–344.
37. Taylor MR, Godfrey S. Exercise studies in congenital heart block. Br Heart J 1972; 34: 930–935.
38. Ten Harkel ADJ, Takken T, Van Osch-Gevers M, Helbing WA. Normal values for cardiopulmonary exercise testing in children. Eur J Cardiovasc Prev Rehabil 2010; 18: 48–54S.
39. Thambo J-B, Bordachar P, Garrigue S, et al. Detrimental ventricular remodeling in patients with congenital complete heart block and chronic right ventricular apical pacing. Circulation 2004; 110: 3766–3772.
40. Thorén C, Herin P, Vávra J. Studies of submaximal and maximal exercise in congenital complete heart block. Acta Paediatr Belg 1974; 2: Suppl 132–143.
41. Villain E.Indications for pacing in patients with congenital heart disease. Pacing Clin Electrophysiol 2008; 31: S17–S20.
42. Wang JW, Al-Ahmad A, Hsia HH, Zei PC. Modes of pacemaker function. In: Kusumoto FM, Goldschlager NF (eds) Cardiac pacing for the clinician, 2nd ed. Springer, New York, pp 647–694, 2008.
43. Watson G, Freed D, Strieder J. Cardiac output during exercise in children with idiopathic complete heart block. Front Act Child Health 1977; 297: 743–47.
44. Whipp BJ, Davis JA, Torres F, Wasserman K. A test to determine parameters of aerobic function during exercise. J Appl Physiol 1981; 50: 217–221.
45. Winkler RB, Freed MD, Nadas AS. Exercise-induced ventricular ectopy in children and young adults with complete heart block. Am Heart J 1980; 99: 87–92.
46. Yater W, Lyon J, McNabb P. Congenital heart block—review and report of the second case of complete heart block studied by serial sections through the conduction system. JAMA 1933; 100: 183–1837.

CHAPTER 3

Rewiring the heart: stem cell therapy to restore normal cardiac excitability and conduction

Rewiring the heart: stem cell therapy to restore normal cardiac excitability and conduction

A.C. Blank, T.A.B. van Veen, M.K.B. Jonsson, J.S.J. Zelen, J.L. Strengers, T.P. de Boer, M.A.G. van der Heyden

Curr Stem Cell Res Ther *2009; 4: 23-33*

Department of Paediatric Cardiology, Wilhelmina Children's Hospital, University Medical Center Utrecht (UMCU), Utrecht, the Netherlands
AC Blank
JL Strengers

Division of Heart and Lungs, Department of Medical Physiology, UMCU, Utrecht, the Netherlands
AC Blank
TAB van Veen
MKB Jonsson
JSJ Zelen
TP de Boer
MAG van der Heyden

Cardiac Mechano-Electric Feedback Group, University of Oxford, Department of Anatomy, Physiology and Genetics, Oxford, United Kingdom
TP de Boer

Abstract

The regenerative capacity of the mammalian heart is insufficient to recover from myocardial infarction. Stem cells are currently considered as a promising and valuable tool to replace the, often large, loss of contractile tissue. One of the bottlenecks hampering fast clinical application is the large amount of cells required to replace a single damaged region combined with an appropriate strategy to succeed in homogeneous repair. A second class of major cardiac disorders for which stem cell therapy might be fruitful and would require less cells for repair, are chronic rhythm disorders. In this area, most research has been focused on stem-cell based biological pacemakers, but increasing amounts of data on AV nodal repair appear in literature. Both therapies, in principle, could eventually replace current instrumentation with electronic pacemakers. Finally, an emerging field of interest explores transplantation of stem cells expressing specific ion channels aiming at suppression of focal arrhythmias, providing an alternative strategy for surgical and catheter-mediated ablation. Since in this second class of applications the number of transplanted cells required may be relatively low, effective clinical therapy may be within close range. Here, we will review recent achievements in the fields of stem-cell based biological pacemakers, AV nodal repair and biological ablation.

Introduction

Cardiac electrophysiology

From early embryonic development on, the heart provides the body with proper perfusion of the tissues. Starting with peristaltic contractions in the heart tube stage, the mammalian heart develops into a four-chambered pump that maintains two circulations; the pulmonary and systemic circulation. Though influenced by innervation (vagal and sympathetic), the heart beats autonomously at a rhythm that is generated by the sinoatrial (SA) node, a small structure located close to the superior caval vein of the right atrium (Figure 1). In the SA-node spontaneously active cardiomyocytes are present that are able to impose their beating rate on the surrounding atrial tissue. The impulse is propagated via the atrial myocardium toward the atrioventricular (AV) node, located at the border between atria and ventricles, right above the interventricular septum. After a delay generated by the cells of the AV-node that allows proper filling of the ventricles, the impulse is forwarded to the bundle of His. From here, subsequently the bundle branches and the Purkinje system is activated allowing rapid propagation of the electrical impulse toward the ventricles. Finally, the Purkinje system activates the working myocardium from endo- to epicardium.

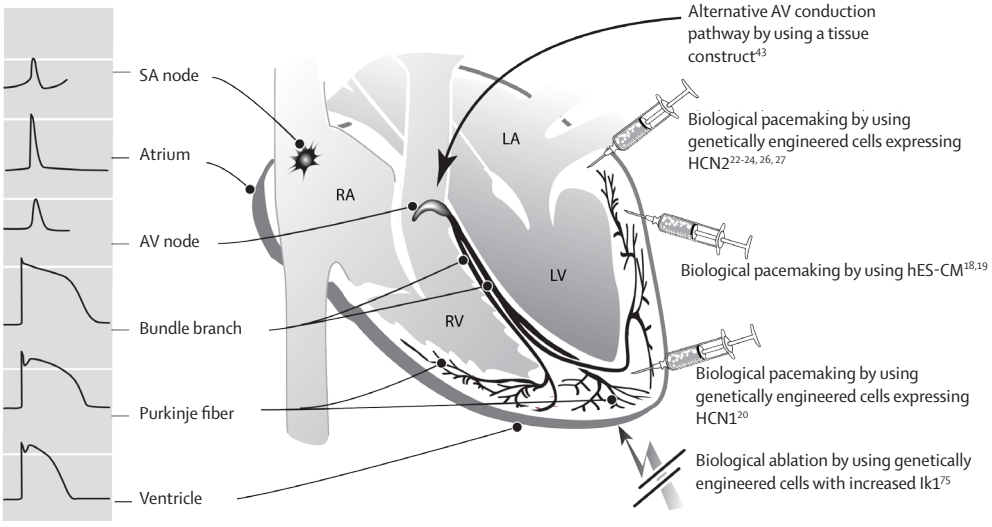

***Figure 1*: The cardiac conduction system.** Diagram of the different components of the cardiac conduction system with its different action potential morphologies: sinoatrial (SA) node, atrioventricular (AV) node, bundle branches, and Purkinje fibers (modified with permission from Mikawa *et al*)[76]. The action potentials are shown at the left side of the diagram. The white lines represent a membrane potential of 0 mV. RA: right atrium, RV: right ventricle, LA: left atrium, LV: left ventricle. The pictograms and their corresponding numbers at the right side of the diagram summarize concepts of cell therapy for cardiac arrhythmias.

Electrical properties of cardiomyocytes

Cardiomyocytes are excitable cells, i.e. they are capable of producing transient depolarizations, called action potentials (APs), when triggered by a depolarizing stimulus large enough to reach threshold. Firing an AP results in contraction of the cell, a phenomenon called excitation-contraction coupling that depends on intracellular calcium handling.[1] The human AP can be divided into five phases. At rest, adult human ventricular cardiomyocytes have a stable membrane potential of approximately -85 mV (see Fig. (2A)). When triggered to fire an AP, rapid depolarization to +40 mV en-sues (phase 0), followed by a transient repolarisation (phase 1), a slow repolarisation called the plateau phase (phase 2), and a relatively fast repolarisation to resting membrane potential (phase 3). Finally, the resting membrane potential is reached again in phase 4. In contrast to ventricular cardiomyocytes, cardiomyocytes from the SA node are spontaneously active (Fig. (2B)). This is due to their less negative and unstable resting membrane potential (approximately -55 mV) that allows a spontaneous but slow depolarization towards the threshold potential, resulting in firing of an AP. The underlying mechanism that allows the AP to occur is interplay between different ion channels. Differences in ion channel expression between ventricular and SA node cardiomyocytes underlie the different AP morphologies.

Ion channel proteins form pores in the plasma membrane that selectively conduct one or more ions and their state, i.e. open or closed, is controlled by the membrane potential.[2] The phases of the human cardiac AP are the result of the changing balance between the depolarizing and repolarising currents carried by specific ion channels (see Figure 2).

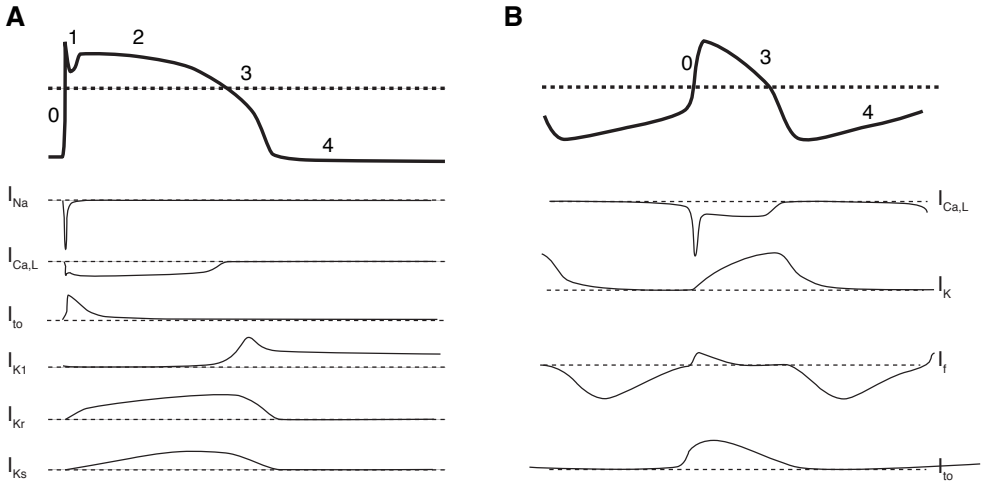

***Figure 2*: Ventricular and nodal action potentional. A**: Schematic representation of the cardiac ventricular action potential and underlying ion currents. The action potential (thick line) is the result of subsequent activation of depolarizing currents, (I_{Na}, I_{Ca-L}) and repolarising currents (I_{to}, I_{Kr}, I_{Ks} and I_{K1}). **B**: Schematic representation of the cardiac sino-atrial action potential and underlying ion currents. The action potential (thick line) is the result of subsequent activation of diastolic depolarising current (I_f), systolic depolarizing current, (I_{Ca-L}) and repolarising currents (I_K and I_{to})

In the ventricular AP, phase 0, the rapid depolarization is caused by a fast increase in sodium conductance, which is attributable to activation of the cardiac sodium channel (Nav1.5) encoded by the SCN5A gene. This initial depolarization is followed by an early repolarisation that is mediated by activation of transient outward potassium channels; Kv4.2 and Kv4.3. During the plateau phase (phase 2), calcium inward current via the Cav1.2 channels (L-type calcium channel) is dominant and maintains the membrane potential at a depolarized value. In the last part of the plateau phase, the potassium channels Kv7.1 and Kv11.1 become predominant. These channels re-main active during the first part of phase 4. Finally, phase 4 is mostly determined by the potassium conductance resulting from activity of Kir2.1, 2.2 and 2.3 inward rectifier channels.

Impulse propagation in the heart

Impulse propagation, i.e. travelling of the AP through the heart, is not only determined by excitability, but also depends on intercellular electrical coupling via gap junction channels. These channels are composed of two hemichannels, which are hexamers of connexin proteins, each contributed by one of the two connected cells. There are twenty-one human connexin (Cx) isoforms identified.[3] Cardiomyocytes mainly express Cx40, -43 or -45 isoforms that are functionally different and are also differentially expressed with respect to the location in the heart.[4] In the working myocardium of the ventricles, Cx43 is the predominant isoform.

A third crucial factor influencing impulse propagation is the extracellular matrix. Interspersed between the cardiomyocytes are blood vessels and fibroblasts. The latter deposit a network of collagen and associated proteins in between and surrounding cardiomyocytes that provides the heart with structure and elasticity. Initially, the extracellular matrix between cells is relatively thin, but upon aging it becomes thicker, although this poses no threat to cardiac function per se. In several pathologies however, such as myocardial infarction and end stage heart failure, cardiomyocytes become apoptotic or necrotic and are replaced by collagen. This so-called replacement fibrosis may create regions of slow conduction or conduction block that promote the occurrence of arrhythmias.[5]

When several factors involved in impulse propagation are impaired, the heart becomes less resistant to the occurrence of arrhythmias. Changes in excitability, tissue architecture or intercellular coupling can provide an arrhythmogenic substrate.[6] Human cardiac diseases often cause changes in more than one parameter affecting conduction. As mentioned before, increased collagen deposition is found in cardiac disease, but changes in expression of ion and gap junction channels often accompany the structural alteration. However, abnormalities in function of ion or gap junction channels also can have a genetic basis[7], as seen in the long QT-syndromes, Andersen-Tawil syndrome, sick sinus syndromes and Naxos disease. Furthermore, adaptation processes in hearts challenged with heart failure result in so-called electrical remodelling. Depending on the nature of the disease, or the experimental intervention, changes in expression levels of all cardiac ion channels have been reported.[8] Also calcium-handling in failing hearts is known to be altered. Thorough discussion of the many possible mechanisms involved in arrhythmia are beyond the scope of this review, but a distinction should be made between mechanisms involving a change in inherent excitability of the cardiomyocytes and changes that

involve altered impulse propagation for reasons that these factors are included in the attempts to improve cardiac function by means of cell therapy.

It is important to discern two potential applications of stem cells for cardiac repair therapy. First, *de novo* generated cardiomyocytes may be applied to compromised heart, thus increasing the functional muscle mass and improving cardiac function (we will refer to this goal as myocardial repair). Notwithstanding that stem cell therapy is commonly considered as a promising tool to treat a variety of cardiovascular disorders resulting from muscle loss, its initial success to support hearts compromised by myocardial infarction is still limited. The underlying causes for the lack of desired straightforward and long-term improvements are diverse. Besides the fact that repopulation of myocytes in scar tissue is difficult (e.g. due to lack of vascularisation), many other problems such as the huge amount of cells that need to be generated, efficient mode of transplantation, immunorejection of non autologous cells, heterogeneity within the donor cell source, viral and bacterial contamination, tumourgenicity risk of non-differentiated cells, to name some, have to be coped with. Though improvements in cardiac output are in general limited (2-4% increase in ejection fraction), transplantation with a variety of cells derived from bone-marrow, cord blood and adipose tissue commonly resulted in a preservation of the ischemic area that might result from paracrine stimulation.[9]
Second, a distinct goal is to repair the specialized rhythm generation and propagation structures of the heart, i.e. the SA node and AV node with its associated bundles of His and Purkinje fibres (we will refer to this as biological pacemaking). Those sources of stem cells that can be differentiated into *de novo* cardiomyocytes share one thing in common; the cardiomyocytes often display spontaneous activity. Like skeletal myoblasts[10], this equips them with characteristics that might trigger development of arrhythmias upon transplantation in the intrinsically quiescent ventricular working myocardium. On the other hand, as has been recognized by many groups all over the world, this characteristic could be beneficial when the aim is to generate a biological pacemaker.

Making this distinction in stem cell applications is essential since both aims impose different requirements on the stem cell-derived myocytes used for the purpose. For myocardial repair, cardiomyocytes have to resemble the native ventricular or atrial cardiomyocyte as closely as possible with respect to electrical phenotype and gap junctional coupling. Cells for biological pacemakers on the other hand, need to be only moderately coupled in order to preserve their spontaneously beating phenotype.[11]

In this paper we first review biological pacemaking by stem cell-derived cardiomyocytes, which have been applied mainly to activate the ventricles instead of replacing the original pacemaker localized in the right atrium. Secondly, we discuss the complex structure-function relationship of the AV node and review literature on restoring AV conduction. Since stem cell-derived cardiomyocytes may trigger ventricular ectopic activity as a negative side-effect in myocardial repair, we emphasize mechanisms by which these arrhythmias may occur and strategies for preventing these. Finally, we review the concept of stem cell-mediated biological ablation, which aims at inhibition of abnormal and undesired automaticity in the heart, and can therefore be considered as the opposite of pacemaking.

Generation of biological pacemakers through stem cell therapy

As mentioned, spontaneous depolarization of cells within the SA node determines cardiac rhythm. Crucial in this process are the electrophysiological characteristics of the myocytes in the SA node. Opposite to ventricular myocytes, these cells lack a stable resting membrane potential, which is also less negative as compared to working myocardial cells in the atrium and ventricle (Fig. 2B). Once repolarisation of an SA node myocyte is complete, a continuous leakage of sodium ions through so called I_f channels underlie the spontaneous phase-4 depolarization that initiates the next beat. This phenomenon is facilitated through a delicate balance between very low amounts of outward I_{K1} current that is counteracted by the inward I_f. Once threshold is reached, gating of primarily inward $I_{Ca\text{-}L}$ channels facilitate the upstroke of the AP. Adaptations in heart rhythm under changing physiological demands (e.g. exercise) rely on the influence of the autonomic nervous system, in particular on $I_{Ca\text{-}L}$ and I_f within SA node myocytes.[12]

Several sources of stem cells have been tested in an attempt to initiate differentiation into cardiomyocytes. For some sources it has yet to be fully determined whether they have potency to differentiate into cardiomyocytes (e.g. bone-marrow derived stem cells). Currently, human ES cells (hES) are generally accepted to be the most potent. Electrophysiological characterization of hES-derived cardiomyocytes (hES-CM) revealed a large heterogeneity in electrical phenotypes with, interestingly, a high predominance of the nodal phenotype. Several reports commonly describe presence of I_f, $I_{Ca\text{-}L}$ and I_{Kr} with AP upstroke velocities ranging from 4-8 V/s, which is typical for nodal myocytes.[13,14] More conflicting are the data presented on functional presence of I_{K1} and I_{Na}.[15]

In culture, both monolayers of hES-CM and hES embryoid bodies (hES-EB) displayed spontaneous activity that was sensitive to adrenergic stimulation. In addition hES-CMs do express functional gap junction channels required for electrical integration with recipient myocardium upon transplantation. These observations elicited the logical idea to exploit these characteristics in an approach to generate a biological pacemaker that ultimately would be applicable in patients with a dysfunctional SA or AV node.

Commonly such patients are instrumented with electronic pacemaker devices in order to achieve or control cardiac rhythm. Though improvements in technology have resulted in more sophisticated pacemakers, still the instrumentation has serious drawbacks. In the paediatric age group, complete AV block (CAVB) is the main indication for pacemaker implantation. There, CAVB is predominantly caused by surgery associated or maternal autoantibody-induced damage of the AV conduction system. Because paediatric cardiac surgery is nowadays performed at younger age and to alleviate more complex heart defects than before, a growing number of patients are expected to require a pacemaker[16] Due to growth and a more active lifestyle the pacing system in paediatric patients is more prone to complications as infection, erosion, fracture and dislodgment hence requiring frequent re-operations.[16] However, instrumentation in elderly patients also has some drawbacks as depleted pacemaker batteries have to be replaced regularly. Moreover conventional long-term pacing can lead to left ventricular (LV) remodelling, LV dilatation, LV asymmetrical hypertrophy, and low exercise capacity.[17] The latter point can be

explained by the fact that such electronic pacemakers have limited capacity to respond to adrenergic stimulation elicited by the autonomous nervous system. For these reasons, a long-term functional biological alternative for electronic pacemakers will be beneficial for a large patient group.

As a proof of principle towards biological pacemaking, hES-EB and hES-CM have been transplanted in several (predominantly large) animal models with experimentally induced abrogation of normal AV-conduction. Since the natural pacemaker is only a tiny structure, this approach not only benefits from the intrinsic spontaneous activity of hES-CM/EB but also from the fact that only a limited amount of material is required which can be delivered by a single injection. Transplantations have mainly been performed in the left ventricular free wall (LVFW). Besides allowing for the determination whether the transplanted construct truly is able to drive the ventricles, intrinsic beating rates of the ventricles in large animal models (escape rhythm) is often very low which is necessary to enable the faster beating transplants to dominate. Without AV-block, beating rates especially of rodent hearts are too fast, which would mask activity from the transplant (overdrive suppression). Kehat *et al*. were the first to establish this principle by transplanting spontaneously beating parts of hES-EB into pig hearts with CAVB. First they showed electrical integration within 24 h of hES-EB with spontaneously beating rat cardiomyocytes *in vitro*. Upon a few days after transplantation in the LVFW of pig CAVB hearts, hES-EB derived pacemaker activity could be allocated to the site of transplantation.[18] Later, a comparable study was performed in a guinea pig model by Xue *et al*. that additionally confirmed that I_f was responsible for the pacemaking behaviour.[19]

Even though the initial success of introducing artificial pacemaker activity elicited much enthusiasm, the road to clinical application still has not been paved. Many countries have resolved ethical obstructions and installed permissive legislation for hES research. The current principle obstacles are safety (like creating an arrhythmic substrate or focus, viral or bacterial contamination, teratoma formation) and immune rejection.

Since pacemaking activity is more based on the electrical characteristics of nodal cells than on their contractile performance (which is limited), it was envisioned that bare gene delivery (focussed mainly on attenuation of I_{K1} activity or introduction of I_f) or transplantation of autologous cells in which 'pacemaking-genes' were introduced, could also be used.[20] Several groups have followed this road in order to circumvent mentioned problems and to temper the risk of rejection. Though attenuation of I_{K1}, as shown by Miake, *et al*.[21], clearly enables pacemaker activity, uncontrolled spatial delivery of adenovirus in their approach could also increase the propensity to arrhythmias, which is a serious drawback. Adenoviral delivery of HCN2 (encoding I_f) into the left atrial appendage.[22], or the left bundle branch[23] successfully enhanced rhythm which was confirmed to originate from the site of adenoviral infection. Using the same approach, expression of a synthetic pacemaker channel into the LVFW of bradycardic guinea pigs resulted in idioventricular beats that originated from the site of injection.[24]

In general, most data describe a short-term result, which is adequate for testing proof-of-principle, but physiological sense demands a longer follow-up. In that perspective, adenoviral interference might be incompatible since effects fade within weeks and, secondly, inflammatory responses are enhanced.[25] Application of lentivirus or adeno-associated virus might avoid these problems although caution in clinical application will still be advisable.

As an alternative, nonexcitable (possibly autologous) cells have been used to deliver the I_f current to induce pacemaker activity. The group of Rosen used human mesenchymal stem cells (hMSC) transduced (via electroporation thereby circumventing the use of viral vectors) with HCN2 to create pacemaker activity in the LVFW of CAVB dogs.[26,27] The advantages of hMSC are that these cells seem to be immune-privileged meaning that rejection can be tempered[28], and that they express sufficient amounts of gap junction protein allowing integration upon transplantation. To avoid dependence on gap junctions to mediate transfer of the pacemaker current, Cho and co-workers generated an elegant model of cell fusion.[20] In this model, fibroblasts stably expressing HCN1 (a family member of HCN2 also generating I_f) were injected in guinea pig hearts in the presence of polyethylene-glycol. This agent stimulated cell fusion of the injected fibroblasts with the native cardiomyocytes in the injected myocardium hereby providing them with I_f which resulted in pacemaker activity.

Recently, we and several other groups have reported on the isolation and characterisation of cardiomyocyte progenitor cells (CMPC) from different (including human) species.[29-32] These undifferentiated cells appear naturally resident in both foetal and adult hearts, can be isolated based on stem cell biomarkers and differentiate, at least in culture, to cardiomyocytes. Thereby they enervate the assumption that the myocardium is terminally differentiated and has no regenerative capacity.[33] In culture, differentiated CMPC appeared quiescent but became spontaneously active upon administration of serum. Since these cells display a proper level of gap junctional communication, once it is unravelled which factors are responsible for their spontaneous activity, it raises the possibility of applying these cells in autologous regeneration of pacemaker activity.

Restoring normal AV conduction by means of stem cells

In the normal heart the AV node is the only connection between the atrial and ventricular part of the specialized cardiac conduction system. From its first description in 1906[34,35] until now, the AV node causes intense debate about its structure and function as reviewed recently by Efimov *et al.*[36] Functionally, the AV node can be viewed as: (1) conductor, (2) subsidiary pacemaker and (3) (frequency) controller. The AV node receives its electrical input via various atrial myocardial fibres and nodal extensions.[37,38] The electrical impulse is then slowly conducted through the AV node itself. If no atrial electrical impulse arrives at the AV node, the AV node itself can function as a subsidiary pacemaker.

Finally, in the case of an atrial tachyarrhythmia the AV node can limit the amount of conducted impulses to the ventricles. The conducting properties of the AV node are determined by active ('source', i.e. excitability by membrane ion channel activity) and passive electrical factors ('sink', i.e. cell/tissue architecture and membrane gap junctions).[39]

Structurally, the AV node is composed of different cell types positioned in a complex 3-dimensional configuration.[38] Moreover, each of these possesses their own cell type specific gap junction and ion channel expression pattern.[37,40,41] Finally, it should be mentioned that all these aspects vary between mammalian species. Modern imaging technologies, which combine both functional and structural information in a 3-dimensional dataset, could establish a species-specific blueprint for AV nodal repair by stem-cell therapy. Recently, such dataset for the rabbit AV node was provided.[42] In this elegant study, a rabbit AV nodal preparation was treated with a voltage-sensitive dye, and electrical activity during AV nodal pacemaking and AV nodal reentry was recorded. Thereafter, the AV nodal preparation was extensively sectioned and histological analyzed. Adjacent sections were immunoenzymatically labelled for Cx43 and neurofilament as a marker of nodal tissue. All sections were used to construct a 3-dimensional computer model of the AV nodes' anatomy. This model shows a continuing tract of nodal tissue at the AV junction that can be divided into two morphological and histochemically distinct entities: an inferior nodal extension (INE) and a penetrating bundle (PB). The Cx43 expression levels of the INE and the PB change along their path through the AV node. Most of the INE did not express Cx43. The upper part of the PB showed a weak Cx43 labelling. The lower part of the PB expressed Cx43 strongly. Most of the INE and the upper part of PB were covered by transitional tissue (i.e. nodal cells loosely packed into fibrous tissue). To establish a structure-function relationship, a map of the electrical activation was superimposed on the anatomic model. This shows that AV nodal pacemaking was initiated in the INE.

In theory, stem cells should be able to restore a dysfunctional AV node. However, given the structural and functional complexity of the AV node as briefly described above, this particular field of stem-cell-based regeneration is in its infancy. Choi *et al*. showed that it is possible to create an alternative AV conduction pathway in rats[43] by producing an *in vitro* tissue construct from skeletal myoblasts in a collageneous matrix. At the outside of the heart the tissue construct was attached to the AV groove, thereby physically bridging the atrial and ventricular structures. By optical mapping and electrophysiological analysis it was subsequently demonstrated that permanent AV conduction via the alternative AV conduction pathway in one-third of recipient animals did occur.

In another study, injections with autologous fibroblast were performed to alter the conducting and controlling properties of the AV node.[44] This study started with a search for an alternative to radiofrequency ablation of the AV node in therapy-resistant atrial fibrillation, for which we wish to use the term 'biological ablation'. Although not originally designed for the purpose of restoring AV function, this study, in our opinion, established important prerequisites for (stem) cell therapy of a disturbed AV node. The study showed that cell injections could be precisely placed into chosen parts of the AV node by catheter intervention under electrophysiological and anatomical guidance.

Potential of proarrhythmic consequences of ventricular cell therapy

Normal impulse conduction in the heart can be challenged by factors that decrease conduction velocity or introduce regions with spontaneous triggered activity.[6] Such factors are associated with cardiac disease and infarction, and are therefore often observed in patients that could benefit from future myocardial repair therapy. In this setting however, attempts to enhance the contractile function of the heart with stem cell-derived-cardiomyocytes should not result in introducing more arrhythmias.

Several clinical and preclinical studies have shown that spontaneous activity of stem cell-derived cardiomyocytes can result in ectopic pacemaking and ventricular tachyarrhythmias upon transplantation.[18,45,46] As discussed, this is beneficial if a biological pacemaker is desired, it is however incompatible with the aim of myocardial repair. A number of mechanisms underlying the observed arrhythmias upon transplantation have been identified.

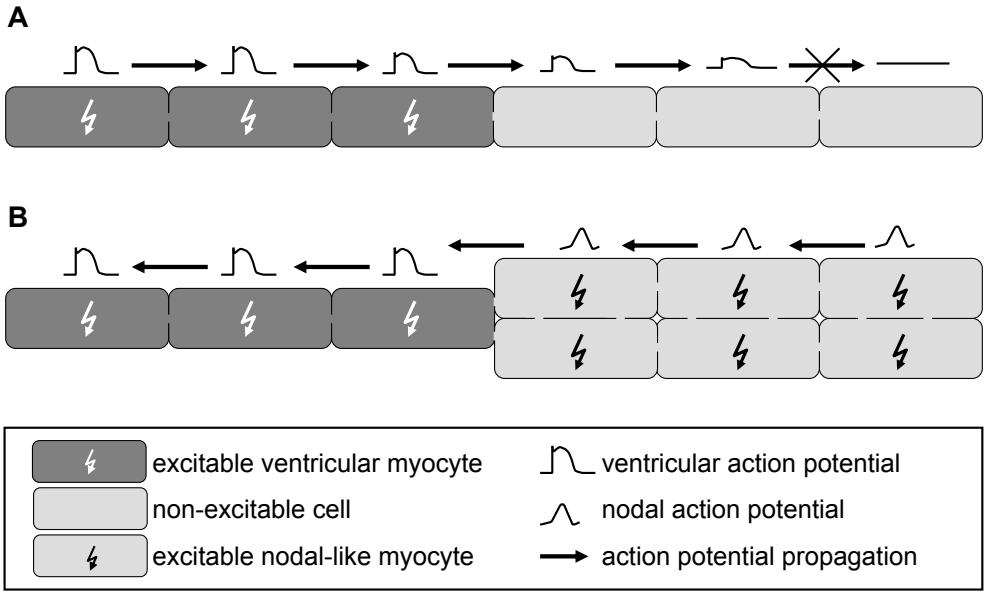

***Figure 3*: Source-sink and pacemaking concept. A**: Source-sink. Schematic representation of a strip of cardiac ventricular myocytes coupled by gap junctions to non-excitable cells, like undifferentiated mesenchymal or embryonic stem cells. The action potential (originating from the the non-depicted SA node to the left) is propagated from cardiomyocyte to cardiomyocyte, each time re-established by ion channels expressed in the cell itself. Upon coupling to the non-excitable stem cells, the action potential fades, resulting in block of action potential propagation. **B**: Pacemaking. A cluster of spontaneous active stem cell derived cardiomyocytes is coupled by gap junctions to ventricular cardiac myocytes. When the frequency of action potential formation exceeds that of the non-depicted SA node, the cluster propagates the action potential to the ventricular cells resulting in ectopic pacemaking.

Inherent intrinsic automaticity of stem-cell-derived cardiomyocytes is a large dissimilarity with cardiomyocytes of the host myocardium that contract only in response to external electrical impulses. When one of two adjoining electrically coupled cardiomyocytes fires an AP, a difference in membrane potential between the cells will develop as the AP initiates. This difference in potential will drive an electrical current between the two cells, its magnitude being a function of the resistance of the electrical coupling. The gap-junctional current that is flowing from the 'source' cardiomyocyte will depolarize the 'sink' cardiomyocyte, which under physiological conditions will result in subsequent firing of an AP by the 'sink' cardiomyocyte and thus propagation of the electrical impulse (Fig. 3A). This mechanism is referred to as the source-sink relationship. The resting membrane potential of embryonic stem cell-derived cardiomyocytes is between -55 and -45 mV[15,47], while native cardiomyocytes have a membrane potential between -80 and - 90 mV. If the two cell types are weakly coupled, stem-cell-derived cardiomyocytes will not be silenced by the native cardiomyocytes and retain spontaneous activity that might be transmitted to the host myocardium (Fig. 3B). Moreover, at such intermediate coupling levels, grafted stem-cell-derived cardiomyocytes will present a continuous depolarizing 'sink', promoting spontaneous activity in otherwise quiescent native cardiomyocytes.

Clustering of stem-cell-derived cardiomyocytes worsens the source-sink relationship, as a larger cluster is better able to maintain its intrinsic membrane potential, and therefore is more proarrhythmic.[11,27] In the context of myocardial repair, this means that clustering which is likely to occur if the mode of transplantation is intramyocardial injection, should be avoided unless the differences in electrical phenotype between native and grafted cells are negated. In an *in vitro* study[11], we investigated this proarrhythmic potential of spontaneously active cardiomyocytes. Rat neonatal cardiomyocytes (NCMs), here used as a model for spontaneously active stem cell-derived cardiomyocytes, were co-cultured with canine adult ventricular cardiomyocytes (ADCs). Isolated ADCs display no spontaneous APs due to a positive balance between I_{K1} and depolarizing currents, whereas NCMs are spontaneously active (like embryonic stem cell derived cardiomyocytes, albeit that these become spontaneous active through intracellular calcium oscillations[48]). When cultured together, both cell types were coupled by Cx43 mediated gap junctions. In the event of one ADC coupled to one or two NCMs, these cells became quiescent, indicating a positive balance between the counteracting currents. When three or more NCMs were coupled to one ADC, this balance reversed and all cells were spontaneously active. It appeared that a delicate window existed in which triggered activity was possible, depending on the amount of coupled cells and the absolute level of intercellular coupling.

A second mechanism involved in stem cell-related proarrhythmia is re-entry. Under normal physiological conditions, electrical impulses are propagated throughout the heart rapidly. Conduction velocity in the heart is rather uniform, but higher parallel to, than perpendicular to fiber orientation. Loss of rapid conduction within a region predisposes it to become an arrhythmogenic substrate. If conduction slowing is significant, normally conducting tissue can first excite the compromised region, than recover from excitation itself and once recovered, it can on its turn be re-excited by the slowly conducting region. This sequence of events constitutes a re-entry circuit, and can be the basis for self-perpetuating circular excitation waves.[6]

As was shown by a number of groups, slowing of conduction can be observed in mixed cell populations containing cardiomyocytes and skeletal myoblasts or mesenchymal stem cells.[49,50] In the case of skeletal myoblasts, which themselves are excitable but do not couple electrically with cardiomyocytes, slowing of conduction is caused by lengthening of the path of conduction; the impulse must revolve around the transplanted myoblasts. Non-excitable cells such as mesenchymal stem cells can additionally slow conduction by constituting a 'sink' that slows the depolarization of native cardiomyocytes.[51]

Identification of these two mechanisms underlying stem cell-related proarrhythmia tells us that (1) clustering is not beneficial in the context of myocardial repair, and (2) evenly distributed stem cells can still provoke slowing of conduction if their electrical properties are obstructively aberrant from native cardiomyocytes. Thus, in order to optimize myocardial repair strategies, differentiation techniques have to be developed that give rise to sufficiently electrical mature cardiomyocytes. At the same time, tissue engineering skills are necessary that allows delivery of cells in a controlled fashion, in order to avoid clustering and ensure rapid impulse propagation.

As mentioned, cardiac progenitor cells that can be differentiated *in vitro* into cardiac myocytes have been isolated from heart tissue of different animal species.[29,52-54] The electrical phenotype of cardiomyocytes derived from such stem cells may be more mature and homogeneous than those observed in cardiomyocytes derived from embryonic stem cells. This idea is instigated by the thought that these so-called cardiac stem cells are committed to the mesodermal lineage, and therefore differentiate more efficiently to cardiomyocytes. Recent work by our group has shown that this is indeed the case.[55] Cardiomyocytes derived from human fetal cardiomyocyte progenitor cells are not spontaneously active in the absence of serum, but are excitable and have a membrane potential in the order of -70 mV (unpublished data, de Boer *et al.*). While this phenotype still is not equal to the phenotype of normal mature cardiomyocytes, it does constitute a step into the right direction as the lack of spon-taneous activity is particularly essential in myocardial repair. Recent reports indicate that adult hearts contain a pool of small cardiomyocytes that may develop during adulthood, and have physiological properties that are compatible with a less mature identity.[56] Since adult cardiomyocyte progenitor cells can be isolated from, for instance, human atrial appendages obtained during heart surgery[29], it might be possible to induce differentiation of cardiomyocytes with even better physiological properties using adult cardiomyocyte progenitor cells.

With recent progress in finding proper cells to use in myocardial repair, it is becoming increasingly clear that the mode of cell delivery will be essential. Present experimental data on myocardial repair have clearly demonstrated that delivery of large amounts of cells is cumbersome. Common methods are intramyocardial and intracoronary injection. Both techniques are hampered by very low efficiencies; after delivery of millions of cells, the number of retrievable cells is often dramatically low (up to a few hundred). Most likely, cells are massively lost to the systemic circulation, flow back through the injection tract or die during the injection procedure itself due to mechanical stress.
To overcome these problems, several tissue-engineering approaches have been devised. The general concept is that transplantation effectiveness can be improved if cells are

provided with an extracellular matrix. This idea has been followed in two approaches[57]; firstly it is possible to obtain a genuine cardiac extracellular matrix by removing cardiomyocytes from myocardial biopsies, or to create a matrix *in vitro* using collagen, matrigel, alginate or other biomaterials. Such matrices can subsequently be seeded with cells and applied to the heart.[58] Alternatively, liquid matrix components can be mixed with cells and, by using a casting-mould, tissue constructs of defined shape can be created. Employing matrigel and culture medium mixed with a whole heart cell suspension, Zimmermann *et al*. created artificial myocardial tissue *in vitro* containing vasculature that generated im-proved cardiac function and normalized epicardial impulse conduction upon transplantation onto infarcted rat hearts.[59]

A second approach is to mix cells with extracellular matrix components and inject the mixture, thereby creating an artificial tissue in situ. Acellular injections of collagen, fibrin or matrigel into myocardial infarctions resulted in similarly improved angiogenesis, while collagen injections appeared to induce recruitment of myofibroblasts.[60] Co-injection of fibrin and skeletal myoblasts as well as matrigel and murine embryonic stem cells resulted in markedly improved cell retention and survival.[61,62]

Finally, while several studies have demonstrated that cell therapy can lead to sustained presence of transplanted cells in the myocardium and functional improvement, potential proarrhythmic consequences of ventricular cell therapy are largely overlooked. This is partly due to an inherent insensitivity of the mouse model to proarrhythmic instability. Mouse hearts are too small to sustain the re-entry arrhythmias observed in human hearts, and their sinus rhythm is much faster than the beating rate of (human) stem-cell-derived cardiomyocytes. These two factors make it very unlikely that cell therapy will result in proarrhythmia in mice. In order to design clinically relevant strategies for cell therapy, it is essential to employ larger animal models such as the pig or dog. Follow-up of treated animals should be much longer than the usual three months, and heart rhythm should be monitored regularly based on ECG recordings, preferably combined with in situ mapping of impulse conduction in the treated region of myocardium.

Biological ablation — excitability control by electronic inward rectifier current application

Developed in the eighties of the last century, catheter-based ablation is currently a widely used technique for treatment of atrial and ventricular fibrillation caused by either re-entry circuits or ectopic activity (recently reviewed in refs 63, 64). Although the basic mechanisms underlying these arrhythmias are totally different as described above, they can be terminated by a common mechanism as demonstrated by the catheter ablation. The molecular equivalent to radiofrequency or cryo-ablation can be found in suppression of excitability of the arrhythmogenic substrate by application of a stabilizing ion current like the inward rectifier potassium current (I_{K1}).
I_{K1} mainly operates in between subsequent APs (Fig. 2A) and is responsible firstly for generating and stabilizing the resting membrane potential at a rather negative potential between -75 and -90 mV, and secondly for the initial depolarization (indirectly, opposing depolarizing currents) and final repolarisation (directly, contributing repolarising cur-

rents) of the AP.[65] In mammals, several different but closely related ion channels constitute the cardiac I_{K1}.[66] Of these, the KCNJ2 and KCNJ12 gene products Kir2.1 and Kir2.2 are the main determinants. Furthermore, Kir2.3 coded by the KCNJ4 gene contributes to cardiac I_{K1}. To function as an ion channel, Kir2.x proteins form either homotypic or heterotypic tetramers.

In the heart, an inverse relationship between I_{K1} and focal activity can be inferred from nodal tissue, where the absence of strong I_{K1} and Kir2.x expression is a prerequisite for spontaneous pacemaker activity. On the other hand, inhibition of endogenous I_{K1} by dominant negative Kir2.1 in the working ventricular myocardium of guinea pigs induces ectopic focal pacemaker activity.[21] In humans, loss-of-function mutations in Kir2.1 lead to Andersen-Tawil syndrome characterized by potentially lethal ventricular arrhythmias.[67] While less I_{K1} favours excitability, it has been questioned whether an increase in the levels of I_{K1} would render tissue inexcitable. In several elegant studies it was demonstrated indeed that increased levels of I_{K1}, mediated by Kir2.1 overexpression in the ventricle, resulted in AP shortening and even in regions of conduction block, likely due to the inability of depolarizing currents to overcome the stabilizing I_{K1}.[21,68,69]

These data demonstrate that, in principle, triggered and re-entry based arrhythmias can be terminated by dramatically increasing I_{K1}. In such approaches, care should be taken however to add sufficient amounts of I_{K1} to reach inexcitability, rather than suppression of excitability, as becomes eminent from the study of Xia.[70] In that work, a gain-of-function mutation in Kir2.1 has been linked to congenital atrial fibrillation, likely due to its effect of AP shortening leading to decreased effective refractory period allowing multiple wavelet formation. Although many conflicting data concerning gain- and loss-of function of I_{K1} with respect to arrhythmia still exist and need to be resolved[71], it is clear that a delicate balance between stabilizing I_{K1} and 'pacemaker' currents in the different regions of the heart exists, and that manipulating I_{K1} densities can result in either enhancing (focal pacemaking[21], re-entry based rotors[72]) or inhibiting (silencing) excitability. As a proof-of-principle, biological ablation of re-entry based arrhythmias in infarct border zones has been demonstrated in a porcine model of myocardial infarction, by application of a dominant negative form of potassium ion channel Kv11.1, normally carrying the delayed rectifier current I_{Kr}. In that study, adenovirus mediated gene therapy resulted in increased refractoriness of the tissue, thereby preventing running of re-entry circuits in this region.[73]

When using stem cell therapy for application of specific ion currents in the heart, i.e. I_{K1}, it should be established that these cells can provide their current to the cardiac myocytes by electrotonic coupling. As explained in the section on ventricular cell therapy, the absolute level of intercellular coupling and the number of functionally coupled cells determines the efficacy of exogenous provided currents on native cardiomyocytes.[11] In a follow-up study[74], NCMs were co-cultured with HEK cells expressing ectopic wild-type Kir2.1 (KWGF). Upon gap-junctional communication, KWGF cells were able to silence the spontaneous APs of the NCMs in a dose-dependent fashion. These data provide *in vitro* proof of concept for I_{K1} mediated regulation of heart cell excitability by electrotonic coupling.

In vivo examination on the concept of I_{K1}-mediated biological ablation by cell therapy is limited to a single study. Yankelson *et al.* generated NIH-3T3 fibroblasts expressing Kir2.1 based ion channels.[75] Upon transplantation into the pig right ventricle, transplanted cells electrotonically coupled to the host myocardium and increased the local effective refractory period (a measure of reduced excitability). Similar results were found with fibroblasts expressing the non-cardiac ion channel Kv1.3.

Many issues still have to be addressed with respect to the optimal cell type, ion channel, amount of current, mode of application, durability, efficacy and so on before clinical applicability of biological ablation might even be considered. Though cardiac Kir2.1, Kir2.2 and Kir2.3 all display inward rectification, they display distinct current-voltage relationships. This will differentially affect AP shortening[66], which is an unwanted side effect of stabilizing the resting membrane potential in an arrhythmogenic substrate or ectopic focus. With regard to the optimal cell type several prerequisites can be defined. The cell should be relatively small compared to the cardiomyocytes to limit its 'sink' and to prevent dilution of ion currents other than the one provided by the donor cell. Furthermore, the cell should establish adequate gap-junctional communication with the host tissue and should not influence the hearts architecture by, for instance, depositing large amounts of extracellular matrix. As mentioned before, the amount of current applied by the donor cells is essential for the ablation effect versus proarrythmia. One way to achieve this is to generate stem cells containing the ion channel in question under an inducible promoter.

Conclusion

In this review we have discussed current approaches for resolving electrical disorders of the heart by stem cell-based-transplantation therapy. Due to the inherent characteristic of spontaneous beating behaviour of many types of stem cell-derived cardiomyocytes, progress in the field of biological pacemaking has advanced furthest thus far. Biological pacemakers can be created by stem cells, and in principle they are able to respond to adrenergic drive.
AV node repair is more challenging due to the complex structural and functional organization of the AV node itself that combines different functions as slow conduction, subsidiary pacemaking and frequency control. Achievements have been made in manipulating the individual functions of the AV node, such as pacemaking or slow AV conduction. The main challenge is found in combining these into one stem cell based functional tissue construct.
Stem cell based myocardial repair of muscle loss carries the inherent risk of introducing an arrhythmogenic substrate into an already electrically vulnerable heart. We indicated that the electrophysiological phenotype of the donor cells is of crucial importance. Here, attention should be given to generating mature cardiomyocytes that are not spontaneous active, that display a ventricular-like AP and can be well coupled to the surrounding cardiomyocytes by Cx43 based gap junctions.

Furthermore, donor cells should be homogenously distributed throughout the recipient tissue to avoid clustering-mediated 'sink' and 'pacemaking' effects.
The usage of stem cells for delivery of specific ion currents into the diseased heart in order to resolve electrical disorders is an emerging field. Especially, I_{K1}-mediated biological ablation may evolve into new clinical alternatives for classical catheter based ablation techniques.

For all applications mentioned, the optimal stem cell type and its mode of (efficient) differentiation has not been elucidated currently, and certainly requires much attention. For now, immature-like cardiomyocytes derived from embryonic stem cells or genetically manipulated autologous mesenchymal stem cells best serve the requirements for biological pacemaking, while cardiac progenitor cells appear well-suited for myocardial muscle mass repair.

Acknowledgements

We thank Professor Emeritus David A. de Wolf for careful reading the manuscript. This work was supported by the Technology Foundation (STW program DPTE, grant UGT.6746), the Netherlands Organization for Scientic Research (NWO, grant 916.36.012), and the Ter Meulen Fund, Royal Netherlands Academy of Arts and Sciences, The Netherlands.

References

1. Díaz M, Graham H, O'Neill S, Trafford A, Eisner D. The control of sarcoplasmic reticulum Ca^{2+} content in cardiac muscle. Cell Calcium 2005; 38: 391-6.
2. Roden DM, Balser JR, George Jr AL, Anderson ME. Cardiac ion channels. Annu Rev Physiol 2002; 64: 431-75.
3. Söhl G, Willecke K. An update on connexin genes and their nomenclature in mouse and man. Cell Commun Adhes 2003; 10: 173-80.
4. van Veen TA, van Rijen HV, Jongsma HJ. Physiology of cardiovascular gap junctions. Adv Cardiol 2006; 42: 18-40.
5. de Bakker JMT, van Rijen HVM. Electrocardiographic manifestation of anatomical substrates underlying post-myocardial infarction tachycardias. J Electrocardiol 2007; 40: S21-5.
6. Kléber AG, Rudy Y. Basic mechanisms of cardiac impulse propagation and associated arrhythmias. Physiol Rev 2004; 84: 431-88.
7. Marbán E. Cardiac channelopathies. Nature 2002; 415: 213-8.
8. Michael G, Xiao L, Qi XY, Dobrev D, Nattel S. Remodelling of cardiac repolarization: How homeostatic responses can lead to arrhythmogenesis. Cardiovasc Res 2008; doi:10.1093/cvr/cvn266.
9. Gnecchi M, He H, Liang OD, et al. Paracrine action accounts for marked protection of ischemic heart by Akt-modified mesenchymal stem cells. Nat Med 2005; 11: 367-8.
10. Menasché P, Alfieri O, Janssens S, et al. The Myoblast Autologous Grafting in Ischemic Cardiomyopathy (MAGIC) trial: first randomized placebo-controlled study of myoblast transplantation. Circulation 2008; 117: 1189-1200.
11. de Boer TP, van der Heyden MAG, Rook M, et al. Proarrhythmogenic potential of immature cardiomyocytes is triggered by low coupling and cluster size. Cardiovasc Res 2006; 71: 704-14.
12. Boyett MR, Honjo H, Kodama I. The sinoatrial node, a heterogeneous pacemaker structure. Cardiovasc Res 2000; 47: 658-87.
13. He JQ, Ma Y, Lee Y, Thomson JA, Kamp TJ. Human embryonic stem cells develop into multiple types of cardiac myocytes: action potential characterization. Circ Res 2003; 93: 32-9.
14. Sartiani L, Bettiol E, Stillitano F, Mugelli A, Cerbai E, Jaconi ME. Developmental changes in cardiomyocytes differentiated from human embryonic stem cells: a molecular and electrophysiological approach. Stem Cells 2007; 25: 1136-44.
15. Satin J, Kehat I, Caspi O, et al. Mechanism of spontaneous excitability in human embryonic stem cell derived cardiomyocytes. J Physiol 2004; 559: 479-96.
16. Silvetti MS, Drago F, Grutter G, De Santis A, Di Ciommo V, Ravà L. Twenty years of paediatric cardiac pacing: 515 pacemakers and 480 leads implanted in 292 patients. Europace 2006; 8: 530-6.
17. Thambo JB, Bordachar P, Garrigue S, et al. Detrimental ventricular remodelling in patients with congenital complete heart block and chronic right ventricular apical pacing. Circulation 2004; 110: 3766-72.
18. Kehat I, Khimovich L, Caspi O, et al. Electromechanical integration of cardiomyocytes derived from human embryonic stem cells. Nat Biotechnol 2004; 22: 1282-9.
19. Xue T, Cho HC, Akar FG, et al. Functional integration of electrically active cardiac derivatives from genetically engineered human embryonic stem cells with quiescent recipient ventricular cardiomyocytes: insights into the development of cell-based pacemakers. Circulation 2005; 111: 11-20.
20. Cho HC, Kashiwakura Y, Marbán E. Creation of a biological pacemaker by cell fusion. Circ Res 2007; 100: 1112-5.
21. Miake J, Marbán E, Nuss HB. Biological pacemaker created by gene transfer. Nature 2002; 419: 132-3.
22. Qu J, Plotnikov AN, Danilo P, Jr., et al. Expression and function of a biological pacemaker in canine heart. Circulation 2003; 107: 1106-9.
23. Plotnikov AN, Sosunov EA, Qu J, et al. Biological pacemaker implanted in canine left bundle branch provides ventricular escape rhythms that have physiologically acceptable rates. Circulation 2004; 109: 506-12.
24. Kashiwakura Y, Cho HC, Barth AS, Azene E, Marbán E. Gene transfer of a synthetic pacemaker channel into the heart: a novel strategy for biological pacing. Circulation 2006; 114: 1682-6.
25. Gilgenkrantz H, Duboc D, Juillard V, et al. Transient expression of genes transferred in vivo into heart using first-generation adenoviral vectors: role of the immune response. Hum Gene Ther 1995; 6: 1265-74.
26. Potapova I, Plotnikov A, Lu Z, et al. Human mesenchymal stem cells as a gene delivery system to create cardiac pacemakers. Circ Res 2004; 94: 952-9.
27. Plotnikov AN, Shlapakova I, Szabolcs MJ, et al. Xenografted adult human mesenchymal stem cells provide a platform for sustained biological pacemaker function in canine heart. Circulation 2007; 116: 706-13.
28. Liechty KW, MacKenzie TC, Shaaban AF, et al. Human mesenchymal stem cells engraft and demonstrate site-specific differentiation after in utero transplantation in sheep. Nat Med 2000; 6: 1282-6.
29. Goumans MJ, De Boer TP, Smits AM, et al. TGF-β1 induces efficient differentiation of human cardiomyocyte progenitor cells into functional cardiomyocytes in vitro. Stem Cell Res 2007; 1: 138-49.
30. Oh H, Bradfute SB, Gallardo TD, et al. Cardiac progenitor cells from adult myocardium: homing, differentiation, and fusion after infarction. Proc Natl

Acad Sci USA 2003; 100: 12313-8.
31. Beltrami AP, Barlucchi L, Torella D, et al. Adult cardiac stem cells are multipotent and support myocardial regeneration. Cell 2003; 114: 763-76.
32. Matsuura K, Nagai T, Nishigaki N, et al. Adult cardiac Sca-1-positive cells differentiate into beating cardiomyocytes. J Biol Chem 2004; 279: 11384-91.
33. Anversa P, Leri A, Kajstura J. Cardiac regeneration. J Am Coll Cardiol 2006; 47: 1769-76.
34. Tawara S. Das Reizleitungssystem des Säugetierherzens. Eine anatomische-histologische studie über das Atrioventricularbündel und die Purkinjeschen Fäden. 1906; Jena, Verlag v. Gustav Fischer.
35. Silverman ME, Grove D, Upshaw Jr CB. Why Does the Heart Beat? The Discovery of the Electrical System of the Heart. Circulation 2006; 113: 2775-81.
36. Efimov IR, Nikolski VP, Rothenberg F, et al. Structure-function relationship in the AV junction. Anat Rec A Discov Mol Cell Evol Biol 2004; 280: 952-65.
37. Anderson RH, Ho SY. The atrial connections of the specialized axis responsible for AV conduction. In: Mazgalev TN, Tchou PJ, Eds. Atrial-AV nodal electrophysiology: a view from the millennium. New York, Futura publishing company, Inc; 2000; 3-24.
38. Bharati S. Anatomic-morphologic relations between AV nodal structure and function in the normal and diseased heart. In: Mazgalev TN, Tchou PJ, Eds. Atrial-AV nodal electrophysiology: a view from the millennium. New York, Futura publishing company, Inc; 2000; 25-48.
39. Desplantez T, Dupont E, Severs NJ, Weingart R. Gap junction channels and cardiac impulse propagation. J Membr Biol 2007; 218: 13-28.
40. Petrecca K, Shrier A. Spatial distribution of ion channels, receptors, and innervation in the AV node. In: Mazgalev TN, Tchou PJ, Eds. Atrial-AV nodal electrophysiology: a view from the millennium. New York, Futura publishing company, Inc; 2000: 89-105.
41. Boyett MR, Inada S, Yoo S, et al. Connexins in the sinoatrial and atrioventricular nodes. Adv Cardiol 2006; 42: 175-97.
42. Li J, Greener ID, Inada S, et al. Computer three-dimensional reconstruction of the atrioventricular node. Circ Res 2008; 102: 975-85.
43. Choi YH, Stamm C, Hammer PE, et al. Cardiac conduction through engineered tissue. Am J Pathol 2006; 169: 72-85.
44. Bunch TJ, Mahapatra S, Bruce GK, et al. Impact of Transforming Growth Factor-β1 on atrioventricular node conduction modification by injected autologous fibroblasts in the canine heart. Circulation 2006; 113: 2485-94.
45. Hagège A, Marolleau J, Vilquin J, et al. Skeletal myoblast transplantation in ischemic heart failure: long-term follow-up of the first phase I cohort of patients. Circulation 2006; 114: 108-13.
46. Smits P, van Geuns R, Poldermans D, et al. Catheter-based intramyocardial injection of autologous skeletal myoblasts as a primary treatment of ischemic heart failure: clinical experience with sixmonth follow-up. J Am Coll Cardiol 2003; 42: 2063-9.
47. Mummery C, Ward-van Oostwaard D, Doevendans P, et al. Differentiation of human embryonic stem cells to cardiomyocytes: role of coculture with visceral endoderm-like cells. Circulation 2003; 107: 2733-40.
48. Yang HT, Tweedie D, Wang S, et al. The ryanodine receptor modulates the spontaneous beating rate of cardiomyocytes during development. Proc Natl Acad Sci USA. 2002; 99: 9225-30.
49. Abraham M, Henrikson C, Tung L, et al. Antiarrhythmic engineeringof skeletal myoblasts for cardiac transplantation. Circ Res 2005; 97: 159-67.
50. Beeres S, Atsma D, van der Laarse A, et al. Human adult bone marrow mesenchymal stem cells repair experimental conduction block in rat cardiomyocyte cultures. J Am Coll Cardiol 2005; 46: 1943-52.
51. van Veen TA, de Bakker JMT, van der Heyden MAG. Mesenchymal stem cells repair conduction block. J Am Coll Cardiol 2006; 48: 219-20.
52. Bearzi C, Rota M, Hosoda T, et al. Human cardiac stem cells. Proc Natl Acad Sci USA 2007; 104: 14068-73.
53. Urbanek K, Cesselli D, Rota M, et al. Stem cell niches in the adult mouse heart. Proc Natl Acad Sci USA 2006; 103: 9226-31.
54. Wu SM, Chien KR, Mummery C. Origins and fates of cardiovascular progenitor cells. Cell 2008; 132: 537-43.
55. de Boer TP, van Veen TAB, Jonsson MKB, et al. The functional electronome of cardiomyocytes differentiated from human cardiac progenitor cells. Heart Rhythm 2007; 4: S3.
56. Chen X, Wilson RM, Kubo H, et al. Adolescent feline heart contains a population of small, proliferative ventricular myocytes with immature physiological properties. Circ Res 2007; 100: 536-44.
57. Christman K, Lee R. Biomaterials for the treatment of myocardial infarction. J Am Coll Cardiol 2006; 48: 907-13.
58. Leor J, Aboulafia-Etzion S, Dar A, et al. Bioengineered cardiac grafts: A new approach to repair the infarcted myocardium? Circulation 2000; 102: 56-61.
59. Zimmermann WH, Melnychenko I, Wasmeier G, et al. Engineered heart tissue grafts improve systolic and diastolic function in infarcted rat hearts. Nat Med 2006; 12: 452-8.
60. Huang NF, Yu J, Sievers R, et al. Injectable biopolymers enhance angiogenesis after myocardial infarction. Tissue Eng 2005; 11: 1860-6.
61. Christman KL, Vardanian AJ, Fang Q, et al. Injectable fibrin scaffold improves cell transplant survival, reduces infarct expansion, and induces neovasculature formation in ischemic myocardium. J Am Coll Cardiol 2004; 44: 654-60.

62. Kofidis T, Lebl DR, Martinez EC, et al. Novel injectable bioartificial tissue facilitates targeted, less invasive, large-scale tissue restoration on the beating heart after myocardial injury. Circulation 2005; 112: 173-7.
63. Wilber DJ. Catheter ablation of ventricular tachycardia: two decades of progress. Heart Rhythm 2008; 5: S59-63.
64. Lubitz SA, Fischer A, Fuster V. Catheter ablation for atrial fibrillation. BMJ 2008; 336: 819-26.
65. Dhamoon AS, Jalife J. The inward rectifier current (IK1) controls cardiac excitability and is involved in arrhythmogenesis. Heart Rhythm 2005; 2: 316-24.
66. Dhamoon AS, Pandit SV, Sarmast F, et al. Unique Kir2.x properties determine regional and species differences in the cardiac inward rectifier K^+ current. Circ Res 2004; 94: 1332-9.
67. Plaster NM, Tawil R, Tristani-Firouzi M, et al. Mutations in Kir2.1 cause the developmental and episodic electrical phenotypes of Andersen's syndrome. Cell 2001; 105: 511-9.
68. Miake J, Marbán E, Nuss HB. Functional role of inward rectifier current in heart probed by Kir2.1 overexpression and dominantnegative suppression. J Clin Invest 2003; 111: 1529-36
69. Li J, McLerie M, Lopatin AN. Transgenic upregulation of IK1 in the mouse heart leads to multiple abnormalities of cardiac excitability. Am J Physiol Heart Circ Physiol 2004; 287: H2790-802.
70. Xia M, Jin Q, Bendahhou S, et al. A Kir2.1 gain-of-function mutation underlies familial atrial fibrillation. Biochem Biophys Res Comm 2005; 332: 1012-9.
71. Piao L, Li J, McLerie M, Lopatin AN. Transgenic upregulation of IK1 in the mouse heart is proarrhythmic. Basic Res Cardiol 2007; 102: 416-28.
72. Noujaim SF, Pandit SV, Berenfeld O, et al. Up-regulation of the inward rectifier K^+ current (IK1) in the mouse heart accelerates and stabilizes rotors. J Physiol 2007; 578: 315-26.
73. Sasano T, McDonald AD, Kikuchi K, Donahue JK. Molecular ablation of ventricular tachycardia after myocardial infarction. Nat Med 2006; 12: 1256-8.
74. de Boer TP, van Veen TAB, Houtman MJC, et al. Inhibition of cardiomyocytes automaticity by electrotonic application of inward rectifier current from Kir2.1 expressing cells. Med Biol Eng Comput 2006; 44: 537-43.
75. Yankelson L, Feld Y, Bressler-Stramer T, et al. Cell therapy for modification of the myocardial electrophysiological substrate. Circulation 2008; 117: 720-31.
76. Mikawa T, Hurtado R. Development of the cardiac conduction system. Semin Cell Dev Biol 2007; 18: 90-100.

CHAPTER 4

Computer 3D reconstruction of the canine atrioventricular conduction axis under physiologic and pathologic conditions

Computer three-dimensional reconstruction of the canine atrioventricular conduction axis under physiologic and pathologic conditions

A.C. Blank, L. van Stuijvenberg, D. van den Brink, E. van der Esch, R.A. de Weger, P. Loh, V.M. Christoffels, T. Delhaas, M.A. Vos, T.A.B. van Veen

Manuscript submitted

Department of Pediatric Cardiology, Wilhelmina Children's Hospital, University Medical Center Utrecht (UMCU), Utrecht, The Netherlands
AC Blank

Department of Medical Physiology, Division of Heart and Lungs, UMCU, Utrecht, The Netherlands
L van Stuijvenberg
MA Vos | TAB van Veen

Department of Pathology, UMCU, The Netherlands
D van den Brink
E van der Esch | RA de Weger

Department of Cardiology, Division of Heart & Lungs, UMCU, Utrecht, The Netherlands
P Loh

Department of Anatomy, Embryology and Physiology, Heart Failure Research Center, Academic Medical Center, Amsterdam, The Netherlands
VM Christoffels

Cardiovascular Research Institute Maastricht, Departments of Biomedical Engineering/Physiology, Maastricht University, Maastricht, The Netherlands
T Delhaas

Abstract

Background Recent studies in small animal models using immunohistochemistry, gene expression analysis and three-dimensional image processing, have deepened our understanding of the atrioventricular (AV) conduction axis. The dog could bridge the line of comparative anatomy from small animals to the human. The last extensive description of the canine AV conduction axis has been published decades ago, without the use of modern molecular and imaging-processing techniques.

Objective To provide an up-to-date description of the canine AV conduction axis under physiological and pathological conditions.

Methods Formalin-fixed and paraffin embedded tissue sections were derived from: (1) physiological/ normal AV junction, (2) AV junction in acquired complete AV block, (3) AV junction after ablation of AV node. The sections were stained with Masson's trichrome stain and van Gieson's stain, immunolabeled with antibodies against connexin 43, pan-cadherin and neurofilament, and in situ hybridized with probes against dog-specific mRNA encoding for gap junction-, ion channel-, and marker proteins. Digitalized 2D sections were transformed into interactive 3D models by surface rendering.

Results and conclusions This study refined the 2D histological structure of the canine AV conduction axis from earlier studies, proved that Cx43 is absent from the canine transitional zone, inferior nodal extensions, compact AV node and AV bundle. Thereby this study provides the first interactive 3D models of the canine AV conduction axis under physiological and pathological conditions.

Introduction

The atrioventricular (AV) conduction axis comprises the AV node, AV bundle and bundle branches. Since its first description by Tawara in 1906, especially the AV node has caused a lot of controversy about its location, structure and function. Species related differences and the use of non-uniform nomenclature also contributed to these controversies. In rodents, most of these matters have been resolved by recent studies using immunohistochemistry (IHC), gene expression analysis and three-dimensional (3D) image processing, sometimes combined with functional 3D imaging using microelectrodes or fluorescent dyes.[1-5]

These studies together demonstrate that the AV node is part of an extended tissue circuit that shares (and retains) the same embryological origin from AV canal myocardium.[1-5] Within that circuit the AV node connects two tissue rings around the atrioventricular valves, and receives dual electrical input: (1) fast, from the interatrial septum via a transitional zone and (2), slow from the atrial terminal crest via (right inferior) nodal extensions. However, all of these studies were conducted in small animal models, most commonly mouse[1,5] and rabbit[2-5], and comparable data for the human are lacking. The dog could bridge the line of comparative anatomy from small mammals to the human and is a commonly used experimental model in cardiac electrophysiology. Moreover, the last extensive descriptions of the canine AV conduction axis have been published decades ago[6-9], and data have been obtained without the use of modern molecular and image-processing techniques.

Therefore, the objective of this study was to provide an up-to-date description of the canine AV conduction axis under physiological and pathological conditions in order to bridge the line of comparative anatomy from small mammals to the human. Reconstruction of the AV conduction axis has been made using histology, IHC, gene expression analysis by in situ hybridization of dog-specific mRNA, and 3D image processing.

Glossary of abbreviations

A — artery
ABL — ablation
AM — ordinary atrial myocardium
AO — arteriole
Ao — aorta
AoV — aortic valve
AV — atrioventricular
CFB — central fibrous body
CN — compact AV node
Cx40 — connexin 40
Cx43 — connexin 43
Cx45 — connexin 45
DAB — diaminobenzidine
DIG — digoxigenin
G — ganglion
IHC — immunohistochemistry
IAS — interatrial septum
INE — inferior nodal extensions
ISH — in situ hybridization
IVC — inferior vena cava
IVS — interventricular septum
LA — left atrium
Lcx — left circumflex coronary artery
LMCA — left main coronary artery
LV — left ventricle
mRNA — messenger RNA
OF — oval fossa
PBS — phosphate buffered saline
RA — right atrium
RAA — right atrial appendage
RV — right ventricle
SVC — superior vena cava
Tbx3 — T-box factor
TT — tendon of Todaro
TV — tricuspid valve
TZ — transitional zone
V — vena
VM — ventricular myocardium
2/3D — two/three-dimensional

Methods

Tissue preparation

Six hearts from adult dogs were used. The hearts of dog 1-3 were used for 3D reconstruction. Their characteristics are presented in Table 1. The hearts of dog 4-6 were used for reference staining. Animal handling of all dogs was in accordance with the European Directive for the Protection of Vertebrate Animals Used for Experimental and Other Scientific Purposes (86/609/EU) and the Dutch Law on Animal Experimentation. The Committee for Experiments on Animals of the Utrecht University approved the use of the hearts. The heart of dog 2 was obtained from autopsy and provided by the Department of Animal Companions of Utrecht University.

Dog/heart/AV junction number	1	2	3
Dog	Beagle Weight: 14-16 kg Age: 1.6 year	Dachshund Weight: unknown Age: 11.2 year	Bastard Weight: 22.5 kg Age: 1 year
Number of sections	146	159	175
Thickness of sections (µm)	4	6	6
Mean distance of sections (µm)	115	121	120
Range of sections (µm)	52-340	48-252	81-153
Clinical information	Normal heart, sinus rhythm	Acquired complete heart block. Autopsy heart, provided by Department of Animal Companions	T0: Ablation of the AV node under electroanatomical guidance (Ensite NavX), complete heart block. RF ablation with 25 W, 30 seconds, approximately 50°C. T0+3 weeks: MRI and sacrifice

***Table 1*: Characteristics of the dogs used for 3D reconstruction.**

After rapid removal, the hearts (except from heart 2) were flushed with ice-cold Tyrode solution until the flushing solution became clear. To preserve normal cardiac architecture the whole hearts were fixed in 10% neutral buffered formalin for 3-5 days.

From the fixed hearts a rectangular tissue block of the AV junction was excised from the posterior border of the coronary sinus to the anterior edge of the septal leaflet of the tricuspid valve, containing ≈6 mm of atrial tissue and ≈12 mm of ventricular tissue.

The inferior margin was cut beneath the ostium of the coronary sinus. The tissue blocks were dehydrated, cleared and embedded in paraffin and sectioned serially on a microtome in 4 µm (heart 1) – 6 µm (heart 2 and 3) thick sections, parallel to the long axis (transverse or perpendicular plane) of the heart. From each 10 sections the first 3 or 4 sections were mounted. To prevent distortion all sections were uniformly mounted on

SuperFrost glass slides (Menzel-Gläser, Braunschweig, Germany) in the following manner: (1) placing the dry section on the glass slide, (2) hydration in aquadest during 5 min on a heated plate at ≈42 °C, (3) aspiration of water, (4) drying 1-2 hours on a heated plate at ≈33-35 °C followed by drying overnight in an incubator at 37°C.

Histology and immunohistochemistry

Histology: The sections were deparaffined, hydrated in a graded ethanol series, washed in PBS and subsequently stained with Masson's trichrome stain (Trichrome Staining Kit, HT15, Sigma-Aldrich) and van Gieson's stain. The Masson's trichrome stain was carried out with slightly adapted incubation times for phosphotungstic/phosphomolybdic acid (10 min.) and 1% acetic acid (5 min.). The van Gieson's staining was carried out using the automatic stainer Artisan Link Pro (Dako, www.dako.com). After staining, tissue sections were dehydrated through graded ethanols (70-100 %), cleared and sealed with a coverslip.

Immunohistochemistry: Sections were deparaffined, hydrated in a graded ethanol series and washed in PBS. Next, sections were heat pretreated with citrate buffer pH6, and endogenous peroxidase was blocked with 1.5% H2O2 in buffer. The sections were incubated with rabbit anti-rat connexin 43 (Cat.nr. 483000, Zymed) diluted 1:200 in PBS and pan-cadherin (Sigma), diluted 1:100; followed by Brightvision (poly-HRP goat-anti-mouse/rabbit/rat IgG, Immunologic). Finally signals were visualized with DAB, 3-3'diaminobenzidine tetrahydrochloride, (D5637, Sigma-Aldrich). Between incubations, the sections were washed in PBS/Tween. After counterstaining with haematoxylin, the sections were dehydrated through graded ethanols (70-100%), cleared and sealed with a coverslip.
Immunolabeling for neurofilament using mouse anti-human neurofilament (70 kD/200 kD pp)(MON 3004, Monosan) diluted 1:800 in PBS, was carried out using the BOND immunostainer (Leica, http://www.leicabiosystems.com) following the standard protocol.

In situ hybridization (ISH): For ISH, the method as described by Moorman *et al.*[10] was used. Briefly, the method includes: deparaffining, rehydration, proteolytic digestion, washing with glycine, re-fixation with paraformaldehyde, washing, prehybridization and hybridization with digoxigenin (DIG)-labeled probes against the following mRNAs connexin 40 (Cx40) and 45 (Cx45), T-box factor 3 (Tbx3), alpha subunit of sodium channel Nav1.5 and potassium/sodium hyperpolarization-activated cyclic nucleotide-gated channel 4 (Hcn4).
Probes were designed using the NCBI Dog genome (http://www.ncbi.nlm.nih.gov/genome/guide/dog/) and PrimerQuest (http://eu.idtdna.com/PrimerQuest/Home/Index). After hybridization and washing in formamide/SSC/PBS-Tween/buffer, the expressed RNA was visualized through staining with anti-DIG-alkaline phosphatase solution.

3D reconstruction

For 3D reconstructions, Masson's trichrome or van Gieson-stained sections with a mean distance of 115-121 µm were selected (distance in between two subsequent stained sections). The selected sections were digitalized by a digital slide scanner system (ScanScope, Aperio, Vista, CA, USA) at ≈0.5 µm resolution. From the digital color images a prede-

fined section of the scan was extracted with ImageScope software (version 11.0.2.780 for Windows; Aperio, Vista, CA, USA) and saved in JPEG format with a resolution reduced to 10% of the original image. The color images were split into RGB grayscale channels using Photoshop. The grayscale channel providing the best tissue contrast (red (R) in Masson's trichrome stained images, green (G) in van Gieson stained images) was used for further image processing. ThumbsPlus (version 8 SP1 for Windows, Cerious Software Inc., Charlotte, NC, USA) was used to crop all images to a standardized pixel size, inverting grayscale color and reducing image resolution further by 50%, resulting in a final pixel size of 10 µm.

The images were loaded into 3D visualization software Amira (version 5.3.4 for Windows, VSG, www.vsg3d.com) as Stacked Slices file format. This format allowed a stack of individual one-channel image files to be read with optional z- values for each slice. The z-value defined the position of an individual slice within a 3D stack. X- and y- values represented the voxel size and were determined by the image resolution and slice thickness. The images were aligned using the 'Least-squares' alignment mode and misaligned images were manually corrected. Based on morphological tissue characteristics[9,11-13], using the Segmentation Editor in Amira, the following structures were labeled: atrial myocardium, ventricular myocardium, fibro-fatty tissue (including the valves and the central fibrous body), compact AV node (CN), AV bundle with bundle branches, arteries and veins. However, morphological characteristics failed to identify the exact boundaries of the transitional zone (TZ) and of the inferior nodal extensions (INE).
Before creating a 3D surface all labels were resampled to obtain equal voxel dimensions, and smoothened. From these data sets Amira created corresponding polygonal surface models. Using Acrobat 3D (Adobe Systems, Inc.) surface models were converted into 3D PDF files. These 3D models are available as supplementary material.

Orientation

To facilitate comparison with the human, all views are shown in an, to the human, attitudinally appropriate manner[14], but attitudinally inappropriate for the dog.

Results

Dog/ AVJ 1: normal AV conduction axis

Gross anatomy, global position and arterial supply of the AV conduction axis

Figure 1A shows an illustration of the normal AV junction with its anatomical landmarks. The AV junction is viewed from the right side of the heart, after removal of the lateral walls of the right atrium and ventricle. After exposure of the AV junction the so-called triangle of Koch (marked in broken lines in Figure 1A-D) can be constructed by drawing a first line from the hinge point of the septal leaflet along the orifice of the tricuspid valve (= anterior border of the triangle of Koch), a second line from the hinge point of the septal leaflet to the posterior border of the ostium of the coronary sinus (= posterior border of the triangle of Koch), and a third (base) line, connecting the other two lines along the border of the ostium of the coronary sinus. The apex of the triangle of Koch is

drawn across a visible bulge of the right atrial surface (marked by a bullet (•) in Figure 1A-D), caused by the wedged position of the aorta into the base of the heart. This bulge begins approximately 5 mm above the ostium of the coronary sinus. As will be described later, the compact AV node is situated just inferior to that bulge. Figure 1B depicts the wedged position of the aorta and the origin of the left main coronary artery and its bifurcation into the left circumflex coronary artery (marked by arrows). From the AV junction a tissue block (see photo composition in Figure 1A and 1B) can be excised, containing

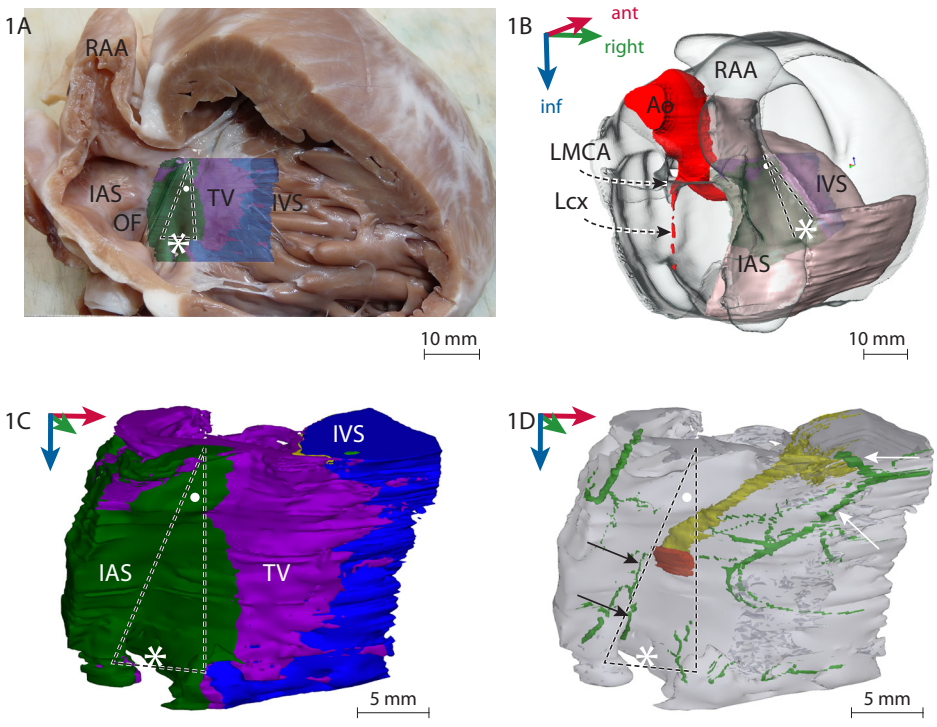

Figure 1

1A: Photograph of the canine AV junction showing the anatomical landmarks and the position of the excised and reconstructed tissue block. The broken lines on the tissue block mark the margins of the triangle of Koch, with in its base the ostium of coronary sinus (*). The bullet (•) marks a bulge caused by the aortic root. **1B**: 3D reconstruction from 2D MRI slices showing the position of the excised and reconstructed tissue block. The aorta (red) is wedged into the base of the heart. The tissue walls of the atrioventricular junction are colored light brown. Arrows mark the origin of the left main coronary artery and its bifurcation into the left circumflex coronary artery. **1C**: 3D reconstruction (an interactive 3D PDF is available in the supplementary material) of the excised tissue block containing the AV conduction axis: atrial myocardium (green), fibro-fatty tissue (purple), ventricular myocardium (blue). The broken lines mark the margins of the triangle of Koch, with in its base the ostium of coronary sinus (*). The bullet (•) marks a bulge caused by the aortic root. **1D**: 3D reconstruction of the AV conduction axis: compact AV node (red), AV bundle and bundle branches (yellow) and its arterial supply (green): black arrows assign the terminal branch of the left circumflex coronary artery, white arrows point at terminal branches of the septal artery (from left anterior descending or left main coronary artery).

Abbreviations: Ao- aorta, OF- oval fossa, IAS- interatrial septum, IVS- interventricular septum, Lcx- left circumflex coronary artery, LMCA- left main coronary artery, RAA- right atrial appendage, TV- tricuspid valve

the components of the AV conduction axis. Figure 1C shows a 3D reconstruction of this tissue block with atrial (working) myocardium (labeled green), ventricular myocardium (labeled blue), and fibro-fatty tissue (labeled purple). After virtual removal of these tissues in the 3D reconstruction, the AV conduction axis becomes visible. An interactive 3D PDF is available in the supplementary material. Figure 1D depicts the position and course of the AV conduction axis: the compact AV node lies in the center of the triangle of Koch, approximately 5 mm above the ostium of the coronary sinus, and just inferior to the bulge caused by the (wedged) aortic root (marked by a bullet). The AV bundle rises superiorly along the crest of the ventricular septum and divides into the left and right bundle branches. Figure 1D also shows the dual arterial supply of AV conduction system as described first by Lumb[16] and illustrated by Woods.[17] The compact AV node is supplied by a terminal branch of the left circumflex artery (marked by black arrows).
The AV bundle and the bundle branches are supplied by terminal branches of the septal artery (from the left main coronary artery or the left anterior descending coronary artery; marked by white arrows).

Structure of the atrial part of the AV conduction axis

Figure 2 illustrates the histology of the atrial part of the AV conduction axis. The tendon of Todaro (TT) forms a prominent orientation point. There are variable amounts of fatty tissue around the tendon (Figure 2A). Transverse cut ordinary atrial myofibers, covered in a perimysium from collagen, approach the tendon from the left, posterior and the right. These ordinary atrial working myofibers are (weakly) positive for Cx43 (Figure 2d). Around the anterior part of the tendon of Todaro the transverse cut ordinary atrial myofibers make contact with transverse cut myofibers of the transitional zone. The amount of collagen becomes more extensive and the pattern more irregular. From the right, longitudinally cut myofibers of the INE approach the transitional zone. The myofibers of the transitional zone (Figure 2d and 3h) and the INE (Figure 3d) are negative for Cx43. All myofibers enter/contact the superior part of the compact AV node from posterior (broken arrows in Figure 2B). The compact AV node lies approximately 0.5-1 mm underneath the right atrial endocardial surface and measures in superior-inferior direction: 1.5 mm, in anterior-posterior direction 0.6 mm, left-right direction 1.5 mm. In the compact AV node transversely cut myofibers intermingle with longitudinally cut fibers, causing a 'twisted' appearance (Figure 2B). This 'twisted' appearance becomes particularly clear after pan-cadherin labeling (Figure 2a, 3a and 3c; high-resolution images are available in the supplementary material, details are best observed after magnification). Positive pan-cadherin labeling (dark brown) indicates the presence of sparse adherens junctions (marked by arrows) in between the cardiomyocytes (aspecifically light brown stained) which are imbedded into a matrix of mesenchymal cells (light blue stained), nerve fibers (neurofilament positive, Figure 2e) and collagen (red in the van Gieson's stain, Figure 2A-C). Despite the presence of adherens junctions the compact AV node is negative for Cx43 (Figure 2b, 3b and 3d, high-resolution images are available in the supplementary material, details are best observed after magnification). The cardiomyocytes of the compact AV node are thinner and shorter than ordinary atrial and ventricular cardiomyocytes and show a rounded nucleus. The nuclei of the mesenchymal cells are smaller, more irregular and more elongated. The compact AV node has no own main artery supply.

2A. Overview

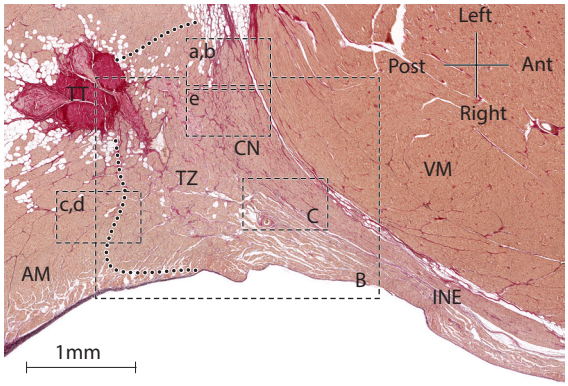

2B. Compact AV node-gross histology

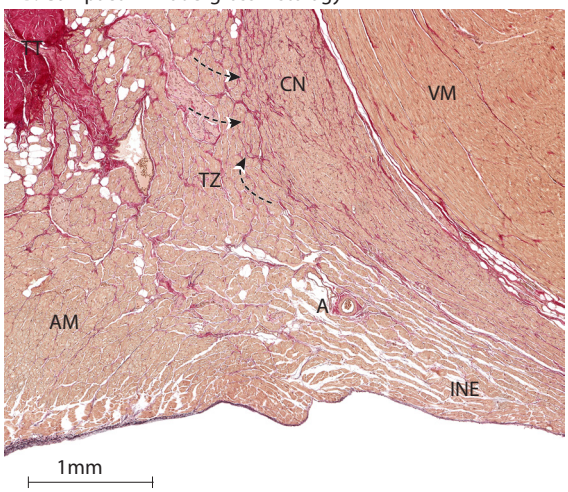

2C. Compact AV node-fine histology

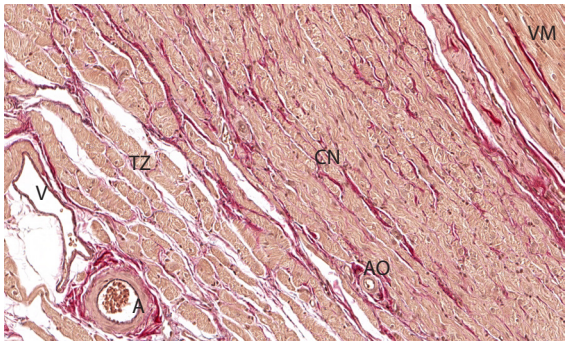

2a. Compact AV node-Cadh

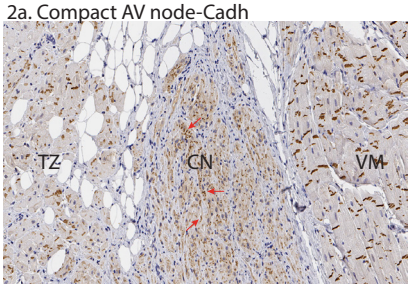

2b. Compact AV node-Cx43

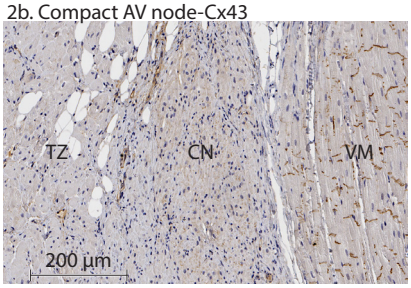

2c. Atrial myocardium/transitional zone-Cadh

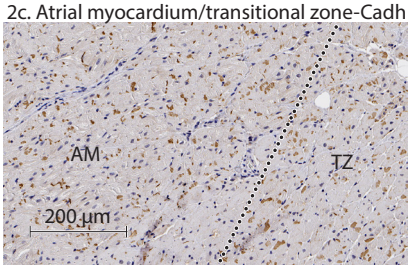

2d. Atrial myocardium/transitional zone-Cx43

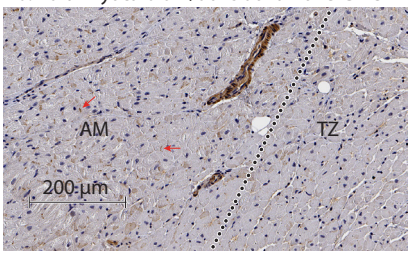

2e. Compact AV node-Neurofilament

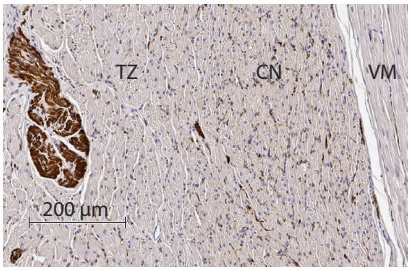

Figure 2 *—see previous page*
2A. Overview: Transverse section through the compact AV node (van Gieson's stain: collagen (red), cytoplasm (yellow)). The broken lines mark the approximate position of magnifications 2B, 2C and 2a-e. The dotted lines mark the approximate border between Cx43 (weak-) positive ordinary atrial myocardium and Cx43 negative transitional zone.
2B. Compact AV node – gross histology: van Gieson's stain magnification of the compact AV node, transitional zone and inferior nodal extensions. The broken lines with arrow depict the place and direction of myofiber input into the compact node.
2C. Compact AV node – fine histology: van Gieson's stain magnification showing the cardiomyocyte and myofiber structure of the transitional zone and compact AV node.
2a. Compact AV node - Cadh: IHC Cadherin labeling (dark brown); the cardiomyocytes of the transitional zone and ventricular myocardium show abundant adherens junctions, the cardiomyocytes of the compact node show sparse adherens junctions (marked by arrows) and are are imbedded into a matrix of mesenchymal cells and collagen. High-resolution images are available in the supplementary material, details are best observed after magnification,
2b. Compact AV node – Cx43: IHC Cx43 labeling (dark brown); the transitional zone and the compact node show no Cx43 co-localization at the adherens junctions, the ventricular myocardium shows strong Cx43 co-localization.
2c. Atrial myocardium/ transitional zone - Cadh: IHC Cadherin labeling (dark brown); the ordinary atrial myocardium and the transitional zone show abundant adherens junctions. The dotted line marks the approximate border between the Cx43 (weak-)positive ordinary atrial myocardium and Cx43 negative transitional zone.
2d. Atrial myocardium/ transitional zone – Cx43: IHC Cx43 labeling (dark brown); the ordinary atrial myocardium shows some weak Cx43 co-localization at the junctions (marked by arrows), the transitional zone shows no Cx43 co-localization. The dotted line marks the approximate border between the Cx43 (weak-) positive ordinary atrial myocardium and Cx43 negative transitional zone.
2e. Compact AV node – Neurofilament: IHC Neurofilament labeling (dark brown); there are abundant nerve fibers (brown) and some neuronal cells (dark brown) present within the compact AV node; also the transitional zone shows many (albeit less than the compact node) nerve fibers, some neuronal cells and a ganglion.
Abbreviations: A- artery, AO- arteriole, AM- ordinary atrial myocardium, CN- compact AV node, G- ganglion, INE- inferior nodal extensions, TZ- transitional zone, TT- tendon of Todaro, V- vena, VM- ventricular myocardium

Instead, there are small arterioles seen (Figure 2C), branching from arteries within the transitional zone. As described earlier, these arteries stem from terminal branches of the left circumflex coronary artery (black arrows in Figure 1D). The compact AV node is richly innervated (see Figure 2e). There are ganglia present in the transitional zone (see Figure 2e) and around the tendon of Todaro.

3a. Compact AV node-Cadh

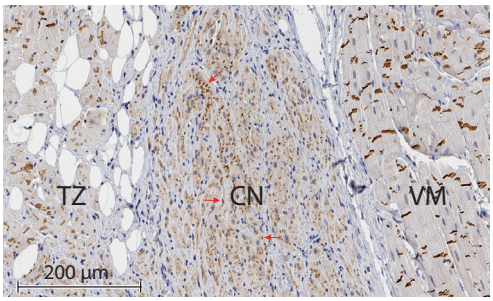

3b. Compact AV node-Cx43

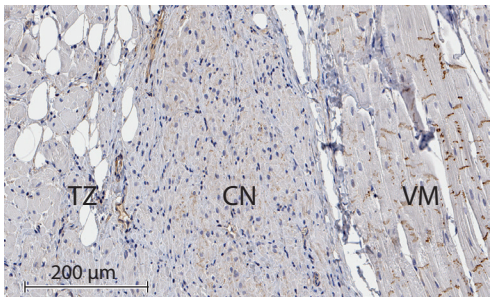

3c. Compact AV node and INE-Cadh

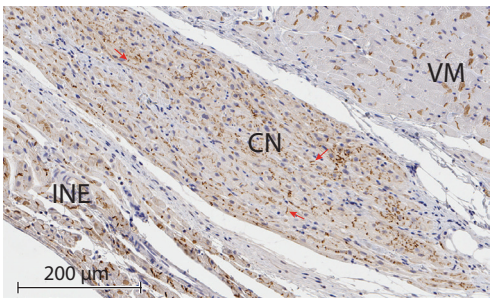

3d. Compact AV node and INE-Cx43

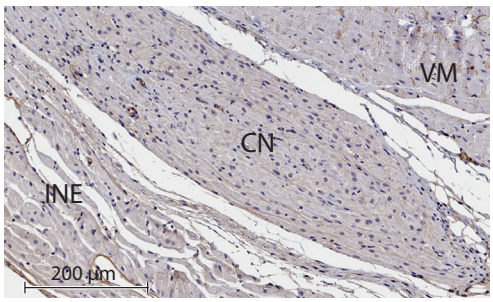

3e. Penetrating AV bundle-Cadh

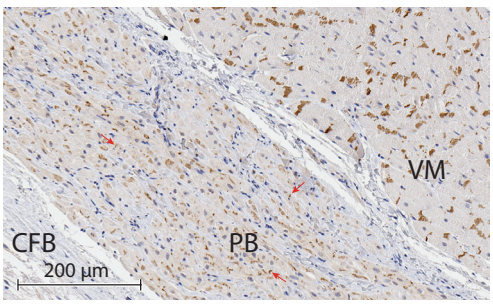

3f. Penetrating AV bundle-Cx43

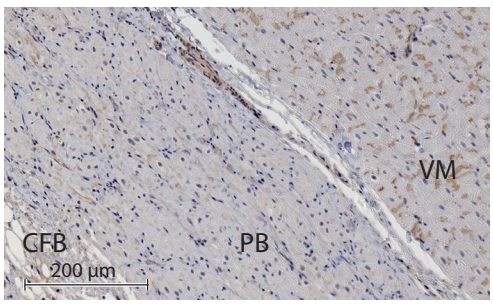

3g. Atrial myocardium and transitional zone-Cadh

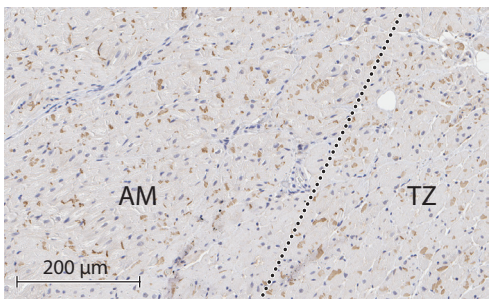

3h. Atrial myocardium and transitional zone-Cx43

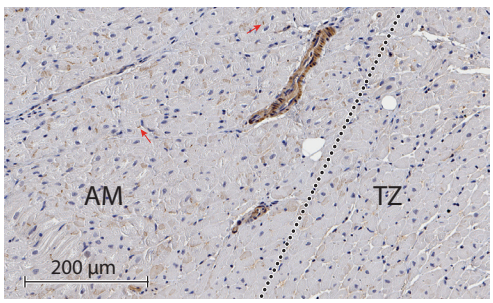

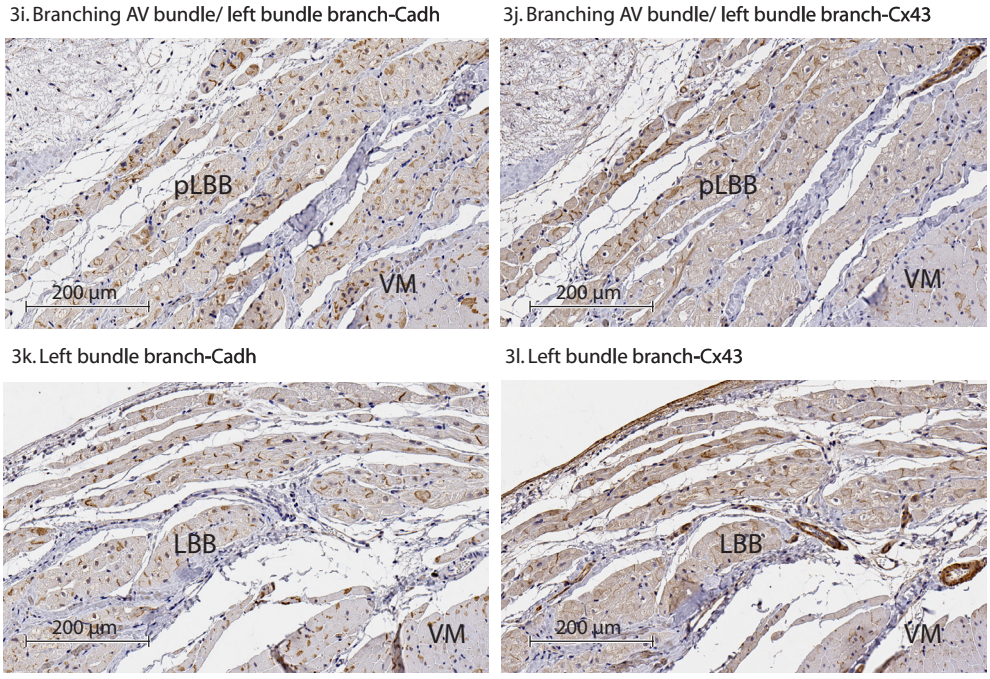

***Figure 3*: Source-sink and pacemaking concept.** A. Source-sink. Schematic representation of a strip of cardiac ventricular myocytes coupled by gap junctions to non-excitable cells, like undifferentiated mesenchymal or embryonic stem cells. The action potential (originating from the the non-depicted SA node to the left) is propagated from cardiomyocyte to cardiomyocyte, each time re-established by ion channels expressed in the cell itself. Upon coupling to the non-excitable stem cells, the action potential fades, resulting in block of action potential propagation. B. Pacemaking. A cluster of spontaneous active stem cell derived cardiomyocytes is coupled by gap junctions to ventricular cardiac myocytes. When the frequency of action potential formation exceeds that of the non-depicted SA node, the cluster propagates the action potential to the ventricular cells resulting in ectopic pacemaking.

AV bundle and bundle branches

The AV bundle is the direct continuity of the superior compact AV node when it enters the central fibrous body. Since the aorta is wedged from the left on the interventricular septum, the AV bundle runs a bit more on the right side of the crest of the interventricular septum. This causes a V-shape of the AV bundle. The proximal AV bundle runs in close relationship with the non-coronary cusp of the aortic valve. The distal and branching AV bundle runs in close relation with right- coronary cusp of the aortic valve.

The non-branching part of the AV bundle measures approximately 7 mm, the branching part 3 mm. First branches go to the left (left bundle branch). The left bundle branches fan-like, the right bundle branches cord like.[15] The penetrating AV bundle is negative for Cx43 (Figure 3f). The branching AV bundle is weakly positive for Cx43 (Figure 3j). In the bundle branches, the outer myofibers are stronger positive for Cx43 than the deeper fibers (Figure 3j and 3l). Labeling of pan-cadherin on sections serial to the ones used for labeling of Cx43 indicates the actual presence of adherens junctions in between the cardiomyocytes in the respective area's (Figure 3e, 3g, 3i and 3k, high-resolution images are available in the supplementary material, details are best observed after magnification).

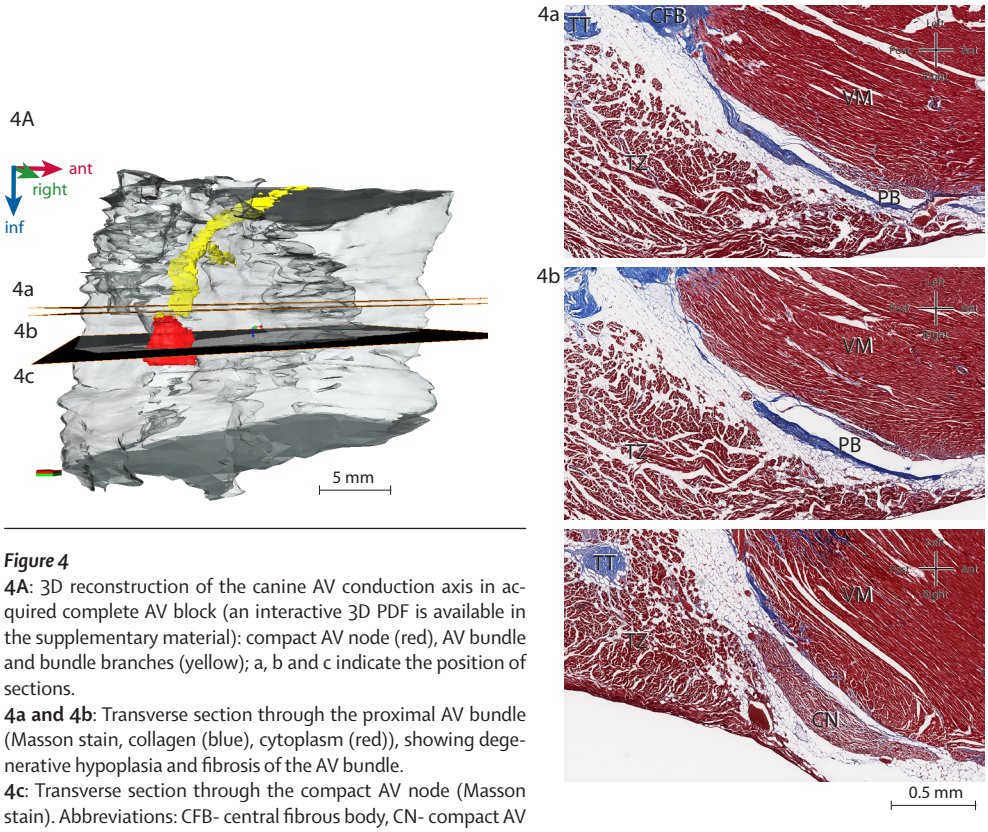

Figure 4
4A: 3D reconstruction of the canine AV conduction axis in acquired complete AV block (an interactive 3D PDF is available in the supplementary material): compact AV node (red), AV bundle and bundle branches (yellow); a, b and c indicate the position of sections.
4a and 4b: Transverse section through the proximal AV bundle (Masson stain, collagen (blue), cytoplasm (red)), showing degenerative hypoplasia and fibrosis of the AV bundle.
4c: Transverse section through the compact AV node (Masson stain). Abbreviations: CFB- central fibrous body, CN- compact AV node, TT- tendon of Todaro, TZ- transitional zone, VM- ventricular myocardium

Dog/ AVJ 2: AV conduction axis in acquired complete AV block

Global and fine composition of the AV conduction axis in acquired complete AV block

The position of the AV conduction axis of this dog with acquired complete AV block is similar to that in the healthy dog. Also, all components of the AV conduction axis are present. However, conventional histology from serial sections revealed degenerative hypoplasia and fibrosis of a small segment (≈750 µm) of the proximal penetrating AV bundle (Figure 4a and 4b) leading to its interruption.

Dog/ AVJ 3: AV conduction axis after AV nodal ablation

Global and fine composition of the AV conduction axis in complete AV block after AV nodal ablation

Figure 5A-5C show the (remnants of the) AV conduction axis after ablation of the AV node. The ablation caused a fibrotic lesion (marked with an asterisk (*) in Figure 5A-5C, 5a and 5E) with maximum dimensions of about 5.5 x 6.5 x 6.5 mm, replacing ordinary atrial myocardium, the transitional zone, the compact AV node and the most proximal part of the AV bundle.

Discussion

This study provided the first 3D reconstruction of the canine AV conduction axis under physiologic and pathologic conditions by digitally labeling its major components in 2D histological sections and transforming them into interactive 3D models by surface rendering. The thus obtained 3D models were used to illustrate the positions of sections that provided details of the cellular and molecular structure of the AV conduction axis. In the following, these details are discussed in the light of current knowledge of the AV conduction axis, with the focus on its most complex part, the AV node. The AV node consists of multiple components (compact AV node, transitional zone and nodal extensions) and different cell types with distinctive gene expression profiles.[18] The function of the AV node is determined by: cell size and shape, microscopic tissue structure, expression of ion channels and cell-to-cell coupling.[19]

Because structure is the determinant of function, and because of the complexity of the AV node, we need accurate knowledge of 3D structure on tissue, cellular and molecular level. Histology offers the best combination of resolution and discrimination of cellular and subcellular structures.[20] It involves tissue fixation and embedding. Studies so far have used different techniques for fixation and embedding. Since each technique has advantages and disadvantages, there is no consensus about the techniques obtaining best results. In our opinion, earlier studies providing excellent histology used paraffin[4,9,13], or paraplast[1] embedding. By using formalin fixation and paraffin embedding, the histological quality of this study could compare with those earlier studies. Tawara[13] was the first to describe the histology of the AV node and its position in the AV conduction axis in different species, including dog and human. Baird and Robb[12] were the first that provided a 3D reconstruction of the canine AV conduction axis by modeling its structure from beeswax. James[11] described the detailed (2D) histology of the canine AV conduction axis, and Ho[9] compared it to the human. Overall, we confirmed the (2D) histologic results from the above-mentioned studies: an oval compact AV node, measuring 1.5 x 1.5 x 0.6 mm (in James[11]: 2 x 2 x 0.5-1 mm, in Ho[9]: 1-1.5 mm), is in continuity with an AV bundle, that branches after a course of 7 mm (in James[11]: 1-3 mm) over a range of 3 mm (in James[11]: 3-4 mm), into a fan-like[15] left bundle branch and a cord-like[15] right bundle branch. However, the 3D reconstruction from 2D histology provided extra benefit: it enhanced mental and visual understanding of the region and improved the identification of the compact AV node. Tawara[13] assigned the compact node on the atrial part of the AV junction. From the point that the compact node was entering the central fibrous body he

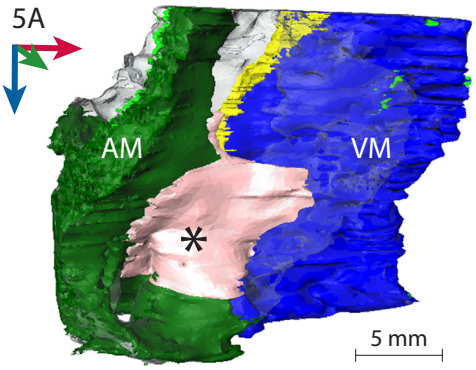
5A
AM
VM
5 mm

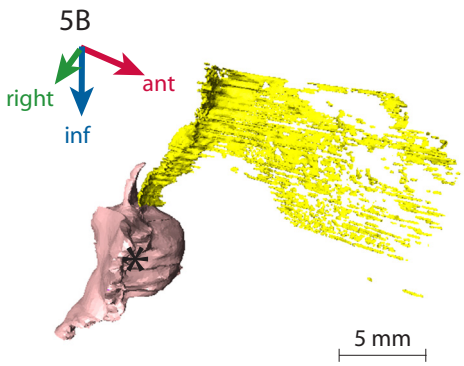
5B
right
ant
inf
5 mm

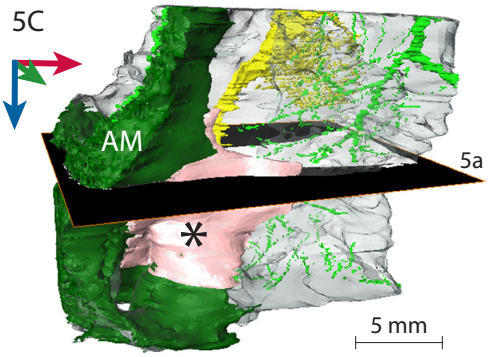
5C
AM
5a
5 mm

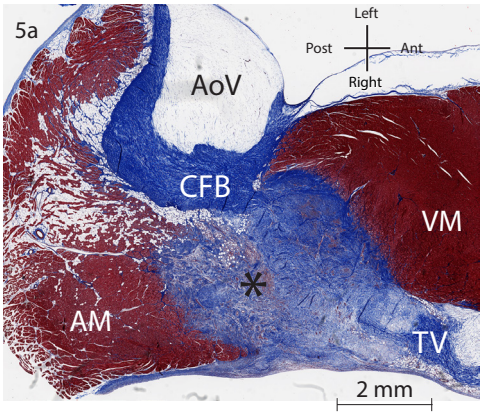
5a
Left
Post
Ant
Right
AoV
CFB
VM
AM
TV
2 mm

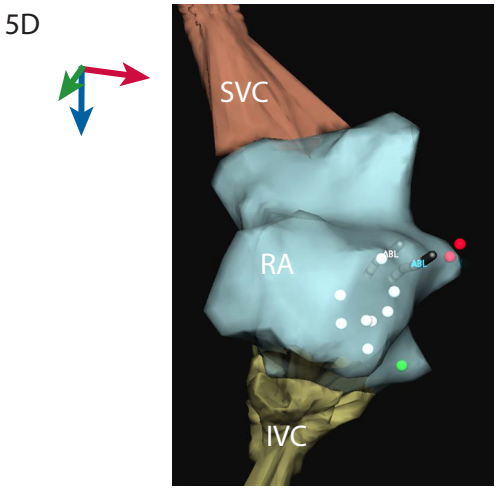
5D
SVC
RA
IVC

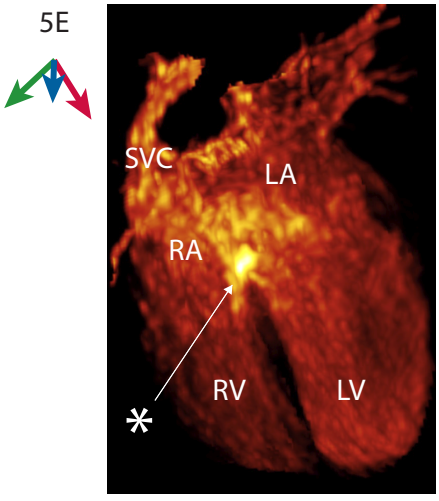
5E
SVC
LA
RA
RV
LV

Figure 5 *—see previous page*
5A: 3D reconstruction of the ablated canine AV conduction axis (an interactive 3D PDF is available in the supplementary material): atrial myocardium (dark green), ablation lesion (pink, marked with a black asterisk (*)), AV bundle and bundle branches (yellow) and ventricular myocardium (blue).
5B: 3D reconstruction of the ablated canine AV conduction axis with atrial en ventricular myocardium removed: ablation lesion (pink, marked with a black asterisk (*)), remaining AV bundle and bundle branches (yellow).
5C: 3D reconstruction of the ablated canine AV conduction axis: atrial myocardium (dark green), ablation lesion (pink, marked with a black asterisk (*)), AV bundle and bundle branches (yellow), arterial supply (light green); a. indicates the position of the section.
5a: Transverse section showing the ablation lesion (marked with a black asterisk (*)), Masson stain, collagen (blue) and cytoplasm (red).
5D: Electroanatomical 3D surface reconstruction (Ensite NavX) from ablation procedure: superior vena cava (brown), inferior vena cava (olive green), right atrium (grey), white spots mark tricuspid valve annulus, red spots mark localization of His potential, green spot mark the ostium of coronary sinus.
5E: 3D surface rendering of gadolinium-enhanced MRI showing the ablation lesion (assigned by a white arrow and a white asterisk (*)).
Abbreviations: ABL- ablation, AM- atrial myocardium, AoV- aortic valve, CFB- central fibrous body, CN- compact AV node, IVC- inferior vena cava, LA- left atrium, LV- left ventricle, RA- right atrium, RV- right ventricle, SVC- superior vena cava, TV- tricuspid valve, VM- ventricular myocardium)

called it AV bundle. Thus, before the labeling of the compact AV node in 2D we labeled the central fibrous body first and used its 3D reconstruction to assign the compact node. Ignoring the original definition by Tawara can result in a non-uniform nomenclature, creating indistinctness and controversy (as occurred by the studies of Racker[8,21], that assigned the compact node within the central fibrous body and coined a 'new' structure called proximal AV bundle on the atrial side of the AV junction; triggering arguments by Ho[9] and Anderson[22]).

Unfortunately, excellent histology and adherence to a uniform nomenclature alone are unfit to unravel the complex structure-function relation of the AV node, and additional techniques are needed. IHC has been applied to study the membrane expression of gap junction and ion channel proteins within the AV node. However, its use is hampered by the availability of specific antibodies that recognize these proteins in the dog. From the cardiac gap junction and ion channel proteins, this study found only an antibody against the gap junction protein Cx43 working on the (formalin-fixed and paraffin-embedded) tissue. Although Cx43 is the major cardiac connexin, its expression is limited within the AV conduction system (see recent review by Dobrzynski15). In humans and small animals Cx43 is largely absent in the compact AV node.[15] In the rat also the nodal extensions, transitional zone and AV bundle show no[23] or very low[5] expression of Cx43. Our study showed that this also holds for the dog. In the rabbit and the human Cx43 is largely absent from the nodal extensions, reduced in the transitional zone and expressed in the lower AV bundle (i.e. the first, most proximal part of the bundle).[15]

Theoretically, the lack of specific antibodies for application of IHC can be circumvented by other molecular techniques studying the regional gene expression. Recent earlier studies analyzed the expression of genes encoding for structural markers, gap junctions, ion channels and calcium handling within the different components of the AV conduction system in mice[1], rabbits[2] and humans[24] by quantitative polymerase chain reaction or in situ expression of mRNA (= in situ hybridization (ISH)). Albeit our ISH-technique wor-

ked on short-fixed tissue on a gene product with a high copy number (i.e. myosin heavy chain), the obtained labeling was too weak to work for genes with a smaller copy number or on specimen that required extensive periods of fixation (like our specimen), thus we abandoned this technique.

One appeal of this study is that it provided direct 3D visualization of the AV conduction axis during pathologic conditions. The 3D model of acquired complete AV block illustrates why routine pathologic examination of AV block (during autopsy) requires the microscopic evaluation of the tissue containing the AV conduction system on multiple levels.[26] The degenerative changes described in this case were restricted to such a small segment of the AV bundle that it might have escaped from routine examination.
Another 3D model showed the fibrotic lesion and the (remnants of the) AV conduction axis after radio-frequency ablation of the AV node. Although (cardiac) fibrosis can be visualized noninvasively by gadolinium-enhanced magnetic resonance imaging (Figure 5E), the visualization is only indirect[27] and the resolution limited.
The objective of this study was to bridge the line from recent elegant studies that analyzed the cellular and molecular 3D structure (sometimes even function) of the AV conduction axis in small animals to the human. Due to technical limitations this objective has only partly been realized. Nevertheless, it should be the aim of future research to overcome these difficulties because we, as others[20], are convinced that the unraveling of the complex structure-function relationship of the AV conduction axis (especially of the AV node) requires accurate knowledge of its 3D structure and function at multiple scales from cellular, subcellular to molecular level[20]; in all animal models used, up to the human itself.

Study limitations

Analysis of histological data can be affected to a certain degree by the fact that the experimentator has to face potential tissue distortion during fixation, dehydration, paraffin embedding, cutting and mounting.[20]

Conclusion

In conclusion, this study confirmed the 2D histological structure of the canine AV conduction axis from earlier studies, proved that Cx43 is absent from the canine transitional zone, INE, compact AV node and AV bundle and provided the first interactive 3D models of the canine AV conduction axis under physiologic and pathologic conditions. These models were used to illustrate positions of detailed histological and IHC sections.

Acknowledgements

We thank J. Hagoort, A. Sizarov MD PhD, G. van den Berg MD PhD, for assistance with Amira; A.F. Moorman and J.D.M. Beekman for support; T.I.G. van der Spoel for providing assistance for MRI; and V. Szatmari for providing dog heart 2.

References

1. Aanhaanen WTJ, Mommersteeg MTM, Norden J, et al. Developmental origin, growth, and three-dimensional architecture of the atrioventricular conduction axis of the mouse heart. Circulation Res 2010; 107: 728-736.
2. Greener ID, Tellez JO, Dobrzynski H, et al. Ion channel transcript expression at the rabbit atrioventricular conduction axis. Circ Arrh Electrophysiol 2009; 2: 305-315.
3. Ko Y-S, Yeh H-I, Ko Y-L, et al. Three-dimensional reconstruction of the rabbit atrioventricular conduction axis by combining histological, desmin, and connexin mapping data. Circulation 2004; 109: 1172-1179.
4. Li J, Greener ID, Inada S, et al. Computer three-dimensional reconstruction of the atrioventricular node. Circulation Res 2008; 102: 975-985.
5. Yanni J, Boyett MR, Anderson RH, Dobrzynski H. The extent of the specialized atrioventricular ring tissues. Heart Rhythm 2009; 6: 672-680.
6. Racker DK. The AV junction region of the heart: a comprehensive study correlating gross anatomy and direct three-dimensional analysis. Part II. Morphology and cytoarchitecture. Am J Physiol Heart Circ Physiol 2004; 286: H1853-1871.
7. Racker DK, Kadish AH. Proximal atrioventricular bundle, atrioventricular node, and distal atrioventricular bundle are distinct anatomic structures with unique histological characteristics and innervation. Circulation 2000; 101: 1049-1059.
8. Racker DK. The AV junction region of the heart: a comprehensive study correlating gross anatomy and direct three-dimensional analysis. Part I. Architecture and topography. Anat Rec 1999;256:49-63.
9. Ho SY, Kilpatrick L, Kanai T, Germroth PG, Thompson RP, Anderson RH. The architecture of the atrioventricular conduction axis in dog compared to man: its significance to ablation of the atrioventricular nodal approaches. J Cardiovasc Electrophysiol 1995; 6: 26-39.
10. Moorman AF, Houweling AC, de Boer PA, Christoffels VM. Sensitive nonradioactive detection of mRNA in tissue sections: novel application of the whole-mount in situ hybridization protocol. J Histochem Cytochem 2001;49:1-8.
11. James TN. Anatomy of the A-V node of the dog. Anat Rec 1964; 148: 15-27.
12. Baird JA, Robb JS. Study, reconstruction and gross dissection of the atrioventricular conducting system of the dog heart. Anat Rec 1950; 108: 747-763.
13. Tawara S. Das Reizleitungssystem des Säugetierherzens. Reprint 1906: 229.
14. Anderson RH, Yanni J, Boyett MR, Chandler NJ, Dobrzynski H. The anatomy of the cardiac conduction system. Clinical anatomy (New York, NY) 2009;22:99-113.
15. Dobrzynski H, Anderson RH, Atkinson A, et al. Structure, function and clinical relevance of the cardiac conduction system, including the atrioventricular ring and outflow tract tissues. Pharmacol Ther 2013; 139: 260-288.
16. Lumb G, Shacklett RS, Dawkins WA. The cardiac conduction tissue and its blood supply in the dog. Am J Pathol 1959; 35: 467-487.
17. Woods WT, Sherf L, James TN. Structure and function of specific regions in the canine atrioventricular node. Am J Physiol 1982; 243: H41-50.
18. Christoffels VM, Smits GJ, Kispert A, Moorman AFM. Development of the Pacemaker Tissues of the Heart. Circulation Res 2010; 106: 240-254.
19. Kléber AG. Gap junctions and conduction of cardiac excitation. Heart Rhythm 2011; 8: 1981-1984.
20. Matthew Gibb. LNBI 7605 - Resolving the three-Dimensional histology of the heart 2012: 1-15.
21. Racker DK. Atrioventricular node and input pathways: a correlated gross anatomical and histological study of the canine atrioventricular junctional region. Anat Rec 1989; 224: 336-354.
22. Anderson RH, Ho SY, Becker AE. Anatomy of the human atrioventricular junctions revisited. Anat Rec 2000; 260: 81-91.
23. Yoo S. The sophisticated architecture of the rat atrioventricular node. 2005: 432.
24. Greener ID, Monfredi O, Inada S, et al. Molecular architecture of the human specialised atrioventricular conduction axis. J Mol Cell Cardiol 2011; 50: 642-651.

25. Farragher SM, Tanney A, Kennedy RD, Paul Harkin D. RNA expression analysis from formalin fixed paraffin embedded tissues. Histochem Cell Biol 2008; 130: 435-445.
26. Waters BL. Handbook of Autopsy Practice. Springer, 2010: 608.
27. de Jong S, van Veen TAB, van Rijen HVM, de Bakker JMT. Fibrosis and cardiac arrhythmias. J Cardiovasc Pharmacol 2011; 57: 630-638.

CHAPTER 5

Stem cell therapy to restore conduction in a dog model of complete AV block

Stem cell therapy to restore conduction in a dog model of complete AV block

A.C. Blank, B. Paylor, L. van Stuijvenberg, F. Wegman, H.D.M. Beekman, M.K.B. Jonsson, M.J. Goumans, M.A. Vos, T.A.B. van Veen

Manuscript to be submitted

Department of Pediatric Cardiology, Wilhelmina Children's Hospital, University Medical Center Utrecht (UMCU), Utrecht, The Netherlands
AC Blank

Department of Medical Physiology, Division of Heart and Lungs, UMCU, Utrecht, The Netherlands
B Paylor
L van Stuijvenberg
F Wegman
HDM Beegman
MKB Jonsson
MA Vos
TAB van Veen

Department of Cardiology, Division of Heart & Lungs, UMCU, Utrecht, The Netherlands
MJ Goumans

Abstract

Background Cell therapy is considered as a promising clinical tool for repairing damaged myocardium. In earlier studies, with some success, lost myocardium has partially been replaced by transplantation of cardiac progenitor cells (CPCs). Additionally, it has been shown that transplantation of mesenchymal stem cells (MSCs) might improve the microenvironment of the diseased myocardium by promoting angiogenesis and survival of host cardiomyocytes. Our group has previously isolated Sca-1 expressing CPCs from fetal and adult human hearts. Upon treatment with 5-azacytidine and TGF-beta1 these CPCs could be differentiated into functional cardiomyocytes. By using a dog model of complete atrioventricular block (CAVB) we hypothesized that injection of CPCs or MSCs might be able to restore the compromised AV conduction.

Methods CAVB was induced by catheter ablation in dogs. Heart tissue was used to isolate canine CPCs using Sca-1-coupled magnetic beads. Canine MSCs were isolated from fat tissue and bone marrow. Three weeks after ablation cells (human CPCs in 7 dogs, canine CPCs in 3 dogs, canine MSCs in 1 dog) were injected into the damaged AV conduction system.

Results and conclusions Transplantation of human/canine CPCs or canine MSCs had no effect on the blocked AV conduction. Histopathological examination revealed only sporadic vital transplanted cells in the injection region. Thus, despite aggressive treatment with immunosuppressive therapy, we assume that the cells do not survive long enough after transplantation.

Introduction

In the pediatric age group complete atrioventricular block (CAVB) is the main indication for implantation of a pacemaker. CAVB is predominantly caused by surgically or maternal autoantibody induced damage of the atrioventricular (AV) conduction system. Because pediatric cardiac surgery is nowadays performed at younger age and in more complex heart defects, a growing percentage of patients is expected to require a pacemaker.[1] Due to growth and a more active lifestyle, the pacing system in pediatric patients is more prone to complications as infection, erosion, fracture and dislodgment requiring frequent reoperations.[1] Depleted pacemaker batteries also have to be replaced regularly. Moreover long term right ventricular pacing can result in electromechanical dyssynchrony, leading to adverse LV remodeling with LV dilatation and asymmetric hypertrophy.[1-3] Up to 30% of patients develop dilated cardiomyopathy[4], and 5% to 10% develop heart failure.[3]

A more causative therapy of the damaged AV conduction system may offer an alternative to cardiac pacing. In general, stem cell therapy is considered as a promising clinical tool for repairing diseased hearts. Stem cells are undifferentiated cells with the ability to differentiate into multiple lineages and as such regenerate a given tissue. Because the heart classically has been considered as a terminally differentiated organ without self-regenerating capacity, the search for stem cell sources capable to differentiate into functional cardiomyocytes for a long period of time has been focused on origins outside the heart. Of the investigated stem cell types, only embryonic stem cells (ESCs)[5] and induced pluripotent stem cells (iPSCs)[6] can be differentiated into functional cardiomyocytes. ESCs have a number of drawbacks, hindering their broader use, as potential tumorgenicity (teratoma formation), lack of large-scale availability and ethical issues. Some of these disadvantages have been cleared by the development of iPSCs, which are broadly available and not subjected to ethical concerns.

In the last decade, it has been detected that the heart itself contains a reservoir of stem- and progenitor cells (CPCs), which are suggested to have a self-regenerative potential throughout mammalian adult life.[7,8] Different populations of CPCs have been identified in the fetal, neonatal and adult mammalian heart according to their expression of certain membrane markers (c-kit, Sca-1, Abcg-2, SSEA-1), transcription factors (Isl-1, Wt-1) or their ability to grow in cardiospheres.[9] Our group used Sca-1-coupled magnetic beads to isolate CPCs from fetal and adult human hearts. These CPCs could be differentiated into functional cardiomyocytes upon treatment with 5-azacytidine and TGF-beta1.[10-13]

One of the bottlenecks hampering a fast clinical application of CPCs is the large amount of cells required to replace a single damaged region in combination with an appropriate strategy to succeed in homogeneous repair. The application of CPCs into a very small lesion situated in an area, which is heterogeneous, by nature, like the AV-node, might be more successful. Functionally, the normal atrioventricular (AV) node can be viewed as: (1) slow conductor, (2) subsidiary pacemaker and (3) (frequency) controller[14] and is composed of different cell types positioned in a complex 3-dimensional (3D) configuration.[15]

Thus far, the aim to restore AV conduction in hearts compromised by CAVB has hardly been followed and one of the underlying reasons may be this complexity in structure and function. Two groups have reported that in rats with CAVB, implantation of tissue constructs with skeletal myoblast derived cells[16] or injection of mesenchymal stem cells (MSCs)[17] resulted in restoration of AV-conduction in 33% of treated animals.

Our research group successfully established a dog model of chronic atrioventricular block (CAVB), which recapitulates the sequence of pathological events as observed in patients. In this model, complete AV block is created by radiofrequency (RF) ablation of the AV node. Bunch *et al.*[18] showed that in dogs, cell injection could be precisely placed into chosen parts of the AV node by catheter intervention under electrophysiological and anatomical guidance. Using this model, we hypothesized that restoration of the natural conductive pathway is possible by transplantation of CPCs or their derived cardiomyocytes in the ablated AV nodal region.
This study aims to: (1) isolate canine CPCs using Sca-1-coupled magnetic beads, (2) analyze the *in vivo* effect of injected human and canine CPCs or their derived cardiomyocytes, (3) isolate and characterize canine MSCs from bone marrow and adipose tissue and analyze their potential as adjunct therapy.

Materials and methods

General outline of the experimental approach

The general outline of a transplantation experiment was that normal AV conduction in the dog heart was interrupted through RF ablation (30 seconds of ablation time) of the AV node under ECG control. During this procedure, catheter-based endomyocardial biopsies were taken, bone marrow and adipose tissue was collected for isolation of various sources of autologous MSCs. In the following 3 weeks, chronic AV block developed with associated electrical remodeling of the heart. Three weeks after the ablation, *in vitro* expanded and fluorescently-, SPIO- or BrdU-labeled cells were transplanted into the ablated region through intra-myocardial injections. Transplanted dogs were followed for another 3 weeks through ECG recordings on every third day in order to evaluate alterations in cardiac activation and/or rhythm. Finally, dogs were sacrificed and the transplanted tissue was excised and processed for histology.

Animal procedures

All animal handling was in accordance with the 'Dutch Law on Animal Experimentation' and the 'Directive 86/609/CEE of the Council of European Communities'. The Committee for Experiments on Animals, University Utrecht, provided institutional control. All invasive experiments were performed on anesthetized purpose bred dogs (Marshall America, Butler Pharms USA, Clyde , NY, USA) under aseptic conditions. After an overnight fasting, dogs were sedated with an intramuscular injection of 0.5 mg/kg methadone, 0.5 mg/kg acepromazine and 0.5 mg atropine sulfate i.m. Anesthesia was induced through sodium pentobarbital (25 mg/kg i.v., Nembutal, Sanofi). The dogs were artificially ventilated, respiratory rate of 12-14/min, through a cuffed endotracheal tube with a mixture of oxygen, nitrous oxide (40/60%) and isoflurane (vapor concentration 1.5%). Tidal volume was adjusted (10-25 ml/kg) to maintain end-expired carbon dioxide concen-

trations between 3.5-4%. During the experiments, a thermal mattress was used to maintain body temperature at 37°C. Proper care was taken before and after the experiments, which included the administration of antibiotics (1000 mg ampicillin) and postoperative analgesics (0.015 mg/kg buprenorphine i.m.).
Electrophysiological testing involved registration of 6 surface ECG leads, 4 precordial, and two endocardial monophasic action potentials (MAPs) which were positioned under fluoroscopy at the endocardium of the left (LV) and right ventricle (RV) and simultaneously stored on a hard disk. In 2 dogs, before RF ablation, catheter-based endomyocardial biopsies were taken via a jugular venous approach. In 4 dogs, before RF-ablation, two pieces of subcutaneous fat were excised from the right hip. In 3 dogs bone marrow aspirates were collected from the iliac crest.

Standard ablation procedure: Vascular access was established by introducing a long sheath into the right internal jugular vein. Under fluoroscopic guidance, RF energy was delivered through a local catheter (7F steerable quadripolar catheter with a 4 mm tip (Medtronic)). This catheter was positioned across the tricuspid valve to record bipolar signals. When a (small) His bundle signal was seen in combination with a right atrial ventricular signal ratio > 1, RF current (RF ablator, Medtronic; 50W, 70°C, 30 sec) was delivered between the tip of the catheter and a pad applied to the back of the dog. This approach assures ablation of the proximal AV node, leaving the His bundle and AV node artery intact.
Ablation under electroanatomical guidance (n=1): This method was designed to minimize the size of the ablation lesion. For the use of the three-dimensional (3D) electroanatomical mapping system EnSite (EE3000, St. Jude Medical, Inc., St. Paul, MN, USA) six skin electrode patches were placed on the dog (after shaving the skin) on neck, right and left lateral thorax, dorsal and ventral thorax and right leg. Vascular access was established by insertion of 6F and 8F sheaths in the right femoral vein. The dog was heparinized (1500 EH i.v.). Through the sheath a catheter (Celsius DS diagnostic/ablation deflectable tip, A-type, 92 cm; Biosense Webster) was positioned in the right atrium. A reference electrode (temporary transvenous pacing lead system, 6416-200cm; Medtronic) was screwed in the region of the oval fossa. By moving the catheter within the right atrium a right atrial geometry were created. In that geometry, the tricuspid valve annulus, coronary sinus ostium and position of the AV bundle (His) were marked (Figure 1B). The proximal part of the AV node was identified and ablated with RF current (RF ablator, Medtronic; 25W, 50°C, 30 sec).

Standard cell injection procedure: Three weeks after ablation 2-4 x 10^6 undifferentiated dog CPCs (n=3), undifferentiated human CPCs (n=2) or differentiated human CPCs (n=5) were injected into the ablated tissue. Injections were performed within, proximal and distal to the ablated region. In 3 dogs a fourth injection was placed into vital myocardium of the left ventricular free wall. Atriotomy appeared not always necessary since most often the ablation could be identified by touch from outside of the heart. Cells were injected in 0.2 ml culture medium without serum. Prior to injection, the dogs received an intravenous bolus of tacrolimus (Prograft, 2.5 mg/ 25 kg/ 30 min) in order to temper immunologic rejection. In the days until sacrifice, 5 mg tacrolimus was given orally.

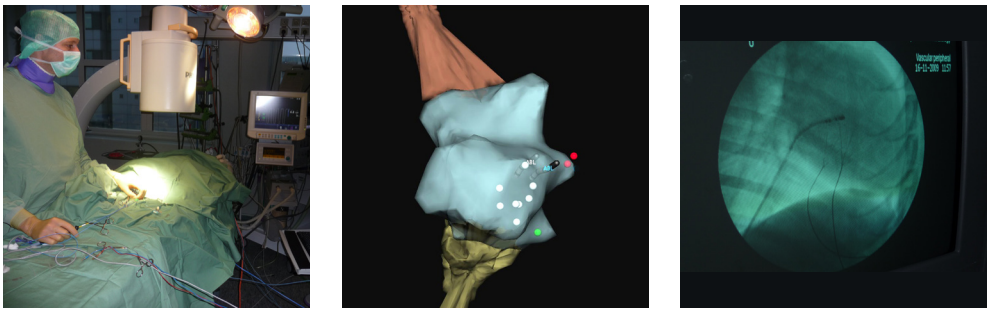

Figure 1
A: Photograph of the setting of the ablation under electroanatomical guidance.
B: Electroanatomical 3D surface reconstruction (EnSite NavX) from ablation procedure: superior vena cava (brown), inferior vena cava (olive green), right atrium (grey), white spots mark tricuspid valve annulus, red spots mark localization of His potential, green spots mark the ostium of coronary sinus.
C: Fluoroscopy showing the position of the ablation catheter in the dog heart.

Cell injection under electroanatomical guidance (n=1): This method was designed to deliver cells by an electroanatomically-guided catheter intervention. Three weeks after ablation, the dog was prepared for the use of the 3D electroanatomical mapping system EnSite as described above. Vascular access was established by insertion of 6F and Agilis (Agilis NxTTM, steerable introducer; St. Jude Medical) sheaths in the right femoral vein. A modified injection catheter (NOGA, A-type; Biosense Webster) was connected with the EnSite system and flushed with 0.1 ml PBS. Under electroanatomical guidance: (1) two injections of SPIO-labeled autologous adipose tissue-derived MSCs (AD-MSCs)(per injection 500.000 cells in 0.1 ml) and (2) five injections of BrdU-labeled AD-MSCs (per injection 500.000 cells/ 0.1 ml) were placed in the ablation area. Three hours after cell injection the dog was transported to the MRI facility and scanned. After MRI scanning the dog was sacrificed.

Sources of cells

Canine bone marrow-derived mesenchymal stem cells (cBM-MSCs)

Bone marrow aspirates were collected under sterile conditions using an 18-gauge needle from the iliac crest of 3 dogs and stored in heparin-coated vials on ice. The amount of bone marrow yield varied from 0.5-2 ml. Bone marrow was strained through a 70µm cell-strainer placed in a 50 ml Falcon tube and the strainer was washed with PBS. The PBS/bone marrow was transferred carefully onto 15 ml of Ficoll-paque, centrifuged at 2000 rpm for 5 minutes and stopped with the slow brake setting on a Multifuge 3 centrifuge (Heraeus). The middle layer of the centrifuged solution was carefully pipetted to a new 50 ml Falcon tube, resuspended to 50 ml with PBS, again centrifuged at 2000 rpm for 5 minutes and the supernatant aspirated. The remaining cell pellet was resuspended in 15 ml of MSC medium (500 ml α-MEM supplemented with 50 ml FBS and 10 ml penicillin/ streptomycin) and plated in T75 culture-flasks. Cells were cultured at 37°C in a CO2 incubator (5% vol/vol). After 24 hours non-adherent cells were washed away with PBS and MSC medium was refreshed. Medium was refreshed every two days.

Canine adipose-derived mesenchymal stem cells (cAD-MSCs)

For cAD-MSCs, subcutaneous tissue was collected under sterile conditions from the hip of 12 dogs (from 4 dogs in this study plus from 8 dogs in other studies). On average 2-3 g of adipose tissue was excised. The isolation procedure in the majority of cases (n=11) included storage in tissue culture medium derived from 500 ml Ham's F12, supplemented with 20mM HEPES, 0.5 g $NaHCO_3$ and 75 ml FBS). Raw weight of adipose tissue was taken. The tissue was then washed twice with M-buffer, twice with PBS and then minced to clear any vascular tissue present. Minced tissue was then digested in a volume (5 ml per gram tissue) of collagenase A (1 mg/ml, Sigma-Aldrich) for two hours at 37°C in a shaker bath. The digestion product was passed through a 70µm cell-strainer which was washed with 5 ml cold M-buffer (1000 ml of PBS supplemented with 10 ml 200mM EDTA and 10 ml FBS) to elute cells. The strained solution was centrifuged at 2000 rpm for 5 minutes. Supernatant was aspirated and cells resuspended in MSC medium (500 ml α-MEM supplemented with 50 ml FBS and 10 ml penicillin/ streptomycin). The suspension was filtered through a 40µm cell-strainer, which was washed with 2 ml MSC medium. 13 ml of MSC medium was added and cells were plated in T75 culture-flasks. After 24 hours non-adherent cells were washed away with PBS and MSC medium was refreshed. Medium was refreshed every two days.

In one procedure (n=1) isolation and culture was performed as described by Neupane *et al.*[19] Briefly, the tissue was washed twice with PBS (Lonza) and digested overnight at 37°C in a volume (5 ml per gram tissue) of D-medium (MEM supplemented with 2mM N-acetyl-L-cysteine (NAC), 0.2mM L-ascorbic acid 2-phosphate (Asc-2P), penicillin, streptomycin and amphotericin), and collagenase A (1 mg/ml, Sigma-Aldrich) in a shaker bath. The next day, the digested tissue solution was centrifuged at 800-1200 rpm for 5 minutes. After removing the supernatant and washing with PBS the cell pellet was resuspended in D-medium supplemented with 10% FBS, plated in a T25 flask and cultured overnight at 37°C. The next day, the flask was careful washed once with PBS. The adherent cells in the flask were covered with K-NAC medium (500 ml Keratinocyte-SFM medium (Invitrogen), supplemented with rEGF (human recombinant epidermal growth factor), BPE (bovine pituitary extract), 2mM NAC, 0.2mM Asc–2P and 5% FBS). The K-NAC medium was refreshed every 3 days. After having reached 90% confluence the cells were passaged. Some aliquots of cells were frozen, used for RNA isolation or immunocytochemistry.

Cardiac progenitor cells (CPCs)

The protocol used to isolate canine CPCs (cCPCs) was modified from Smits *et al.*[20] Canine cardiac tissue was obtained using three different methods: catheter-based endomyocardial biopsy (n=2), needle biopsy (n=4, from dogs in other studies), and mononuclear cell fractions (n=6, from dogs in other studies). For catheter biopsies, a 6F vascular sheath was inserted into the jugular vein through which a bioptome (Cook Biopsy Forceps, 5.2F) was advanced into the right ventricle under fluoroscopic guidance. 3-4 small biopsies were taken from the endomyocardium in the apex of the right ventricle. For needle biopsies, a commercially available biopsy needle (14G, Acecut, TSK, Japan) was used to obtain a transmural biopsy from the septo-apical part of the right ventricle prior to sacrifice. Three biopsies were taken and pooled to increase cell yield. Biopsies were stored on

ice in tissue culture medium. Biopsies were washed twice in cold M-buffer, then twice with PBS. Tissue was then cut into small clumps of approximately 1 mm^3 and transferred into a 15 ml centrifuge tube containing collagenase A solution (1 mg/ml, Sigma-Aldrich). Tissue was incubated at 37°C for 2 h in a water bath. Suspensions were filtered with a 40µm cell-strainer, which was washed five times using 5 ml of cold M-buffer with flow-through being collected. Cells were centrifuged at 1200 rpm for 5 minutes, supernatant aspirated and 5 ml M-buffer added. Cell suspension was centrifuged at 1200 rpm for 5 minutes one additional time and resuspended in 450 µl M-buffer in a 1.5 ml Eppendorf tube.

For mononuclear cell fractionate, methods were adapted from Powell *et al.*[21] Following excision and washing, the entire canine heart was digested using calcium-free solution containing collagenase and proteases. The digestion was filtered through a 220µm filter and cardiomyocytes were pelleted by centrifugation at 300 rpm for 2 minutes and the supernatant transferred to new tube. The remaining total cell fractionate in the supernatant was centrifuged at 1200 rpm for 5 minutes and resuspended in 450 µl M-buffer following supernatant aspiration.
Cell suspensions from all three isolation methods were then incubated with stem cell antigen-1 (Sca-1) specific magnetic microbeads. A double incubation was performed by adding 10 µl of anti-Sca-1/FITC (Miltenyi) and 20 µl anti-c-kit (Miltenyi) microbeads to the cell suspension. The initial three isolations from the mononuclear fractions were performed slightly different because of the availability of beads with direct coupling of the anti-Sca-1 antibody. Incubation was performed under rotation at 4°C for 45 minutes. To wash off the excess of microbeads after incubation, samples were transferred to 15 ml Falcon tubes and 5 ml cold M-buffer was added. Suspension was then centrifuged at 800 rpm for 5 minutes, and the supernatant aspirated. Samples were resuspended in 450 µl of M-buffer and 20 µl anti-FITC (Miltenyi) microbeads added. Incubation was again performed at 4°C for 45 minutes. Samples were washed with 5 ml cold M-buffer and centrifuged at 800 rpm for 5 minutes. The cell pellet was resuspended in 1 ml of cold M-buffer and strained through 40µm cell-strainer. The strainer was washed with 1 ml cold M-buffer. MACS isolation was performed using desinfected MiniMACS magnet system (Miltenyi) as per manufacturer's instructions. Separation columns were pre-wet with 1 ml cold M-buffer and the cardiac cell suspension added 1 ml at a time. Columns were washed three times with 1 ml cold M-buffer and all flow-through was collected as the negative fraction. Columns were then removed from the MiniMACS magnet system, washed with 1 ml of cold M-buffer and flushed using the provided plunger. Following MACS sorting the samples were centrifuged at 1200 rpm for 3 minutes. The positive and negative sorting fraction was then resuspended in 500 µl (c-kit/Sca-1+) or 1500 µl (c-kit/ Sca-1-) of SP++ medium (125 ml of EGM-2 with 375 ml of M199 supplemented with 50 ml FBS, penicillin/streptomycin and 5 ml MEM non-essential amino acids, EGM-2 made of 475 mL EBM-2 supplemented with EGM-2 Single Quots), and 500 µl per well was plated in a 24-well plate coated with 0.1% gelatin. After three days, CPCs were washed with PBS and medium was refreshed.
Human fetal-derived CPCs (hCPCs) were isolated and differentiated into cardiomyoctes as described before[20] and were delivered by Dr. M.J. Goumans (Dept. of Cardiology, UMC Utrecht).

Cell culturing

When cultures reached a 90% confluence they were either frozen or cloned for passage. To split cells culture flasks were washed two times with PBS and 100 µl trypsin (Sigma-Aldrich) was added per 10 cm^2 culture surface. Cells were incubated for 5 minutes at 37 °C and checked to ensure they were detached. Stripped cells were resuspended in 1 ml of the appropriate culture medium (SP++ for CPCs, MSC medium for MSCs). 50 µl was taken, added to 5 ml of CasyTon solution and cell concentration was determined using Casy count system (Innovatis) following manufacturer's instructions.

Differentiation of isolated MSCs and CPCs

Adipogenic, chondrogenic and osteogenic differentiation of MSCs was performed as previously described by Neupane *et al.*[19] Cells were cultured in K-NAC medium until at least 3 x 10^6 cells could be collected (mostly 2x T75 culture flasks, 80-90% confluent). The cells were washed twice with PBS, trypsinized and counted as described above. Cells were plated in a 6-well plate at a concentration of 10,000 cells/cm^2 for adipogenic differentiation, or plated in chamber slides at 1000 cells/cm^2 for osteogenic differentiation. For chondrogenic differentiation micro mass cultures of cells (1x 10^5 cells/10 µl for 2.5 hours) were formed in chamber slides. Adipogenic differentiation was comprised by culturing the cells in D-medium supplemented with 10% FBS, 1µM dexamethasone, 5 µg/ml insulin (Sigma-Aldrich), and 5µM rosiglitazone (Sigma-Aldrich). Cells were cultured for 2 weeks with medium being changed every 3 days. Cells were assessed for adipogenic differentiation after 2 weeks using Oil-Red-O staining, which demonstrates lipid droplets. Chondrogenic differentiation was derived by culturing the cells in D-medium containing 10 ng/ml TGF-beta1, 50µM L-ascorbic acid 2-phosphate and 6.25 µg/ml insulin. Cells were cultured for 2 weeks with medium being refreshed every 3 days. Cells were examined for chondrogenic differentiation with Alcian blue staining, which demonstrates a sulphated proteoglycan-rich matrix. Osteogenic differentiation was derived by culturing the cells in D-medium supplemented with 10% FBS, 0.1µM dexamethasone (Sigma-Aldrich), 10mM beta-glycerophosphate disodium (Sigma-Aldrich) and 50µM Asc-2P. Cells were cultured for 6-8 weeks with medium being changed every 3 days. Cells were assessed for osteogenic differentiation after 6-8 weeks using Alizarin Red or Von Kossa staining.

Cardiac differentiation was performed on both MSCs and CPCs as described by Smits *et al.*[20] Cells were propagated in SP++ medium and after 3-4 passages plated on 0.1% gelatin coated 6-well plates at a density of 100,000 cells/well. Glass cover slips were included in half of the wells (4 slips/well) for later immunocytochemical analysis. After 24 hours medium was changed to differentiation medium (235ml of IMDM with 235 ml Ham's F12 nutrient mixture with GlutaMAX I supplemented with 10 ml horse serum, 5 ml MEM non-essential amino acids, 5 ml insulin-transferrin-selenium, and 10 ml penicillin/streptomycin). 6-8 hours later 40 µl 5-azacytidine was added. This was performed in the dark, since 5-azacytidine is light sensitive. At the end of the next two days 40 µl of 5-azacytidine (250µM) was again added. On the fourth day after initiation the differentiation medium was refreshed. Six days after the changing to differentiation medium 2 µl ascorbic acid (1M) and 2 µl TGF-beta1 (1 µg/ml) were added. Control experiments were performed by only adding ascorbic acid. Cells were cultured in differentiation medium

for 4 weeks with medium changed and TGF-beta1 added twice a week and ascorbic acid added every second day. The effect of activin was tested through addition of 2 µl activin (1000 ng/ml) twice a week. At 2-week and 4-week time points, wells were processed for RNA and protein isolation, and cover slips fixed for immunocytochemical analysis. To facilitate the histological detection of injected cardiomyocytes later on, cells were exposed to different tracker dyes (DiI, 10µM, 30 min; cell-tracker-red, 10µM, 30 min). As a third mode of labeling, bromodeoxyuridine (BrdU)(Sigma)(100 µmol/l) was added to the culture medium 3 days and 1 day before injection. To facilitate detection of the injected cardiomyocytes using MRI, cell cultures were loaded with dextran coated superparamagnetic iron oxide (SPIO)(Endorem).

RNA isolation and PCR

RNA isolation was performed to manufacturer's instructions using an RNeasy mini kit (Qiagen) or an PicoPure RNA isolation kit (Arcturus), and reverse transcribed into cDNA using SuperScript III (Invitrogen) or an iScript cDNA synthesis kit (Bio-Rad). Canine gene sequences were identified using NCBI Dog Genome and primers were designed using Primerquest software (http://eu.idtdna.com/ Scitools/Applications/ Primerquest/). PCR was performed in a C1000 Thermal Cycler (Bio-Rad) with the following protocol: 2 min at 94˚C, followed by 35 cycles of 15s at 94˚C, 30s at 56-60˚C, and 45s at 74˚C. Products were analyzed on ethidium bromide-stained 1% agarose gel. GAPDH was used as RNA input control and gene expression is displayed relative to GAPDH activity. Q-PCR was performed using SYBR green supermix (Bio-Rad), in a MyiQ single-color real time PCR detection system (Bio-Rad) according to the manufacturer's protocol. To quantify the data, the comparative Ct method was used. Relative quantity was defined as $2^{-\Delta\Delta Ct}$ and GAPDH was used as reference gene.

Immunophenotypic characterization of cAD-MSC by FACS

AD-MSCs were washed with PBS. After washing 5 ml pre-warmed (37˚C) PBS/ EDTA buffer (25mM EDTA in PBS, pH 7.4) was added to the cells and the cells were incubated for 15 minutes at 37˚C. After incubation the cells were transferred into a 15 ml tube and PBS/0.5% FCS was added up to 14 ml, and centrifuged at 2000 rpm for 5 minutes. The supernatant was discarded and the pellet resuspended in fresh PBS/0.5% FCS, 10 ml. The cells were counted with Casy count system: 50 µl in 5 ml, and centrifuged at 2000 rpm for 5 minutes. The supernatant was discarded and the pellet resuspended with PBS/0.5% FCS to a cell concentration of 10^6 cells/ml. Aliquots of 50 µl cell suspension were transferred into test tubes. The test tubes were kept on ice. Primary antibody (AB): PE anti-canine CD34 (mouse IgG1)(AbD/Serotec), 1:100; Biotin anti-canine CD45 (rat IgG2b)(Serotec), 1:100, secondary AB: APC/Cy7 Streptavidin, 1:100; anti-human CD73 (mouse IgG2b)(AbD/Serotec), 1:100, secondary AB: RPE anti-mouse IgG, 1:100; anti-canine CD90 (rat IgG2b)(Serotec), 1:20, with secondary AB: FITC anti-rat IgG, 1:20; PE/Cy5 anti-human CD117 (mouse IgG1)(BD Bioscience) was added to the aliquots, and incubated on ice in the dark for 30 minutes. Control aliquots were stained with an isotype-matched antibody. After incubation 1 ml of PBS/0.5% FCS buffer was added to the aliquots, centrifuged at 2000 rpm for 5 minutes. The supernatant was discarded. The pellet was resuspended in 50 µl PBS/0.5% FCS. If necessary, an appropriate secondary reagent was added at the recommended dilution, mixed and incubated on ice in the dark

for 30 minutes. After incubation the cells were washed with 1 ml of PBS/0.5% FCS, centrifuged at 2000 rpm for 5 minutes. The supernatant was discarded and the pellet resuspended in 100 µl of PBS/0.5% FCS and transferred into FACS tubes. Flow cytometry were performed with BD FACS Canto II and analyzed with BD FACS Diva software v6.1.2 and FlowJo software v7.6.5.

Immunohistochemistry

Upon termination of the experiment, the heart was rapidly removed and flushed with ice-cold Tyrode solution until the flushing solution became clear. From the flushed heart a rectangular tissue block of the AV junction was excised from the posterior border of the coronary sinus to the anterior edge of the septal leaflet of the tricuspid valve, containing ≈6 mm of atrial tissue and ≈12 mm of ventricular tissue.
The inferior margin was cut beneath the ostium of the coronary sinus. The tissue block was rapidly frozen in liquid nitrogen (n=7) or mildly fixed as described by Bajanca *et al.*[22], separated into pieces, embedded in tissue-Tek and cryosections of 10 µm thickness were sliced. For analysis of cultured cells, gelatin-coated coverslips with cells were rinsed with PBS, fixed for 2 minutes in –20˚C methanol, washed with, and stored in PBS. To start the labeling, specimen were permeabilized with 0.2% Triton X-100/PBS for 60 minutes. Nonspecific binding of antibodies was blocked with 2% bovine serum albumin (BSA) for 30 minutes. Incubation with primary antibodies was performed overnight in PBS/ 10% normal goat serum (Dako). Antibodies used recognized alpha-actinin (Sigma), vimentin (MAKER), alpha-SMA (Sigma), desmin (Sanbyo), Gata-4 (Santa Cruz), connexin 43 (Zymed), alpha-skeletal actin, c-kit. Following overnight incubation, sections were washed and again blocked with 2% BSA for 30 minutes. Fluorescent immunolabeling was performed using Texas red- or FITC-conjugated secondary antibodies (Jackson) and nuclear 6-diamidin-2-phenylindol (DAPI) staining. All incubation steps were performed at room temperature. In between incubation steps, cells were washed with PBS. Finally, coverslips were mounted in Vectashield (Vector Laboratories) and examined with a Nikon Optiphot-2 light microscope equipped for epifluorescence.

Results

Isolation, culture and characterization of canine MSCs

For cBM-MSC isolation bone marrow aspirants (n=3) from the iliac crest were used. A single puncture resulted in aspiration of 0.5-2 ml of bone marrow. Though two out of three aspirants showed some growth of spindle-shaped cells (see Fig. 2A), only one aspirant resulted in a cell culture that could be passaged. The cells in this culture showed a low growth velocity. After approximately 2 weeks only 30% confluence was reached. Because of the low bone marrow yield and the impossibility to obtain stable cultures, which would result in MSCs in sufficient number for further experiments, this MSC source was abandoned. For cAD-MSC isolation explants of adipose tissue (n=12) were used. All isolations led to proliferating cultures, which were propagated up to 5 passages (Fig. 2B).

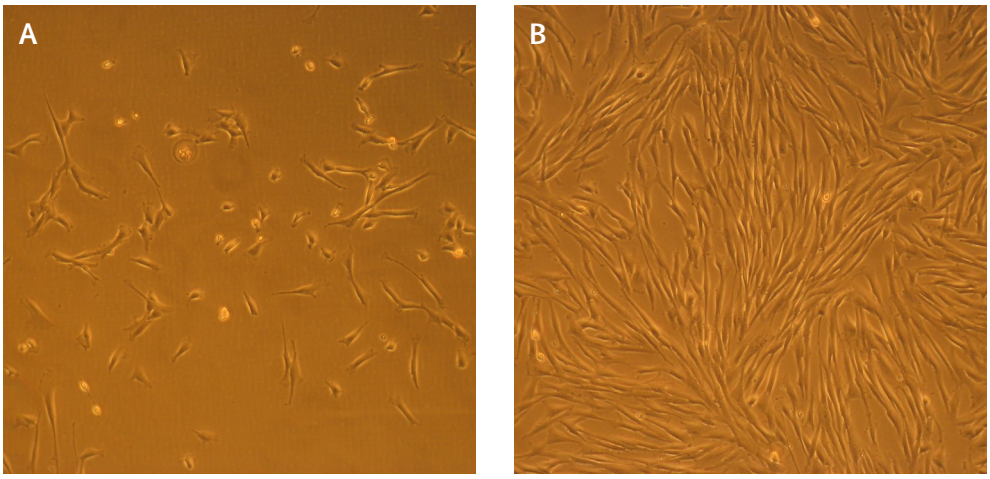

***Figure 2*: Phase contrast photomicrographs. A**: canine bone marrow-derived MSCs, **B**: canine adipose tissue derived MSCs, at day 7 in primary culture (=passage 0), magnification 100x.

Analysis of the expression of cell surface proteins by FACS (Fig. 3) showed that cAD-MSCs after passage 1 were negative for CD34, CD45, CD73, CD271, and positive for CD90 and CD117 (c-kit). Using immunocytochemistry cAD-MSCs stained positive for smooth muscle actin (SMA, Fig. 4A) and vimentin (Fig. 4B). RT-PCR analysis (Fig. 4C), revealed the expression of the following genes at mRNA level: Nkx2.5 and Mef2c, encoding for early cardiac transcription factors, Myh1 (encoding for myosin, heavy chain 1, skeletal muscle), Myh6 (encoding for myosin, heavy chain 6, cardiac muscle), Lpl (encoding for lipoprotein lipase), Cnn1 (encoding for calponin 1, basic, smooth muscle), Ddr2 (encoding for discoid in domain receptor tyrosine kinase 2).
The pluripotency of cAD-MSCs was demonstrated by differentiation into an osteogenic (based on calcified extracellular matrix deposits), adipogenic (based on lipid droplet formation, Fig. 5A)) and chondrogenic lineage (Fig. 5B).

Isolation, culture and differentiation of CPCs

Isolation, purification, cell culture, differentiation and characterization of human fetal CPCs, which were used in the transplantation study, have been described before.[10,11,20] In short, undifferentiated cells were isolated that were positive for CD31 and CD105, c-kit and the cardiac transcription factors Mef2c, Gata4 and Nkx2.5. Upon application of the demethylating agent 5-azacytidine and TGF-beta1, cells nearly uniformly differentiated into cardiomyocytes. The *in vitro* generated human cardiomyocytes displayed robust electrical and mechanical intercellular coupling[11] and near mature electrophysiological characteristics.[10]

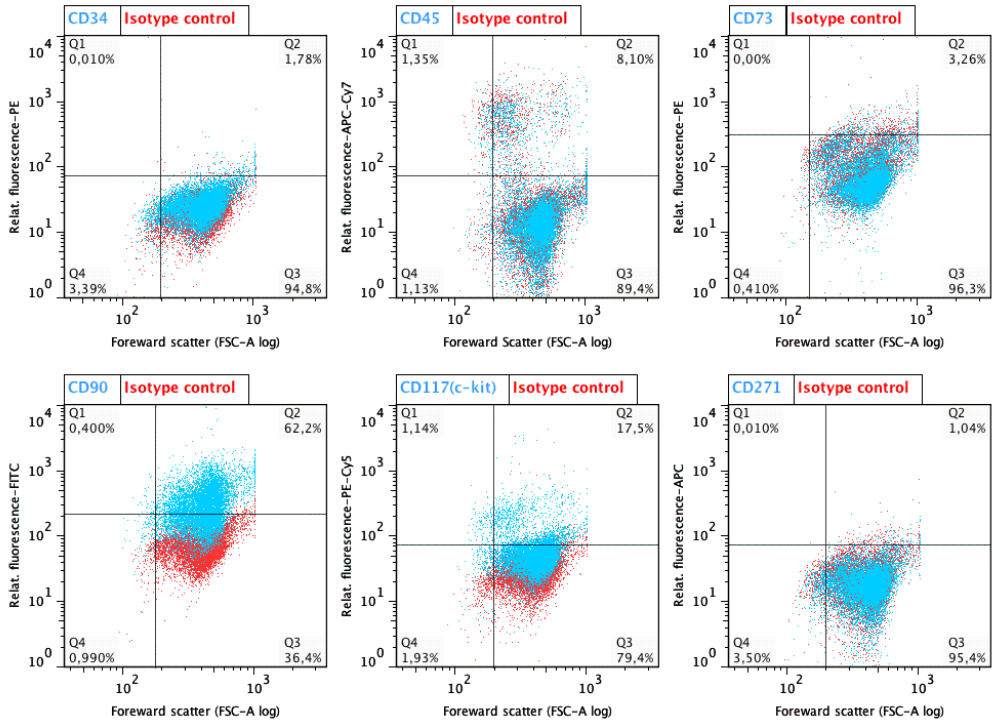

***Figure* 3: FACS analysis of canine AD-MSCs at passage 1**. The graphs are showing dot plots of cells with positive expression of a cell surface marker (blue dots) in comparison to cells with negative expression (red dots); 62.2% of AD-MSCs were positive for CD90, 17.5% of AD-MSCs were positive for CD117 (c-kit).

Dog CPCs isolated during the first 4 isolations from the mononuclear cell fraction (using microbeads with direct coupling of Sca-1antibodies) revealed cells with a high nucleus to plasma ratio typical for stem cell-like cells. The cells were positive for Sca-1, Gata4, Mef2c and c-kit (Figure 6A and 6C). Likewise the human equivalents, the undifferentiated cells robustly expressed the gap junction proteins connexin 43 (Cx43) and connexin 45 (Cx45) while a small minority also expressed connexin 40 (Cx40). Though the majority of protein was found within the cell, typical junctional labelling of Cx43 in between cells was also found (Figure 6A). After an initial lag of 1 or 2 days, cells rapidly expanded in culture with an average doubling time of 1 day. This speed of growth appeared independent whether cells were freshly isolated, subjected to trypsinization and transport, or re-cultured after storage in liquid nitrogen (Figure 6B). However, the general speed of replication slowed down after about 8 passages and growth arrest was observed after 12 passages. Upon differentiation of cells at passage 5-7 using 4 weeks of stimulation with 5-azacytidine and TGF-beta1 the cells started, besides the mentioned connexin isoforms Cx43, Cx45 and Cx40, to express a promising subset of constituents of ion channels involved in action potential generation (e.g., Hcn4a, Kcnd3, Kcnj2 and Kcnh2, Figure

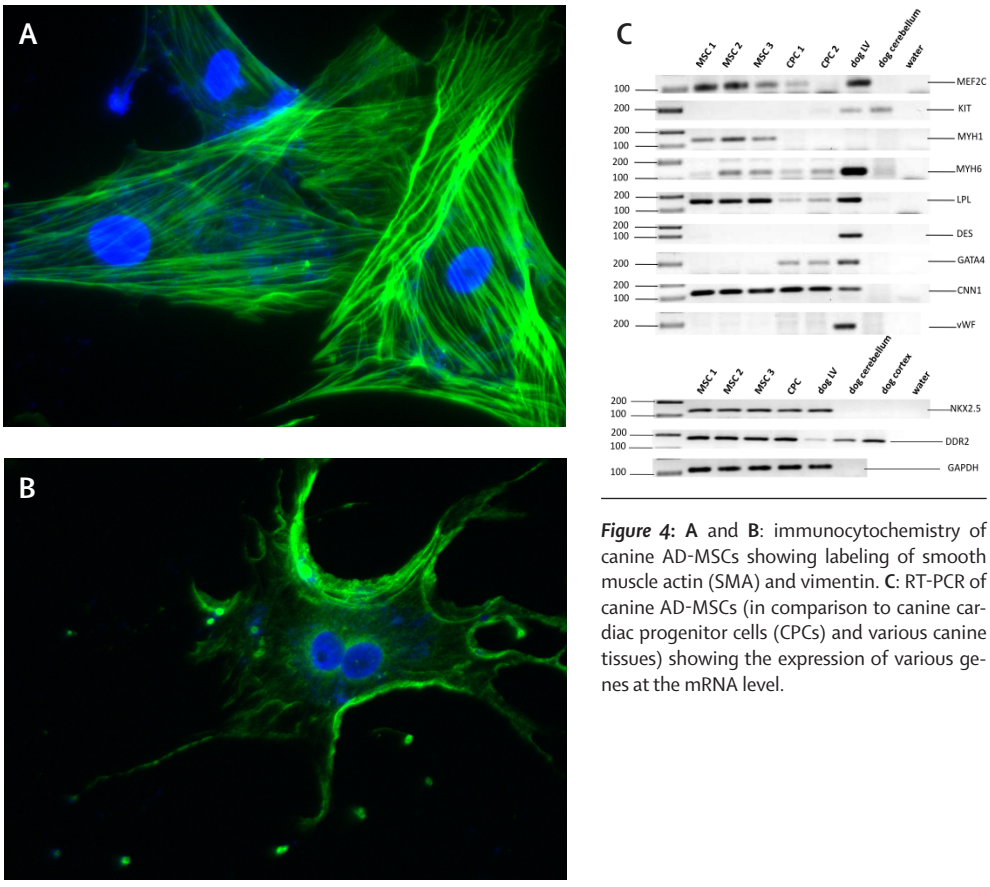

***Figure 4*: A** and **B**: immunocytochemistry of canine AD-MSCs showing labeling of smooth muscle actin (SMA) and vimentin. **C**: RT-PCR of canine AD-MSCs (in comparison to canine cardiac progenitor cells (CPCs) and various canine tissues) showing the expression of various genes at the mRNA level.

6C) and genes involved in regulation of calcium handling (e.g. Cacna1c, Ncx1, Plb, Ryr2 and Serca2a, Figure 6C). Adenoviral infection with a virus encoding beta-galactosidase (in order to induce a marker for recognition upon transplantation) was not tolerated both, by undifferentiated cells and cells during differentiation, and resulted in cell-death (not shown). Immunocytochemistry revealed that after 2 weeks of differentiation, CPCs expressed the cardiomyocyte-specific protein alpha-actinin while expression of the gap junction protein Cx43 was more localized at the intercellular contacts (Figure 6C, right upper panel). The expression pattern of alpha-actinin however did not show the cross-striations typically seen in more mature cardiomyocytes, but rather a pattern of stress fiber-like structures with the highest signal intensity at the cellular boundaries (Figure 6C, right middle panel). Moreover, a subset of cells expressed alpha-skeletal actin (Figure 6C, right lower panel) in a similar fashion, thereby underlining the relative immaturity of the cells or, alternatively, indicating that they developed into myofibroblasts.

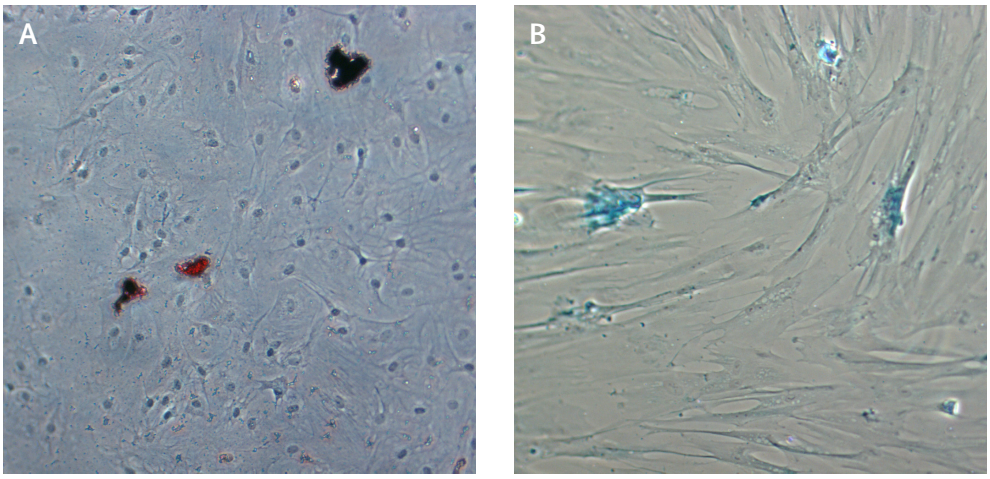

Figure 5: Phase contrast photomicrograph of canine AD-MSCs after: **A**: adipogenic differentiation, Oil-Red-O staining showing lipid droplets; **B**: chondrogenic differentiation, Alcian blue staining demonstrating a sulphated proteoglycan-rich matrix.

To be able to pursue an autologous approach and to test whether sufficient cells could be isolated from a limited amount of tissue, cells were also isolated from endomyocardial right ventricular biopsies that were taken under echocardiographic guidance through insertion of a bioptome via the jugular vein (Figure 7A), or from transmural needle biopsies. In addition to this change in approach, cell isolation had to be performed with different microbeads (Sca-1/FITC) since the former used in earlier experiments were no longer commercially available.

All needle and catheter biopsy material did not produce proliferating cultures following MACS sorting using magnetically coupled c-kit and/ or Sca-1/FITC antibodies. In contrast, comparable to earlier isolations from mononuclear cell fractions (MCF, as derived from the enzymatic digestion of an entire heart), proliferating cultures from both the c-kit/ Sca-1 positive and negative MCF could be obtained. Isolated MCF c-kit/ Sca-1 positive and negative cells had similar proliferative capacities and approximate doubling times of 24 hours for the first five passages. Following treatment with trypsin and subsequent plating for passage, cells reattached to culture flasks within 24 hours. The c-kit/Sca-1 positive and negative cells were propagated for eleven passages. At passage 10, as observed before, cell growth was dramatically reduced (Figure 5.7B), whereas the phenotype of cells in culture changed to one showing extensive formation of dendritic-like structures suggestive for a more fibroblast-like phenotype (Figure 7C). Cells recultured after they had been stored in liquid nitrogen already displayed growth arrest after one passage.

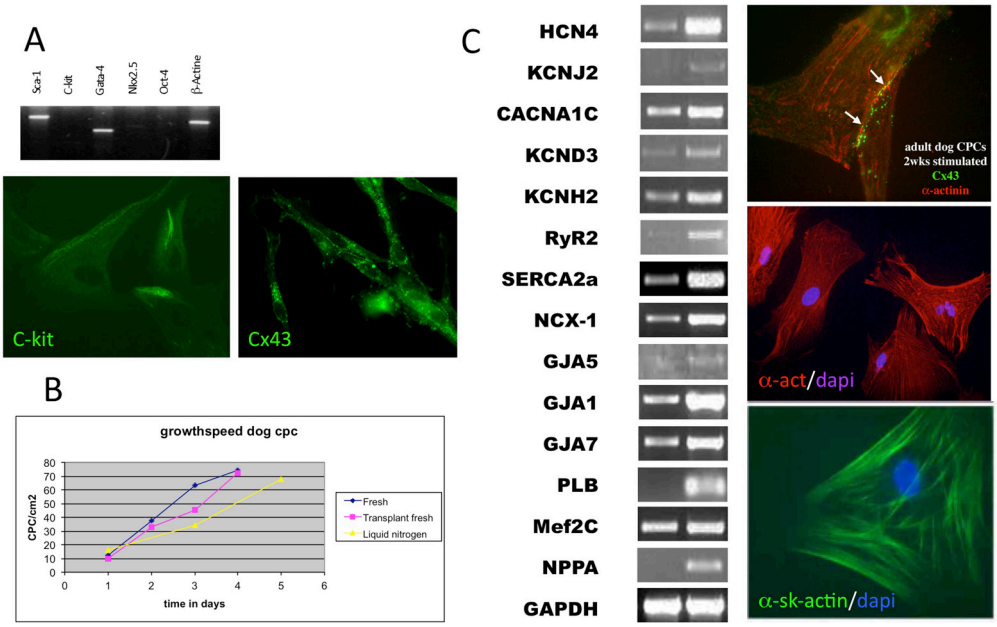

Figure 6
A: upper panel: RT-PCR of canine CPCs showing expression of Sca-1 and Gata4 at mRNA level; lower panel: immunocytochemistry of canine CPSs demonstrating positive labeling for c-kit and connexin 43. **B**: growth speed of canine CPCs. **C**: left panel: RT-PCR showing the expression of various genes at mRNA level in undifferentiated and differentiated canine CPCs; right panel: immunocytochemistry of differentiated canine CPCs demonstrating positive labeling for connexin 43, alpha-actinin and alpha-skeletal actin.

During differentiation of the cells, the impression that their phenotype was more fibroblast-like was further substantiated. Differentiation was performed with, on top of 5-azacytidine and TGF-beta1, activin and oxytocin as potential factors that would support differentiation into cardiomyocytes. Despite of the fact that there was a tendency for increased expression of the cardiac-specific transcription factor Nkx2.5 during differentiation, also expression of the fibroblast marker DDR2 (discoidin-domain receptor-2) followed the same trend (Figure 7D). Immunocytochemical labeling of the cells after 4 weeks of differentiation revealed only weak signals for cardiac alpha-actinin whereas the fibroblast associated proteins alpha-smooth muscle actin and vimentin were strongly positive throughout the culture (Figure 7E).

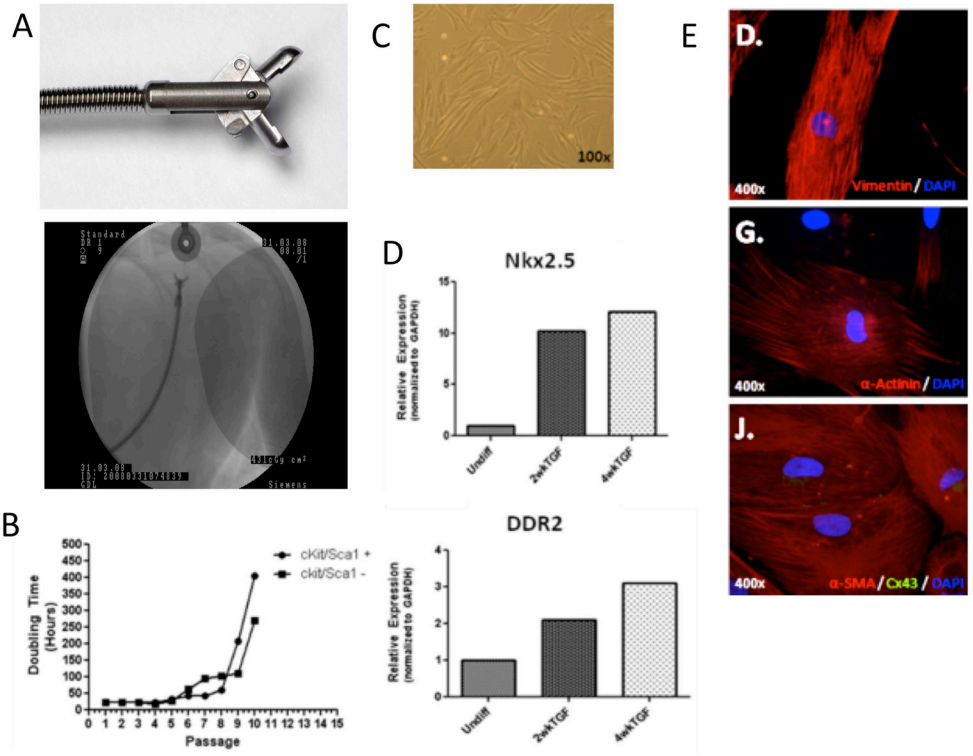

Figure 7
A: upper panel: percutaneous transvenous bioptome; lower panel: fluoroscopy showing the position of the bioptome in the right ventricle. **B**: growth speed of canine CPCs c-kit/ Sca-1 positive or c-kit/ Sca-1 negative, isolated from mononuclear cell fractions (MCF). **C**: phase contrast photomicrograph of canine CPSs at passage 10. **D**: Q-PCR demonstrating increased expression of Nkx2.5 and Ddr2 during cardiac differentiation of canine CPCs. **E**: immunocytochemistry of differentiated canine CPCs demonstrating positive labeling for vimentin, alpha-actinin and alpha-smooth muscle actin.

Transplantation of undifferentiated canine CPCs

In a first set of experiments, 3 dogs (Table 1, Dog experiment number 1 to 3) were transplanted with undifferentiated non-autologous dog CPCs that were derived from incubation of the mononuclear fraction with direct-coupled Sca-1 microbeads. 2 million cells in 0.2 ml serum-free culture medium were injected directly in the ablated area, but also proximal and distal to that. In one of the transplanted dogs atriotomy was necessary in order to locate the ablation while the other two could be transplanted from the epicardial surface, based on finger-touch recognition of the area. A part of the cells was preincubated with DiI and cell-tracker-red while in one dog also additional fluorescent microspheres were co-injected. In this latter dog, a fourth injection with cells was placed into the left ventricular free wall (LVFW), an area of muscle unaffected by the ablation. ECG analysis in all three dogs revealed no restoration of AV-conduction within the 3 weeks of follow-up after transplantation. Dogs remained in complete AV-block as shown in Figure 8A and no additional changes in rhythm were observed.

Dog experiment number	Cell type	Site of injection	Tacrolimus	ECG change	Termination
1	$1x10^6$ undiff cCPCs, fluoresc. microsph.	ablation	5 mg/day	neg	3 weeks
2	$2x10^6$ undiff cCPCs, 50% DiI	ablation	5 mg/day	neg	3 weeks
3	$8x10^6$ undiff cCPCs, 50% cell-tracker-red	ablation, prox and dist + LVFW	5 mg/day	neg	3 weeks
4	$8x10^6$ undiff hCPCs	ablation, prox and dist + LVFW	5 mg/day	neg	3 weeks
5	$8x10^6$ undiff hCPCs	ablation, prox and dist + LVFW	5 mg/day	neg	3 weeks
6	$6x10^6$ diff hCPCs	ablation, prox and dist	5 mg/day	pos	3 weeks
7	$6x10^6$ diff hCPCs	ablation, prox and dist	5 mg/day	neg	3 weeks
8	$12x10^6$ diff hCPCs	ablation, prox and dist	2 x 10 mg/day	neg	8 days
9	$15x10^6$ diff hCPCs	distal to ablation	2 x 5 mg/day	neg	4 days
10	$15x10^6$ diff hCPCs	distal to ablation	none	neg	4 days
11	$2x10^5$ auto cMSCs (SPIO) $5x10^5$ auto cMSCs (BrdU)	ablation	none	NA	0 days

***Table 1*: Overview of experimental procedures**.

Besides the lack of any changes on the ECG, several complicating factors were faced with respect to retrievability of the transplanted cells. Though the co-injected fluorescent microspheres could be identified in sections sliced from the injected area (Figure 8B), transplanted canine CPCs were not retrievable based on immunohistochemistry. Labeling with an antibody against Sca-1 resulted in cross-reactivity, as the signal was similar as obtained with an antibody against alpha-actinin (not shown). Rarely, very weak signals with labeling against c-kit could be found (arrow, Figure 8C). Other tools applied to support retrievability also appeared unsuccessful. Labeling of cells prior to transplantation with DiI or cell-tracker-red was not sufficient to retrieve them 3 weeks after transplantation. Probably the dye faded in the time span between injection and evaluation as indicated by fainting of DiI between day 1 (Figure 8D, left panel) and day 7 (Figure 8D, right panel) after loading during an *in vitro* experiment.

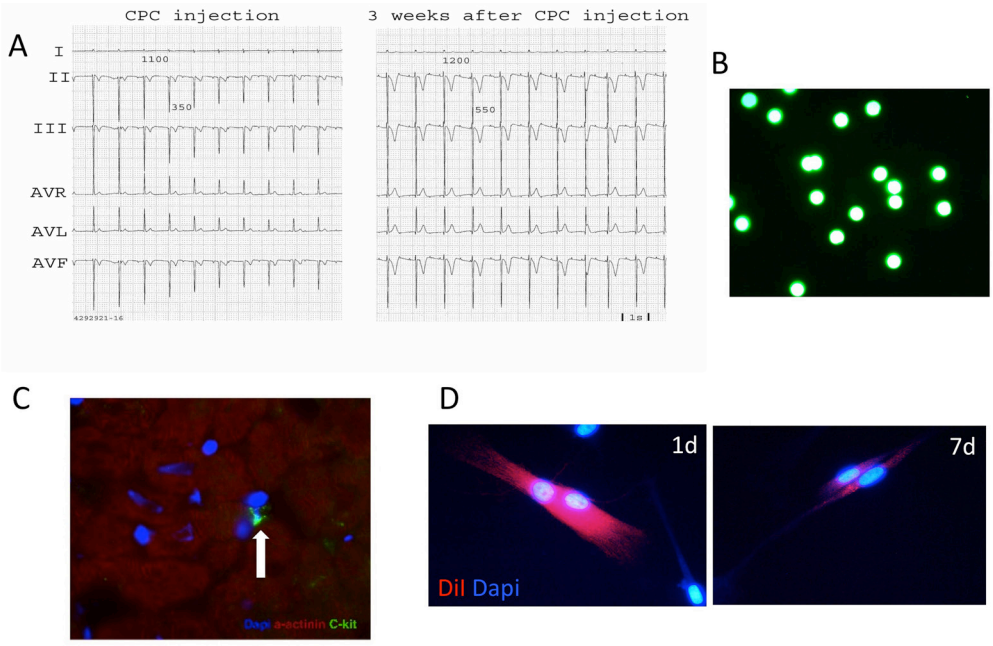

Figure 8
A: ECG at the time of CPC injection (left) and 3 weeks after CPC injection (right), both showing complete AV block. **B**: immunohistochemistry of a tissue section of the ablation/ injection area showing presence of the co-injected fluorescent microspheres but no canine CPCs. **C**: immunohistochemistry of a tissue section of the ablation/ injection area showing cardiomyocytes labeled positive for alpha-actinin with only sporadic positive labelling of c-kit (arrow). **D**: immunocytochemistry of cultured canine CPCs loaded with DiI, 1 day (left panel) and 7 days (right panel) after the loading.

Transplantation of (un)differentiated human CPCs

Due to the lack of functional effects upon transplantation of the dog CPCs and the problems regarding retrievability of the cells, following a similar approach, 7 other dogs (Table 1, Dog experiment number 4 to 10) were transplanted with undifferentiated human CPCs (n=2) or human CPCs differentiated into cardiomyocytes (n=5). For an overview of modifications regarding the approach followed with respect to the transplantation regimen, see Table 1. Theoretically, the use of human CPCs would allow retrieval of the transplanted cells using human specific antibodies like anti-human nuclear factor (HNF) or anti-human mitochondrial factor (both Chemicon). The two dogs that were transplanted with undifferentiated human CPCs did not show any changes on the ECG and CAVB remained present. Histological analysis (H/E staining) revealed small areas of cells with a nucleus/ cytoplasm ratio typical for CPCs (Figure 9B, right panels, arrow) in between the myocardium. However, unfixed cryo-sections serial to the ones used for H/E staining (and positive for co-injected fluorescent microspheres) that were incubated with antibodies specific for human nuclear factor (HNF) appeared to be negative, as was a control cryosection of human ventricle (Figure 9A, right panels).

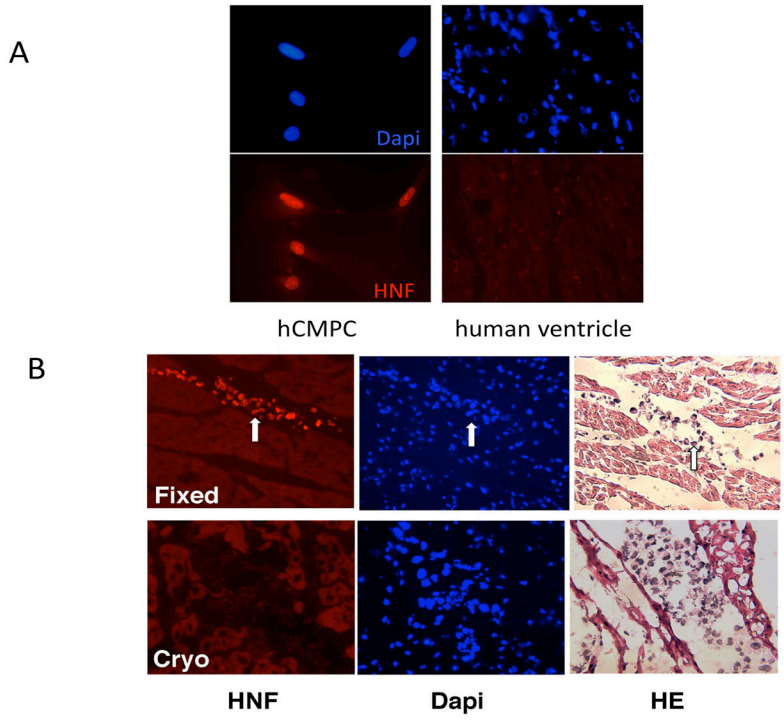

Figure 9
A: Immunocyto-/ histochemistry of fixed human CPCs showing positive labelling for HNF (left panel) and unfixed human control cry-sections that labeled negative for HNF (right panel). DAPI staining indicated the presence of nuclei.
B: canine ventricle after *in vitro* injection of human CPCs; upper row: post-fixed cryo-sections showing a group of HNF positive cells (IHC, left panel, arrow) with the morphology of CPCs (H/E, right panel, arrow); lower row: unfixed cryo-sections appeared negative for HNF (IHC, left panel) though the H/E and DAPI staining suggested the presence of injected cells.

In contrast, HNF-immunolabeling of methanol-fixed human CPCs cultured on glass and post-fixation of cryosections showed convincing nuclear staining (Figure 9A, left panels). Immunolabeling of sections with antibodies against human mitochondrial factor (HMF) did neither result in specific staining.
In the 5 dogs that were sequentially transplanted with differentiated human CPCs, the control injection in the LVFW was omitted to avoid potential pacemaker activity from that transplant. Two dogs received 2 million cells/ injection, 1 received 4 million/injection and in the other two, 15 million cells were injected but only in the remote myocardium distal to the ablation. Only in one (the first) out of these 5 dogs functional alterations could be recorded while the others remained in CAVB. In this one dog, the ECG, taken 48 hours after transplantation, showed a sudden change of beating frequency from 35 bpm to 65 bpm which was accompanied by a change of focus from Purkinje to high septal, resulting in a split morphology of the QRS complex (Figure 10A). Although AV conduction was not restored, these observations were indicative for a functional integration of transplanted cells. The next ECG taken at day 5 after transplantation showed, however, a routine CAVB rhythm and an activation pattern without signs of ectopic pacemaking.

The latter could either mean that the active cells died or that the cells were still present but electrically clamped by the septal cardiomyocytes as a result from an enhanced level of electrical coupling. Before termination of the dogs at three weeks, high frequency atrial pacing in order to force AV conduction appeared unsuccessful. Pacing of the high septum revealed electrical complexes with a morphology comparable to those seen during the temporal period of ectopic pacemaking. Daily recordings of ECGs, shortening of the follow-up period before sacrifice from 3 weeks till only 4 days in the last dog, adjustment of the dose of the immunosuppressive drug and amount of transplanted cells did, unfortunately, not result in any signs of functional integration in the remaining 4 dogs.

In addition, immunohistochemistry revealed comparable but negative results as before. On H/E stainings (arrow, Figure 10B, right panel and Figure 10C, middle panels), large clusters of cells with CPC like nuclei were observed which could be confirmed by DAPI staining. However, clustered cells appeared negative for HNF (Figure 10B, left panel) and, alpha-skeletal actin (Figure 10B, middle panel). In addition, regions were negative for alpha-actinin (red) and Cx43 (green, Figure 10C, left panel). Sirius Red staining (right panels) showed increased fibrosis at the site where CPCs could be recognized at the H/E staining. This was especially dramatically increased in the last dog where immunosuppressive treatment was omitted.

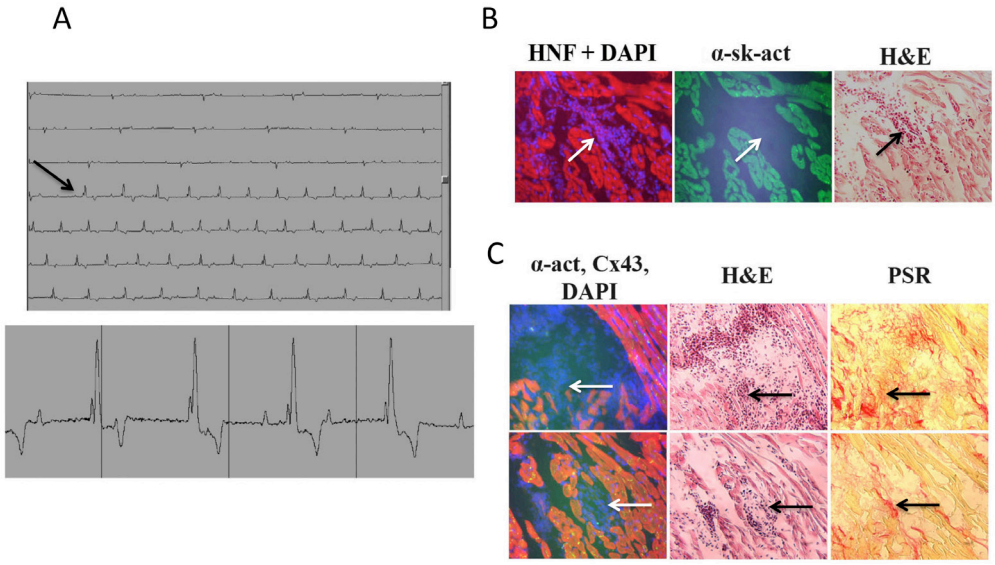

Figure 10
A: ECG, registered 48 hours after transplantation of hCPCs, showing a sudden change of beating frequency from 35 bpm to 65 bpm, with a changed morphology of the QRS complex, fitting to a change of focus from Purkinje to high septal.
B: while H/E staining (right panel) demonstrated a cluster of cells with CPC-like morphology, the cells labeled negative with HNF (IHC, left panel) and alpha-skeletal actin (IHC, middle panel). **C**: H/E staining (middle panels) demonstrated a cluster of cells with CPC-like morphology, embedded in a region of fibrosis (Sirius Red stain, right panels). No labelling for alpha-actinin and Cx43 could be detected.

Transplantation of canine AD-MSCs

In one final experiment (Table 1, Dog experiment number 11), the ablation was guided by a 3D electroanatomical mapping system, in order to attempt to minimize the size of ablation. Three weeks after ablation SPIO- and BrdU-labeled autologous adipose tissue-derived MSCs were injected under 3D electroanatomical guidance through an injection catheter. Shortly after injection the dog was scanned by MRI and sacrificed. MR images showed the ablation lesion after gadolinium enhancement, but failed to reveal signals from the SPIO-labeled cells. In order to study the exact position of the cell injections *in vitro*, after sacrifice, the total tissue block containing the AV conduction axis and the ablation/ injection zone was serially sectioned. From these sections a 3D reconstruction (Figure 11A) was made. Tissue sections from the ablation/ injection region were stained with Perls' prussian blue to detect iron (Fe^{3+}) representing the SPIO-loaded cells. Within the ablation lesion several scattered regions of iron deposition were visible. The iron deposits were mostly situated in the extracellular matrix, and only sporadic in intact cells (Figure 11B, left lower panel). These cells were positive for the surface markers CD68

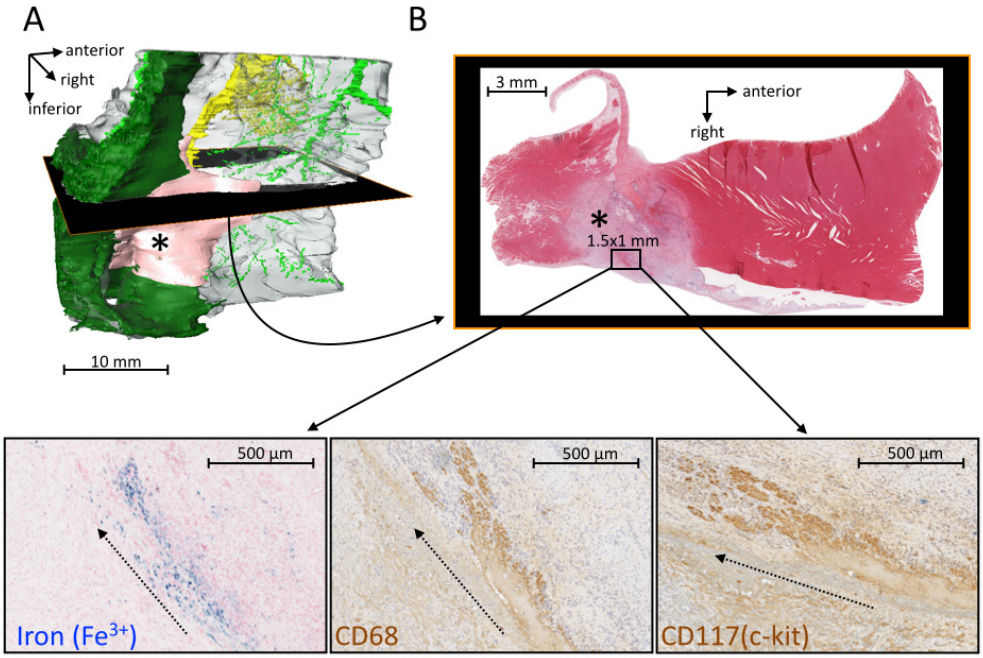

Figure 11

A: 3D reconstruction of the ablated canine AV conduction axis from histological sections: atrial myocardium (dark green), ablation lesion (pink, marked with a black asterisk (*)), AV bundle and bundle branches (yellow), arterial supply (light green); a. indicates the position of the section shown in B. **B**: upper panel: H/E staining of the section shows the ablation lesson (pink, marked with a black asterisk (*)), and the position of the magnifications in the lower panel; lower panel: Perls' stain shows deposits of iron (Fe^{3+}), originating from SPIO-loading. The iron is situated in cells which are positive for CD68 (macrophage-marker) and CD117(c-kit)(stem cel-, but also macrophage-marker); the dotted line with arrow marks a linear structure which might be the injection channel.

and CD117 (c-kit), suggestive for macrophages. Immunohistochemistry with anti-BrdU did not show any specific labeling within the ablation/injection region. All together, the experiment proved that catheter-based cell injections could be placed into a pre-defined region of the canine AV conduction axis. In spite of that, only fragments but no intact cells could be detected in the injection region.

Discussion

The present study represented the first attempt to repair complete atrioventricular block in a large animal model by injection of cardiac progenitor cells. In dogs, normal atrioventricular conduction was first completely blocked by ablation. The area of the resulting lesion was injected with human or canine cardiac progenitor cells. However, the cell injections had no effect on the compromised atrioventricular conduction. Various factors might be responsible for this failure.

In general, to succeed in cardiac repair, the used stem or progenitor cell type should: (1) be able to differentiate into all cell types comprising a particular tissue, (2) be autologous (to minimize rejection), and (3) be able to improve its microenvironment, for instance by providing its own vascularization.

The normal AV conduction axis consists of multiple components (transitional zone, AV nodal ring with compact AV node, nodal extensions, AV bundle), each composed of different cell types with distinctive gene expression profiles[23], resulting in different conduction properties. Simplified, cardiomyocytes comprising the AV ring and compact AV node express the slow-conducting gap junction channel Cx45, the pacemaker channel Hcn4 and the transcription factor Tbx3, while AV bundle cardiomyocytes express the fast-conducting gap junction channel Cx40 and Scn5a.[24] Moreover, these specialized cardiomyocytes are positioned into an extracellular matrix composed of fibroblasts, vessels, nerves, and various types of fibers and amorphous substances. Embryological stem cells (ESCs)(or induced pluripotent stem cells, iPSCs) are the only source that could theoretically provide all cell types of the AV conduction axis. Though canine ESCs and iPSCs have been generated, their use is limited.[25] The present study was fuelled by the discovery of an adult resident stem/progenitor cell, isolated from fetal and adult human enzymatic-digested heart tissue by magnetic cell sorting after binding to magnetic beads directed against the cell membrane protein Sca-1.[10,11,20]

By applying this technique to adult dog heart tissue, we were able to isolate cells with a stemcel-like appearance in culture. In undifferentiated state these cells expressed the early cardiac transcription factors Gata4 and Mef2c. After differentiation with 5-azacytidine and TGF-beta1 the cells expressed cardiomyocyte-specific genes and proteins necessary for the assembly of ion channels, connexons and cytoskeleton, as well as for calcium handling. *In vitro* data derived from both the human and dog CPCs indicated that their molecular profile upon differentiation could fit to the demand provided by the tissue of focus. However, canine CPCs could only been isolated from mononuclear cell fractions (MCF, as derived from the enzymatic digestion of an entire heart), but not from heart tissue obtained by biopsy. The biopsies were taken from the right ventricular wall and the interventricular septum. Earlier studies from our own group have demonstrated that there are different amount of Sca-1-positive CPCs present in the various cardiac compart-

ments. Sca-1-positive CPCs could be found in the atrium, the interatrial septum and in the atrio-ventricular boundary.[12,13] Thus, tissue from right ventricular wall and the interventricular septum might harbor no, or not enough CPCs to be isolated and cultured. On top of that, CPC isolation was hampered by another problem. Due to a production stop of the original beads with direct-coupled anti-Sca-1 antibody, we had to use beads with a new anti-Sca-1 antibody coupled to FITC. This new anti-Sca-1 antibody was not able anymore to isolate CPCs. Instead, the isolation procedure resulted in cells with a fibroblast-like morphology, both in the Sca-1 positive, and negative fraction. This raises the question why the new anti-Sca-1 antibody failed to select canine CPCs. Sca-1 is a murine cell membrane protein of the Ly6-family, potentially responsible for cell-cell adhesion and signaling (reviewed by Holmes *et al.*[26]). There is much doubt about a canine or human Sca-1 homologue. In fact, the region of the Ly6 locus of mouse chromosome 15, encoding Sca-1 and five additional Ly6 genes was deleted between mouse and rat speciation.[26] Thus, in the present study the original anti-Sca-1 antibody probably cross-reacted with another (Ly6-) cell surface protein and the new antibody lost that ability. Beyond the mouse species, Sca-1 expression might not the best way to isolate CPCs. Besides Sca-1-positive CPCs, currently there are the following types of CPCs described: c-kit-positive, cardiosphere-derived, side population-positive, Islet-1-positive, epicardium-derived, and SSEA-1-positive.[27,28] From these types, only c-kit[29-31] and cardiosphere-derived[32] CPCs have been used in the dog. In this study magnetic microbeads against (mouse) c-kit were not able to isolate canine CPCs.

The functional effects of Sca-1-positive canine and human CPCs were studied after injection of these cells into a region of complete AV block. Though *in vitro* the CPCs demonstrated electrical intercellular coupling and the presence of ion channels involved in action potential generation, electrical effects *in vivo* were absent with the exception of a short temporal effect in one dog only. Histopathological examination of the injection region failed to reveal any intact CPCs in the tissue. Though H/E staining suggested the presence of cell clusters with a morphology suggestive of the injected CPCs, we had severe difficulties regarding retrievability of the injected CPCs and with the confirmation of their intact status. The cells did not tolerate transfection with a reporter gene. Also, incubation with various tracker dyes and BrdU, or co-injection of fluorescent microspheres did not result in visualization of the cells. After loading of the cells with super-paramagnetic iron oxide (SPIO) to facilitate *in vivo* MR imaging, we could detect iron deposits in the injection region. However, the iron was situated in the extracellular matrix or in macrophages. One possible explanation for these findings is that the injected cells were just not viably present in the tissue anymore. Previous studies have shown that cell injections display a low rate of engraftment and survival[33], due to mechanical leakage of the cells and poor survival in hostile environment.[27,34] Under best circumstances, about 90% of the successfully retained cells die within the first week after injection, and less than 1% of the cells can be identified 4 weeks after transplantation.[28] Restoration of compromised AV conduction might ask for another delivery mode than cell injection. A conceivable solution would be to design a prefabricated matrix, which is seeded with homogeneously coupled CPC- or iPSC-derived cardiomyocytes. Ideally, this matrix should bridge the regions of intact conduction, before and after the AV conduction block.

Conclusions

After 11 CAVB dogs transplanted with either human/canine CPCs or canine MSCs in and around the ablated region, we have to conclude that thus far we have not been able to restore AV conduction using the tested approaches and tools. Even though, valuable information with respect to the method of ablation, the transplantation procedure, the retrievability of cells and the histopathological examination has been collected. The primary problem to deal with is how to improve the retention of transplanted cells. Despite aggressive treatment with immunosuppressive therapy we assume that the cells do not survive long enough after transplantation.

Acknowledgements

Paul Coffer and all members of the Coffer-lab, Tammo Delhaas, Niels Geijssen, Peter Loh, Bart Spee, Tycho van der Spoel, Giovanni Tahapary, Harry van Wessel, Fred Wittkampf, Harry van Wessel, and all members of the Medical Physiology-lab are kindly acknowledged for their support.

References

1. Silvetti MS, Drago F, Grutter G, et al. Twenty years of paediatric cardiac pacing: 515 pacemakers and 480 leads implanted in 292 patients. Europace 2006; 8: 530-536.
2. Salameh A, Dhein S, Blanke K, et al. Right or left ventricular pacing in young minipigs with chronic atrioventricular block: long-term in-vivo cardiac performance, morphology, electrophysiology and cellular biology. Circulation 2012; 125: 2578-2587
3. van Geldorp IE, Delhaas T, Gebauer RA, et al. Impact of the permanent ventricular pacing site on left ventricular function in children: a retrospective multicentre survey. Heart 2011; 97: 2051-2055.
4. Silvetti MS, Drago F, Ravà L. Determinants of early dilated cardiomyopathy in neonates with congenital complete atrioventricular block. Europace 2010; 12: 1316-1321.
5. Guan K, Hasenfuss G. Do stem cells in the heart truly differentiate into cardiomyocytes? J Mol Cell Cardiol 2007; 43: 377-387.
6. Malliaras K, Marbán E. Cardiac cell therapy: where we've been, where we are, and where we should be headed. British medical bulletin 2011;98:161-185.
7. Bergmann O, Bhardwaj RD, Bernard S, et al. Evidence for cardiomyocyte renewal in humans. Science 2009; 324: 98-102.
8. Hsieh PC, Segers VF, Davis ME, et al. Evidence from a genetic fate-mapping study that stem cells refresh adult mammalian cardiomyocytes after injury. Nat Med 2007; 13: 970-974.
9. Zhang H, Wang H, Li N, Duan CE, Yang YJ. Cardiac progenitor/stem cells on myocardial infarction or ischemic heart disease: what we have known from current research. Heart Fail Rev 2014; 19: 247-258.
10. de Boer TP, van Veen TAB, Jonsson MKB, et al. Human cardiomyocyte progenitor cell-derived cardiomyocytes display a maturated electrical phenotype. J Mol Cell Cardiol 2009: 1-7.
11. Goumans M, de Boer T, Smits A, et al. TGF-ß1 induces efficient differentiation of human cardiomyocyte progenitor cells into functional cardiomyocytes in vitro. Stem Cell Res 2008; 1: 138-149.
12. van Vliet P, Roccio M, Smits AM, et al. Progenitor cells isolated from the human heart: a potential cell source for regenerative therapy. Neth Heart J 2008; 16: 163-169.
13. van Vliet P, Smits AM, de Boer TP, et al. Foetal and adult cardiomyocyte progenitor cells have different developmental potential. J Cell Mol Med 2010; 14: 861-870.
14. Meijler FL, Janse MJ. Morphology and electrophysiology of the mammalian atrioventricular node. Physiol Rev 1988; 68: 608-647.
15. Bharati S. Anatomic-morphologic relations between AV nodal structure and function in the normal and diseased heart. In: Mazgalev TN, Tchou PJ, eds. Atrial-AV nodal electrophysiology: a view from the millenium. Armonk, NY: Futura Publishing Company, 2000:25-48.
16. Choi YH, Stamm C, Hammer PE, et al. Cardiac conduction through engineered tissue. Am J Pathol 2006; 169: 72-85.
17. Yokokawa M, Ohnishi S, Ishibashi-Ueda H, et al. Transplantation of mesenchymal stem cells improves atrioventricular conduction in a rat model of complete atrioventricular block. Cell Transplant 2008; 17: 1145-1155.
18. Bunch T, Mahapatra S, Bruce G, et al. Impact of transforming growth factor-ß1 on atrioventricular node conduction modification by injected autologous fibroblasts in the canine heart. Circulation 2006; 113: 2485.
19. Neupane M, Chang C-C, Kiupel M, Yuzbasiyan-Gurkan V. Isolation and characterization of canine adipose–derived mesenchymal stem cells. Tissue Eng Part A 2008; 14: 1007-1015.
20. Smits AM, van Vliet P, Metz CH, et al. Human cardiomyocyte progenitor cells differentiate into functional mature cardiomyocytes: an in vitro model for studying human cardiac physiology and pathophysiology. Nat Protoc 2009; 4: 232-243.
21. Powell T. Methods for the preparation and characterization of cardiac myocytes. Methods in Studying Cardiac Membranes 1984; 1: 41-62.
22. Bajanca F, Luz M, Duxson MJ, Thorsteinsdottir S. Integrins in the mouse myotome: developmental changes and differences between the epaxial and hypaxial lineage. Dev Dyn 2004; 231: 402-415.
23. Christoffels VM, Smits GJ, Kispert A, Moorman AF. Development of the pacemaker tissues of the heart. Circ Res 2010;106:240-254.
24. Bakker ML, Moorman AF, Christoffels VM. The atrioventricular node: origin, development,

and genetic program. Trends Cardiovasc Med 2010; 20: 164-171.
25. Chronowska E. Induced pluripotent stem (iPS) cells in domestic animals recent achievements —a review. Anim Sci Pap Rep 2013; 31: 89-99.
26. Holmes C, Stanford WL. Concise review: stem cell antigen-1: expression, function, and enigma. Stem Cells 2007; 25: 1339-1347.
27. Ye J, Yeghiazarians Y. Cardiac stem cell therapy: review of the native cardiac progenitor cells and future direction. J Cardiovasc Pharmacol 2014; 63: 85-94.
28. Zhang H, Wang H, Li N, Duan CE, Yang YJ. Cardiac progenitor/stem cells on myocardial infarction or ischemic heart disease: what we have known from current research. Heart Fail Rev 2014; 19: 247-258.
29. Linke A, Muller P, Nurzynska D, et al. Stem cells in the dog heart are self-renewing, clonogenic, and multipotent and regenerate infarcted myocardium, improving cardiac function. Proc Natl Acad Sci USA 2005; 102: 8966-8971.
30. Zhang J, Huang CX, Wu P, et al. Cardiac stem cells differentiate into sinus node-like cells. Tohoku J Exp Med 2010; 222: 113-120.
31. Welt FG, Gallegos R, Connell J, et al. Effect of cardiac stem cells on left-ventricular remodeling in a canine model of chronic myocardial infarction. Circ Heart Fail 2013; 6: 99-106.
32. Hodgkiss-Geere HM, Argyle DJ, Corcoran BM, et al. Characterisation and cardiac directed differentiation of canine adult cardiac stem cells. Vet J 2012; 191: 176-182.
33. Segers VF, Lee RT. Stem-cell therapy for cardiac disease. Nature 2008; 451: 937-942.
34. Teng CJ, Luo J, Chiu RC, Shum-Tim D. Massive mechanical loss of microspheres with direct intramyocardial injection in the beating heart: implications for cellular cardiomyoplasty. J Thorac Cardiovasc Surg 2006; 132: 628-632.

Summary and future perspectives

Samenvatting en toekomstperspectieven

Dankwoord | Curriculum Vitae | Publicaties

Summary and future perspectives

CHAPTER 1

Definition, pathogenesis and therapy of congenital CAVB

Congenital CAVB is a rare cardiac conduction defect with an estimated incidence of 1 in 11.000[1] to 20.000[2] live births. A modern definition of congenital CAVB requires its diagnosis in utero or during the first month of life.[3] When congenital CAVB is diagnosed in a heart without major structural defects, it is mostly associated with the presence of maternal autoantibodies against intracellular ribonucleoproteins SS-A/Ro (especially Ro52) and/or SS-B/La. Following a recent pathophysiological model[3], the maternal autoantibodies cross the placenta and deposit in various fetal tissues, producing a syndrome called neonatal lupus. In the heart a subgroup of antibodies against Ro52 binds to cross-reactive (trans-)membrane molecules, such as the alpha1-subunits of the two L-type calcium channels Cav1.2 and Cav1.3.[4] Subsequent inactivation of these channels causes calcium dysregulation and apoptosis. After apoptosis the intracellular Ro and La proteins are translocated to the cell surface and become the target for the maternal anti-Ro/La autoantibodies. The binding of the autoantibodies triggers an inflammatory reaction causing a wide spectrum of cardiac abnormalities, including CAVB. Case reports and small cohort studies suggested that immunomodulatory agents, such as fluorinated steroids, intravenous immunoglobulin (IVIG) and hydroxychloroquine, might revert or prevent AV block. However, a recent multicenter prospective study demonstrated that the fluorinated steroid dexamethasone could not prevent or revert CAVB.[5] Moreover, two other recent multicenter prospective studies (one in Europe and one in the United States) showed that IVIG administered to mothers with an earlier child with congenital AV block could not prevent recurrence of the CAVB.[6,7]

CHAPTER 2

Cardiopulmonary exercise testing in children with congenital CAVB

The management of patients with congenital CAVB has changed during the last decennia. In the past, only a minority of patients received an electronic pacemaker, whereas the current policy is to pace the majority of patients based on a variety of criteria, among which is limited exercise capacity.[8] Data regarding exercise capacity in congenital CAVB stems from decades-old publications reporting small case series of unpaced patients.[9,10] Although the current policy is to pace patients, it is unknown whether exercise capacity benefits from this approach. Therefore, we studied the exercise capacity of a contemporary group of children with congenital CAVB with, and without a pacemaker. Sixteen children (mean age 11.5 ± 4; 13 with pacemaker, 3 without pacemaker) with congenital CAVB were tested. All patients completed an echocardiogram, a fitness questionnaire and a cardiopulmonary cycle exercise test. Exercise parameters were determined and compared with reference values obtained from healthy Dutch peers. Children with congenital CAVB had a decreased peak oxygen uptake and ventilatory threshold compared to healthy peers, whereas they showed normal peak work rates. This indicates that they generate more energy from anaerobic energy sources during exercise. Paced children with congenital CAVB did not perform better than unpaced children. Possible explanations for that finding might be: (1) a selection bias imposed by the current pacemaker criteria (only the clinically ''best'' congenital CAVB patients stay unpaced), (2) chronic pacing–induced LV dysfunction in some congenital CAVB patients, and (3) suboptimal pacemaker programming.

CHAPTER 3

Stem cell therapy as an alternative treatment to restore normal AV conduction

The current therapy of congenital CAVB, i. e. the implantation of an electronic pacemaker, might be a lifesaving intervention, but it can cause considerable morbidity, and even mortality. Due to growth and a more active lifestyle, the pacing system in pediatric patients is more prone to complications such as infection, erosion, fracture and dislodgment requiring frequent re-operations.[11] Depleted pacemaker batteries also have to be replaced regularly. Moreover, long term right ventricular pacing can result in electromechanical dyssynchrony, leading to adverse LV remodeling with LV dilatation and asymmetric hypertrophy.[11-13] Up to 30% of patients develop dilated cardiomyopathy[14], and 5% to 10% develop heart failure.[13]

A more causative therapy of the damaged AV conduction system may offer an alternative to cardiac pacing. In theory, stem cells should be able to restore a dysfunctional AV node. However, given the structural and functional complexity of the AV node, this particular field of stem-cell-based regeneration is in its infancy. Two groups have reported that in rats with CAVB, implantation of tissue constructs with skeletal myoblast derived cells[15] or injection of mesenchymal stem cells (MSCs)[16] resulted in restoration of AV-conduction in 33% of treated animals.

CHAPTER 4

Computer three-dimensional reconstruction of the AV conduction axis

Because the AV-conduction axis is quite complex in its organization, we first aimed at deepening our understanding of its structure and function. The AV conduction axis comprises the AV node, AV bundle and bundle branches. Its most complex part, the AV node, consists of multiple components (compact AV node, transitional zone and nodal extensions) and different cell types with distinctive gene expression profiles.[17] The function of the AV node is determined by the following: cell size and shape, microscopic tissue structure, expression of ion channels and cell-to-cell coupling.[18] Because structure is the determinant of function, and because of the complexity of the AV node, we need accurate knowledge of its 3D structure on tissue, cellular and molecular levels. Earlier studies have provided that knowledge for the AV node of small animals, mostly rodents. The dog can bridge the line of comparative anatomy from small animals to the human and is, as shown earlier in previous chapters, a commonly used experimental model in cardiology. We studied the canine AV conduction system in (1) normal conduction, (2) naturally acquired CAVB and (3) ablation-induced CAVB. The tissue containing the AV conduction system was fixed with formalin and embedded in paraffin and serially sectioned. The sections were stained with Masson's trichrome stain and van Gieson's stain, immunolabeled with antibodies against connexin 43, pan-cadherin and neurofilament, and in situ hybridized with probes against dog-specific mRNA encoding for gap junction-, ion channel-, and marker proteins. Digitalized 2D sections were transformed into interactive 3D models by surface rendering. This study refined the 2D histological structure of the canine AV conduction axis from earlier studies. Labeling of pan-cadherin indicated the actual presence of abundant adherens junctions in the transitional zone and inferior extensions, while the compact AV node and AV bundle showed sparse adherens junctions. Labeling of Cx43 on sections serial to the ones used for labeling of pan-cadherin proved that Cx43 is absent from the canine transitional zone, inferior nodal extensions, compact AV node and AV bundle. The study provided interactive 3D models that enhance the mental and visual understanding of the AV conduction system under physiologic and pathologic conditions.

CHAPTER 5

Stem cell therapy to restore normal AV conduction in CAVB dogs

In general, stem cell therapy is considered as a promising clinical tool for repairing damaged myocardium. In earlier studies, at a certain rate of success, lost myocardium has partially been replaced by transplantation of cardiac progenitor cells (CPCs). Additionally, it has been shown that transplantation of mesenchymal stem cells (MSCs) might improve the microenvironment of the diseased myocardium by promoting angiogenesis and survival of host cardiomyocytes. Our group has previously isolated Sca-1 expressing CPCs from fetal and adult human hearts. These CPCs could be differentiated into functioning cardiomyocytes upon treatment with 5-azacytidine and TGF-beta1.[19-21] Our hypo-

thesis was that injection of CPCs or MSCs might be able to restore AV conduction in a dog model of CAVB. To investigate the hypothesis, we created CAVB by catheter ablation and isolated canine CPCs using Sca-1-coupled magnetic beads from heart tissue. Canine MSCs were isolated from fat tissue and bone marrow. Three weeks later, cells (human CPCs in 7 dogs, canine CPCs in 3 dogs, canine MSCs in 1 dog) were injected into the ablation area. However, transplantation of human/canine CPCs or canine MSCs had no effect on the blocked AV conduction. Histopathological examination revealed only sporadic vital transplanted cells in the injection region. We assume that, despite aggressive treatment with immunosuppressive therapy or the use of autologous cells, the cells do not survive long enough after transplantation.

FUTURE PERSPECTIVES

1. From the literature and my own experience as a pediatric cardiologist I know that congenital CAVB is a really rare disease. Even though our pediatric heart center belongs to the largest in the Netherlands, we care for only a few dozen children with congenital CAVB. In the past, almost all Dutch pediatric heart centers have published their experience on some aspects of congenital CAVB independent from each other, with only a small number of patients included. We did the same in our study on the exercise capacity in congenital heart disease (see Chapter 2, part III). By combining the patient cohorts of two pediatric heart centers, we could study sixteen (note this number!) patients with congenital CAVB. Some of our experience, though not reported in the publication, is worth describing here, to illustrate the need for a change in our practice. All diagnostic tests in our study were performed by the same, experienced investigators, but on two different locations. To our surprise, there were striking differences in the management of the patients between the two centers. For instance, one center favored DDD-pacing, while the other center preferred VVI(R). There were also differences in the settings of the pacemakers. These differences, together with the low patient numbers, are the major factors that impede clinical research in congenital CAVB in general. Another issue is the lack of data on the incidence and mortality of congenital CAVB in the Netherlands. This problem has at least been addressed by a recent multi-center study by van den Berg *et al.*[22,23] In May 2014, the preliminary results of their study have been presented at the *Annual Meeting of the Association for European Pediatric and Congenital Cardiology*. This study, combining the experience of all Dutch pediatric heart centers on congenital CAVB, should serve as the starting point for a permanent collaboration to establish a nationwide registry and follow-up program in order to: register the incidence and outcome of congenital CAVB, register the indications, modality and complications of pacing and establish longitudinal data on heart function, exercise capacity, neurodevelopmental outcome and quality of life.

2. Another part of our research concerned the 2D and 3D structure of the AV conduction system, with special focus on the AV node. I started the research as an experienced pediatric cardiologist, hence I felt very confident about my up-to-date knowledge regarding the structure and function of the AV node. With confidence, I began to look at tissue sections under the microscope and to study histological images in publications. However, using the microscope for the first couple of times, I couldn't find an AV node at all. Also, while looking at histological images from earlier studies, for example images from frozen sections, I wondered from what location in the heart the section might have been taken. It was only by applying histological techniques that preserve the tissue architecture as much as possible, and after having made 3D reconstructions, that I was fully able to comprehend the complexity of the AV junction. I'm convinced that my experience could be of value to other investigators and clinicians, whether in the laboratory, in the cath-lab or at the bedside of a patient with an unexplained AV block. In the laboratory, efforts should be made to preserve histology in a natural manner and to reconstruct it in 3D. In the clinical setting, already available imaging techniques, such as CT and MRI, should be made ready for imaging the AV junction.

3. The last perspective concerns the most challenging part of this thesis, the use of cell therapy to restore normal AV conduction. After having thoroughly studied the AV nodal structure and having learned from our cell transplantation experiments, I'm convinced that simple cell injections into the AV node will never be able to regenerate a disturbed AV conduction. They imply too much mechanical damage, and too few of the injected cells will survive. Stem cell therapy of CAVB might be attempted by designing a prefabricated matrix, which could be homogeneously seeded with CPC- or iPS-derived cardiomyocytes with the right conduction properties. This matrix might be attached by a heart surgeon to the endocardium of the region of the triangle of Koch. By passing underneath the septal leaflet, it should bridge the region of the triangle of Koch with the endocardial fibers of the right bundle branch, to establish an alternative AV conduction pathway.

References

1. Siren MK, Julkunen H, Kaaja R. The increasing incidence of isolated congenital heart block in Finland. J Rheumatol 1998; 25: 1862-1864.
2. Michaëlsson M, Engle MA. Congenital complete heart block: an international study of the natural history. Cardiovascular Clinics 1972; 4: 85-101.
3. Ambrosi A, Wahren-Herlenius M. Congenital heart block: evidence for a pathogenic role of maternal autoantibodies. Arthritis Res Ther 2012; 14: 208.
4. Karnabi E, Qu Y, Mancarella S, Boutjdir M. Rescue and worsening of congenital heart block-associated electrocardiographic abnormalities in two transgenic mice. J Cardiovasc Electrophysiol 2011; 22: 922-930.
5. Friedman DM, Kim MY, Copel JA, et al. Prospective evaluation of fetuses with autoimmune-associated congenital heart block followed in the PR Interval and Dexamethasone Evaluation (PRIDE) Study. Am J Cardiol 2009;103:1102-1106.
6. Friedman DM, Llanos C, Izmirly PM, et al. Evaluation of fetuses in a study of intravenous immunoglobulin as preventive therapy for congenital heart block: Results of a multicenter, prospective, open-label clinical trial. Arthritis and Rheumatism 2010;62:1138-1146.
7. Pisoni CN, Brucato A, Ruffatti A, et al. Failure of intravenous immunoglobulin to prevent congenital heart block: Findings of a multicenter, prospective, observational study. Arthritis Rheum 2010; 62: 1147-1152.
8. Dolara A, Favilli S. Controversies in the therapy of isolated congenital complete heart block. Journal of Cardiovascular Medicine 2010; 11: 426-430.
9. Paul MH, Rudolph AM, Nadas AS. Congenital complete atrioventricular block: problems of clinical assessment. Circulation 1958; 18: 183-190.
10. Reybrouck T, Vanden Eynde B, Dumoulin M, Van der Hauwaert LG. Cardiorespiratory response to exercise in congenital complete atrioventricular block. Am J Cardiol 1989; 64: 896-899.
11. Silvetti MS, Drago F, Grutter G, et al. Twenty years of paediatric cardiac pacing: 515 pacemakers and 480 leads implanted in 292 patients. Europace 2006; 8: 530-536.
12. Salameh A, Dhein S, Blanke K, et al. Right or left ventricular pacing in young minipigs with chronic atrioventricular block: long-term in vivo cardiac performance, morphology, electrophysiology, and cellular biology. Circulation 2012; 125: 2578-2587.
13. van Geldorp IE, Delhaas T, Gebauer RA, et al. Impact of the permanent ventricular pacing site on left ventricular function in children: a retrospective multicentre survey. Heart 2011; 97: 2051-2055.
14. Silvetti MS, Drago F, Ravà L. Determinants of early dilated cardiomyopathy in neonates with congenital complete atrioventricular block. Europace 2010; 12: 1316-1321.
15. Choi YH, Stamm C, Hammer PE, et al. Cardiac conduction through engineered tissue. Am J Pathol 2006; 169: 72-85.
16. Yokokawa M, Ohnishi S, Ishibashi-Ueda H, et al. Transplantation of mesenchymal stem cells improves atrioventricular conduction in a rat model of complete atrioventricular block. Cell Transplant 2008; 17: 1145-1155.
17. Christoffels VM, Smits GJ, Kispert A, Moorman AF. Development of the pacemaker tissues of the heart. Circ Res 2010; 106: 240-254.
18. Kleber AG. Gap junctions and conduction of cardiac excitation. Heart Rhythm 2011; 8: 1981-1984.
19. de Boer TP, van Veen TAB, Jonsson MKB, et al. Human cardiomyocyte progenitor cell-derived cardiomyocytes display a maturated electrical phenotype. J Mol Cell Cardiol 2009: 1-7.
20. Goumans M, de Boer T, Smits A, et al. TGF-ß1 induces efficient differentiation of human cardiomyocyte progenitor cells into functional cardiomyocytes in vitro. Stem Cell Res 2008; 1: 138-149.
21. van Vliet P, Roccio M, Smits AM, et al. Progenitor cells isolated from the human heart: a potential cell source for regenerative therapy. Neth Heart J 2008; 16: 163-169.
22. van den Berg NWE, van Beynum IM, Clur SA, et al. O1-5 Postnatal outcome of isolated AV-block. A Dutch retrospective analysis. 48th Annual Meeting of the Association for European Paediatric and Congenital Cardiology, with joint sessions with the Japanese Society of Pediatric Cardiology and Cardiac Surgery and Asia-Pacific Pediatric Cardiac Society. Cardiology in the Young 2014; 24: Supplement1: S5.
23. van den Berg NWE, van Beynum IM, de Bruijn D, et al. O2-4 Isolated AV-block in the fetus. A Dutch retrospective analysis. 48th Annual Meeting of the Association for European Paediatric and Congenital Cardiology, with joint sessions with the Japanese Society of Pediatric Cardiology and Cardiac Surgery and Asia-Pacific Pediatric Cardiac Society. Cardiology in the Young 2014; 24: Supplement1: S7.

Samenvatting en toekomstperspectieven

Samenvatting en toekomstperspectieven

HOOFDSTUK 1

Definitie, pathogenese en therapie van congenitaal compleet atrioventriculair blok (CAVB)

Congenitaal CAVB is een zeldzame cardiale geleidingsstoornis met een geschatte incidentie van 1 op 11.000[1] tot 20.000[2] levendgeborenen. Volgens een moderne definitie van congenitaal CAVB moet de stoornis in utero of tijdens de eerste levensmaand gediagnosticeerd zijn.[3] Als congenitaal CAVB wordt gevonden in een hart zonder belangrijke structurele afwijkingen is het meestal geassocieerd met de aanwezigheid van maternale autoantistoffen tegen de intracellulaire ribonucleo-eiwitten SS-A/Ro (vooral Ro52) en/of SS-B/La. Volgens een recent pathofysiologisch model[3], passeren de maternale autoantistoffen de placenta, slaan vervolgens neer in diverse foetale weefsels en produceren een syndroom, dat neonatale lupus wordt genoemd. In het hart bindt een subgroep van antistoffen, gericht tegen Ro52, aan kruisreactieve (trans-)membraan moleculen, zoals de alfa1-subeenheid van de twee L-type calcium kanalen Cav1.2 en Cav1.3[4]. De daaropvolgende inactivatie van deze kanalen veroorzaakt calcium disregulatie en apoptose. Door de apoptose worden intracellulaire Ro en La eiwitten naar het celoppervlak getransloceerd waar zij het doelwit vormen voor maternale anti-Ro/La antistoffen. De binding van de autoantistoffen initieert een ontstekingsreactie, die een wijd spectrum aan cardiale afwijkingen veroorzaakt, onder andere CAVB. Op basis van 'case reports' en kleine cohort onderzoeken is gesuggereerd dat immunomodulerende middelen, zoals gefluoreerde steroïden, intraveneuze immunoglobulinen (IVIG) en hydroxychloroquine, in staat zijn om AV blok om te keren of te vermijden. Echter een recent prospectief multicenter onderzoek heeft aangetoond dat het gefluoreerde steroïd dexamethason de ontwikkeling van CAVB niet ongedaan kan maken.[5] Bovendien hebben twee andere recente prospectieve multicenter onderzoeken (één uitgevoerd in Europa en de andere in de Verenigde Staten) aangetoond, dat IVIG toediening aan moeders, die al eerder een kind met CAVB hadden gekregen, de aandoening bij het nieuwe kind niet kan voorkomen.[6,7]

HOOFDSTUK 2

Cardiopulmonale inspanningstest bij kinderen met congenitaal CAVB

De therapeutische benadering van patiënten met congenitaal CAVB is in de laatste decennia veranderd. Waar in het verleden slechts een kleine minderheid van de patiënten een elektrische pacemaker kreeg, wordt momenteel juist de meerderheid van de patiënten hiermee geïnstrumenteerd, uitgaande van een aantal criteria, waaronder een verminderd inspanningsvermogen.[8] Gegevens met betrekking tot het inspanningsvermogen bij congenitaal CAVB komen uit decennia-oude publicaties en zijn gebaseerd op kleine case series van patiënten zonder pacemaker.[9,10] Hoewel de huidige aanpak is om patiënten te pacen, is niet bekend of het inspanningsvermogen daardoor verbetert. Derhalve bestudeerden wij het inspanningsvermogen van een huidige groep kinderen met congenitaal CAVB, met en zonder pacemaker. De onderzoeksgroep bestond uit 16 kinderen met een gemiddelde leeftijd van 11.5 ± 4 jaar, waarvan 13 met pacemaker en 3 zonder pacemaker. Alle patiënten kregen een echocardiogram, een vragenlijst met betrekking tot sport en bewegen en een cardiopulmonale inspanningstest op de fiets. Verschillende inspanningsparameters werden bepaald en vergeleken met referentiewaarden van gezonde Nederlandse leeftijdsgenoten. Kinderen met congenitaal CAVB hadden een verminderde piek zuurstofopname en ventilatoire drempel vergeleken met gezonde leeftijdsgenoten, waarbij hun piek arbeidsvermogen normaal was. Dit wijst erop dat zij tijdens inspanning meer energie genereren uit anaerobe energiebronnen. Patiënten met een pacemaker presteerden niet beter dan patiënten zonder pacemaker. Mogelijke verklaringen hiervoor zijn: (1) een selectie bias, die door het toepassen van de huidige pacing richtlijnen ontstaat (alleen de klinisch beste patiënten met congenitaal CAVB hoeven geen pacemaker), (2) door chronische pacing geïnduceerde linker kamer disfunctie bij sommige patiënten met congenitaal CAVB, en (3) een suboptimale pacemaker programmering.

HOOFDSTUK 3

Stamceltherapie als een alternatieve methode om abnormale AV geleiding te herstellen

De huidige therapie van congenitaal CAVB, het implanteren van een elektrische pacemaker, is een levensreddende behandeling, maar kan ook aanzienlijke morbiditeit, en zelfs mortaliteit veroorzaken. Door lichamelijke groei en een actievere levensstijl is het pacemakersysteem bij kinderen gevoeliger voor complicaties, zoals infectie, erosie, breuk en verplaatsing, wat frequente re-operaties nodig maakt.[11] Daarnaast moeten lege pacemakerbatterijen regelmatig worden vervangen. Bovendien kan chronisch rechterventrikel pacing resulteren in elektromechanische dyssynchronie, wat kan leiden tot een nadelig linker ventrikel remodeling met linkerventrikel dilatatie en asymetrische hypertrofie.[11-13] Ongeveer 30% van de patiënten ontwikkelt een gedilateerde cardiomyopathie[14], en 5% tot 10% krijgt hartfalen.[13]

Een meer oorzakelijke behandeling van het beschadigde AV geleidingssysteem zou een alternatief kunnen vormen voor cardiale pacing. Hoewel het in theorie mogelijk zou moeten zijn dat stamcellen een disfunctionerende AV knoop regenereren, staat de toepassing ervan, veroorzaakt door de structurele en functionele complexiteit van de AV knoop, nog in de kinderschoenen. Twee onderzoeksgroepen hebben gerapporteerd dat in ratten met CAVB de implantatie van weefselconstructen met cellen uit skeletmyoblasten[15] of het injecteren van mesenchymale stamcellen (MSCs)[16] resulteerde in herstel van AV geleiding bij 33% van de behandelde dieren.

HOOFDSTUK 4

Computer driedimensionale reconstructie van het AV geleidingssysteem

Voor een goed begrip van de complexiteit van het AV geleidingssysteem is een uitgebreide kennis van de structuur en functie vereist. Het AV geleidingssysteem bestaat uit de AV knoop, de AV bundel en bundeltakken. De AV knoop is het meest complexe element en is opgebouwd uit verschillende onderdelen (compacte AV knoop, overgangszone en nodale extensies) en verschillende cel-types met karakteristieke genexpressie profielen.[17] De functie van de AV knoop wordt bepaald door: celgrootte en vorm, microscopische weefselstructuur, expressie van ionkanalen en koppeling tussen cellen.[18] Omdat structuur de functie bepaalt, en omdat de AV knoop zo complex is, dient de driedimensionale structuur van de AV knoop op weefsel-, cel- en moleculair niveau in kaart te worden gebracht. Eerdere studies hebben ons deze kennis betreffende de AV knoop van kleine dieren, meestal muis en rat, geleverd. De hond zou een belangrijke schakel kunnen vormen in de keten van vergelijkende anatomie van kleine dieren naar de mens. Daarnaast is de hond een veel gebruikt diermodel in de cardiologie. We bestudeerden het AV geleidingssysteem in honden bij (1) normale geleiding, (2) natuurlijk-verworven CAVB en (3) ablatie-geïnduceerd CAVB. Het weefsel dat het AV geleidingssysteem bevat werd gefixeerd met formaline, ingebed in paraffine en serieel gesneden. De weefselcoupes werden gekleurd volgens de trichroomkleuring van Masson en de kleuring volgens Von Gieson, gelabeld met antilichamen tegen connexine 43, pan-cadherine en neurofilament, en in situ gehybridiseerd met probes tegen hond-specifieke mRNA coderend voor gap junction-, ionenkanalen- en marker eiwitten. De tweedimensionale coupes werden gedigitaliseerd en door 'surface rendering' getransformeerd in interactieve driedimensionale modellen. Deze studie verdiepte de kennis van de tweedimensionale structuur van het AV geleidingssysteem in de hond zoals verkregen uit eerder onderzoek. Aankleuring van pan-cadherine toonde de ruime aanwezigheid van adherens junctions in de overgangszone en de inferieure extensies, waarbij in de compacte AV knoop en de AV bundel slechts sporadisch adherens junctions aantoonbaar waren. Aankleuring met connexine 43 liet zien dat dit koppelingseiwit afwezig is in de overgangszone, de inferieure nodale extensies, de compacte AV knoop en de AV bundel. Deze studie heeft geleid tot interactieve driedimensionale modellen die het mentale en visuele begrip van het AV conductiesysteem onder fysiologische en pathologische omstandigheden verbeteren.

HOOFDSTUK 5

Stamceltherapie voor het herstel van normale AV geleiding bij CAVB honden

In het algemeen wordt verondersteld dat stamceltherapie een veelbelovend klinisch instrument is voor het repareren van beschadigd myocard. In eerdere studies werd myocard dat verloren was gegaan, met enig succes, vervangen door transplantatie van cardiale progenitor cellen (CPCs). Bovendien is aangetoond dat transplantatie van mesenchymale stamcellen (MSCs) de micro-omgeving van het beschadigde myocard kan verbeteren door angiogenese en het overleven van gast-cardiomyocyten te bevorderen. Onze onderzoeksgroep heeft eerder CPCs, welke Sca-1 tot expressie brengen, uit foetale en adult-humane harten geïsoleerd. Deze CPCs werden door een behandeling met 5-azacytidine en TGF-beta1 gedifferentieerd tot functionerende cardiomyocyten.[19-21] De hypothese ontstond dat injectie van CPCs of MSCs in het CAVB hondenmodel de verstoorde AV geleiding zou kunnen herstellen. Om deze hypothese te testen, werd eerst een compleet AV blok gegenereerd door catheterablatie en werden CPCs van de hond geïsoleerd uit hartweefsel met behulp van Sca-1 bindende magnetische bolletjes. Ook werden uit vetweefsel en beenmerg van de hond MSCs geïsoleerd. Drie weken na de ablatie werden verschillende soorten cellen (humane CPCs bij 7 honden, hond CPCs bij 3 honden, hond MSCs bij 1 hond) in het geableerde gebied gespoten. De injecties van humane/hond CPCs of hond MSCs hadden echter helaas geen effect op de geblokkeerde AV geleiding. Histopathologisch onderzoek toonde slechts sporadisch levende cellen in het injectiegebied. Wij veronderstellen dat de cellen na de injectie onvoldoende lang overleven, ondanks agressieve behandeling met immunosuppressiva of het gebruik van autologe cellen.

TOEKOMSTPERSPECTIEVEN

1. Uit de medische literatuur en mijn eigen ervaring als kindercardioloog weet ik dat congenitaal CAVB een zeldzame ziekte is. Hoewel ons kinderhartcentrum tot de grootste in Nederland behoort zorgen wij maar voor enkele tientallen kinderen met congenitaal CAVB. In het verleden hebben bijna alle Nederlandse kinderhartcentra hun ervaringen met sommige aspecten van congenitaal CAVB onafhankelijk van elkaar gepubliceerd. Ook wij volgden deze lijn met onze studie over het inspanningsvermogen bij congenitaal CAVB (zie Hoofdstuk 2, deel III). Door de patiënten cohorten van twee kinderhartcentra te combineren konden wij zestien patiënten met congenitaal CAVB in onze studie includeren. Naast de uitkomsten die wij in de oorspronkelijke publicatie rapporteerden, zijn er ook andere ervaringen, die wij niet beschreven, het waard om te worden genoemd. Dit met de bedoeling om tot een verandering in beleid te komen. Alle diagnostische testen in de inspanningsstudie werden door dezelfde groep ervaren onderzoekers op twee verschillende locaties uitgevoerd.

Tot onze verbazing waren er grote lokale verschillen in de behandeling van de patiënten. Eén centrum had bijvoorbeeld een voorkeur voor DDD-pacing, waarbij het andere centrum bij voorkeur VVI(R)-pacing uitvoerde. Ook waren er verschillen in de pacemaker instellingen. In het algemeen zijn het deze inter-institutionele verschillen en het kleine aantal patiënten die klinisch onderzoek van congenitaal CAVB zo moeilijk maken. Een ander probleem is dat er geen data beschikbaar zijn over het voorkomen en de sterfte bij congenitaal CAVB in Nederland. Dit laatste probleem werd door de recente multi-center studie van Van den Berg *et al* geadresseerd.[22, 23] In mei 2014 werden de eerste resultaten van deze studie gepresenteerd op het jaarlijks congres van de 'Association for European Pediatric and Congenital Cardiology'. Deze studie, die de ervaringen van alle Nederlandse kinderhartcentra met congenitaal CAVB samenvatte, zou het startpunt moeten zijn voor een landelijke samenwerking voor een registratie- en follow-up programma met als doel de registratie van: (1) incidentie en prognose van congenitaal CAVB, (2) indicatie, model gebruikte pacemaker en complicaties door pacing, (3) longitudinale data van hartfunctie, inspanningsvermogen, neurologische, motorische en cognitieve ontwikkeling en de kwaliteit van leven.

2. Een ander deel van ons onderzoek betrof de 2D en 3D structuur van het AV geleidingssysteem, met een speciaal focus op de AV knoop. Toen ik als ervaren kindercardioloog aan dit onderzoek begon, voelde ik mij vrij zeker over mijn kennis van de structuur en functie van de AV knoop. Met veel zelfvertrouwen begon ik de weefselcoupes door de microscoop te bestuderen en histologische afbeeldingen in publicaties te bekijken. Toen ik echter met de microscoop de AV knoop ging zoeken kon ik hem niet vinden! Bovendien, als ik naar histologische afbeeldingen van de AV knoop in andere studies keek, waarin bijvoorbeeld vriescoupes waren gebruikt, vroeg ik mij af van welke locatie in het hart het materiaal was verkregen. Pas nadat ik histologische technieken had toegepast die de weefselarchitectuur zo natuurlijk mogelijk in stand hielden, en nadat ik seriële weefselcoupes in 3D reconstructies had verwerkt, begreep ik de complexiteit van het AV geleidingssysteem, en kon ik de AV knoop zonder moeite lokaliseren. Mijn ervaring, om door een 3D model tot een beter begrip van het complexe AV geleidingssysteem te komen, zou kunnen worden benut door iedere onderzoeker of clinicus, zij het in een laboratorium, de hartkatheterisatiekamer of naast het bed van een patiënt met een onverklaard AV blok. In het laboratorium zou ernaar moeten worden gestreefd om weefsel zo natuurlijk mogelijk histologisch te verwerken en om de weefselstructuur in 3D af te beelden. In de klinische setting zouden de reeds aanwezige beeldvormende technieken zoals CT en MRI technisch zo moeten worden verfijnd dat visualisatie van het AV geleidingssysteem mogelijk is.

3. Het laatste toekomstperspectief betreft het meest uitdagende en innovatieve onderdeel van dit proefschrift, het gebruik van stamceltherapie om een abnormale AV geleiding te herstellen. De grondige bestudering van de structuur van de AV knoop en de resultaten van onze celtransplantatie experimenten, brengen mij tot de overtuiging dat eenvoudige celinjecties in de AV knoop niet in staat zullen zijn om een verstoorde AV geleiding te herstellen. De injecties zelf veroorzaken te veel mechanische schade en een te kleine fractie van de geïnjecteerde cellen overleeft de injectie. Een andere mogelijkheid voor stamceltherapie van CAVB zou kunnen bestaan uit de fabricage van een matrix, waarin cardiomyocyten met de juiste geleidingseigenschappen, verkregen uit cardiale progenitor cellen of geïnduceerde pluripotente stamcellen, homogeen zijn verspreid. Deze matrix zou door een hartchirurg op het endocard van de driehoek van Koch kunnen worden bevestigd. Door onder het septale blad van de tricuspidaalklep door te steken zou de matrix de driehoek van Koch kunnen verbinden met de endocardiale vezels van de rechter bundeltak, en aldus een alternatieve vorm van atrioventriculaire geleiding kunnen bewerkstelligen.

Referenties

1. Siren MK, Julkunen H, Kaaja R. The increasing incidence of isolated congenital heart block in Finland. J Rheumatol 1998; 25: 1862-1864.
2. Michaëlsson M, Engle MA. Congenital complete heart block: an international study of the natural history. Cardiovascular Clinics 1972; 4: 85-101.
3. Ambrosi A, Wahren-Herlenius M. Congenital heart block: evidence for a pathogenic role of maternal autoantibodies. Arthritis Res Ther 2012; 14: 208.
4. Karnabi E, Qu Y, Mancarella S, Boutjdir M. Rescue and worsening of congenital heart block-associated electrocardiographic abnormalities in two transgenic mice. J Cardiovasc Electrophysiol 2011; 22: 922-930.
5. Friedman DM, Kim MY, Copel JA, et al. Prospective evaluation of fetuses with autoimmune-associated congenital heart block followed in the PR Interval and Dexamethasone Evaluation (PRIDE) Study. Am J Cardiol 2009;103:1102-1106.
6. Friedman DM, Llanos C, Izmirly PM, et al. Evaluation of fetuses in a study of intravenous immunoglobulin as preventive therapy for congenital heart block: Results of a multicenter, prospective, open-label clinical trial. Arthritis and Rheumatism 2010;62:1138-1146.
7. Pisoni CN, Brucato A, Ruffatti A, et al. Failure of intravenous immunoglobulin to prevent congenital heart block: Findings of a multicenter, prospective, observational study. Arthritis Rheum 2010; 62: 1147-1152.
8. Dolara A, Favilli S. Controversies in the therapy of isolated congenital complete heart block. Journal of Cardiovascular Medicine 2010; 11: 426-430.
9. Paul MH, Rudolph AM, Nadas AS. Congenital complete atrioventricular block: problems of clinical assessment. Circulation 1958; 18: 183-190.
10. Reybrouck T, van den Eynde B, Dumoulin M, van der Hauwaert LG. Cardiorespiratory response to exercise in congenital complete atrioventricular block. Am J Cardiol 1989; 64: 896-899.
11. Silvetti MS, Drago F, Grutter G, et al. Twenty years of paediatric cardiac pacing: 515 pacemakers and 480 leads implanted in 292 patients. Europace 2006; 8: 530-536.
12. Salameh A, Dhein S, Blanke K, et al. Right or left ventricular pacing in young minipigs with chronic atrioventricular block: long-term in vivo cardiac performance, morphology, electrophysiology, and cellular biology. Circulation 2012; 125: 2578-2587.
13. van Geldorp IE, Delhaas T, Gebauer RA, et al. Impact of the permanent ventricular pacing site on left ventricular function in children: a retrospective multicentre survey. Heart 2011; 97: 2051-2055.
14. Silvetti MS, Drago F, Ravà L. Determinants of early dilated cardiomyopathy in neonates with congenital complete atrioventricular block. Europace 2010; 12: 1316-1321.
15. Choi YH, Stamm C, Hammer PE, et al. Cardiac conduction through engineered tissue. Am J Pathol 2006; 169: 72-85.
16. Yokokawa M, Ohnishi S, Ishibashi-Ueda H, et al. Transplantation of mesenchymal stem cells improves atrioventricular conduction in a rat model of complete atrioventricular block. Cell Transplant 2008; 17: 1145-1155.
17. Christoffels VM, Smits GJ, Kispert A, Moorman AF. Development of the pacemaker tissues of the heart. Circ Res 2010; 106: 240-254.
18. Kleber AG. Gap junctions and conduction of cardiac excitation. Heart Rhythm 2011; 8: 1981-1984.
19. de Boer TP, van Veen TAB, Jonsson MKB, et al. Human cardiomyocyte progenitor cell-derived cardiomyocytes display a maturated electrical phenotype. J Mol Cell Cardiol 2009: 1-7.
20. Goumans M, de Boer T, Smits A, et al. TGF-ß1 induces efficient differentiation of human cardiomyocyte progenitor cells into functional cardiomyocytes in vitro. Stem Cell Res 2008; 1: 138-149.
21. van Vliet P, Roccio M, Smits AM, et al. Progenitor cells isolated from the human heart: a potential cell source for regenerative therapy. Neth Heart J 2008; 16: 163-169.
22. van den Berg NWE, van Beynum IM, Clur SA, et al. O1-5 Postnatal outcome of isolated AV-block. A Dutch retrospective analysis. 48th Annual Meeting of the Association for European Paediatric and Congenital Cardiology, with joint sessions with the Japanese Society of Pediatric Cardiology and Cardiac Surgery and Asia-Pacific Pediatric Cardiac Society. Cardiology in the Young 2014; 24: Supplement1: S5.
23. van den Berg NWE, van Beynum IM, de Bruijn D, et al. O2-4 Isolated AV-block in the fetus. A Dutch retrospective analysis. 48th Annual Meeting of the Association for European Paediatric and Congenital Cardiology, with joint sessions with the Japanese Society of Pediatric Cardiology and Cardiac Surgery and Asia-Pacific Pediatric Cardiac Society. Cardiology in the Young 2014; 24: Supplement1: S7.

Dankwoord

Dankwoord

Bij toeval raakte ik betrokken bij het onderzoeksproject waaruit dit proefschrift is ontstaan. Ergens in 2007 werd mijn WKZ-kamergenote Mirella gebeld door professor Vos. Hij was op zoek naar een kindercardioloog die interesse had in onderzoek naar reparatie van de AV knoop. Half meeluisterend naar het telefoongesprek, raakte ik direct geïnteresseerd en Mirella heeft mij vervolgens aan hem geïntroduceerd. Diezelfde week ontmoette ik professor Vos en daarmee was de start van mijn promotietraject gemaakt.

Professor dr. M.A. Vos. Beste Marc, dank voor je vertrouwen in mij en je onvoorwaardelijke professionele steun. Ik begrijp niet hoe je het voor elkaar krijgt om je enorme vakinhoudelijke expertise te combineren met zo veel functies. Ik ben blij dat je sabbatical pas begint na de voltooiing van dit proefschrift. Ik wens je veel reisplezier en hoop dat deze ervaring je nieuwe energie en inzichten geeft naast ruimte voor wat rust.

Dr. A.A.B. van Veen. Beste Toon, van meet af aan was jij de drijvende kracht achter het AV-knoop reparatie-project en dit proefschrift. Zonder je nooit aflatende steun, je bewonderenswaardige doorzettingsvermogen en je grote expertise was dit proefschrift niet tot stand gekomen. Mijn dank hiervoor is erg groot.

Dr. J.L.M. Strengers. Beste Jan, sinds mijn komst naar jouw afdeling kindercardiologie heb je het mij mogelijk gemaakt mij te ontwikkelen, als clinicus en onderzoeker. Heel erg veel dank hiervoor. Je welgemeende interesse, je hartelijkheid en je steun heb ik als zeer bijzonder ervaren. Helaas heb je door omstandigheden ervoor gekozen om tijdens de afronding van dit proefschrift naar de zijlijn te stappen. Ik vind dit erg jammer, maar respecteer je besluit.

Dr. T. Takken. Beste Tim, je bent een top-onderzoeker en een top-inspanningsfysioloog: snel, enthousiast en betrouwbaar! Je hebt mij geleerd om inspanningstesten te verrichten en te analyseren en dat heeft geresulteerd in mooie publicaties. Ik hoop in de toekomst nog menig onderzoeksproject met je samen te mogen doen. Erg bedankt voor alles!

Professor dr. F. Haas. Beste Felix, ik voel mij vereerd dat je mijn promotor wilde zijn en verheug mij op de samenwerking in de komende jaren.

Mijn dank aan de leden van de beoordelingscommissie bestaande uit:
prof.dr. R. Goldschmeding (voorzitter), prof.dr. J.M.T. de Bakker, prof.dr. T. Delhaas, prof.dr. N. Geijsen, dr. P. Loh.

Beste Dorine, Eline en Leonie, jullie zijn de beste analisten die ik me had kunnen wensen! Jullie waren precies, gedreven, betrouwbaar en betrokken. Ontelbare uren hebben jullie alleen of samen met mij gewerkt aan de onderzoeken die de basis vormen van een groot deel van dit proefschrift. Heel erg veel dank voor jullie inzet.

Dear Ben, while doing experiments, having fun and lunches, we also worked on improving my English conversational skills. Thank you for your enthusiasm and hard work.

Mijn dank aan alle collega's van de afdeling Medische Fysiologie, Roel (voor je relativerende humor), Marcel (je bent een top-wetenschapper), Jet (de spil van alle dierexperimenten: betrouwbaar en onmisbaar), Marien, Bart, Malin (Zweden, NL, nu Singapore), Lukas (Tsjechië), Peter (voor hulp bij computer- en statistiek problemen), alle 'leden' van de AIO kamer, eerst: Maartje (voor onze gesprekken over muziek), Lukas, Mohammed (voor onze gesprekken over afkomst, familie en religie), Avram, John, Linda, later: Sofieke, Rianne en Rosanne (voor jullie enthousiasme en gezelligheid, vooral in de vroege ochtend), Thom (voor alle computer en statistiek ondersteuning, je gaat een goede dokter worden!), Vincent (voor alle gesprekken over cultuur, kunst, literatuur en maatschappij), Sanne ('moeder' van de AIO kamer), Siddarth, Magda (Portugal), Tonny (voor alle secretariële ondersteuning), Teun (voor je steun op vele fronten), Harold (voor het 'reactiveren' van mijn 'latente Mac-infectie' en voor het oplossen van computerproblemen, een keer moest ik je bellen toen je met jouw gezin op een veerboot in Egypte zat (sorry ☹)), Maria (voor het kritisch bediscussiëren van het inspanningsstuk), Martin (voor alle gesprekken over Engeland, oude auto's en Olivier Bommel), Marti (voor het mogen gebruiken van je "magische" PCR flesjes, PCR was zonder je spullen niet gelukt), Jacques en Tobias (inspirerende voorbeelden), Shirley.

Mijn dank aan alle collega's van het Coffer-lab, allereerst Paul (voor je vertrouwen en alle steun), Jorg (voor je hulp en je enthousiasme), Cornelieke (organisatorisch spil in het lab), Liesbeth en Estel (top-analistes), Jeffrey (voor je hulp en humor), Miranda (voor je hulp bij FACS), Koen (voor alle hulp, enthousiasme en (korte) gesprekken over hardlopen), Anton en Henk Jan (voor jullie hulp en enthousiasme), Marije en Marthe ('brothers (sisters?) in arms', als (kinder)artsen (in spe) vreemde eenden in de lab-bijt, dank voor alle steun).

Mijn dank aan de collega's van de afdeling (Experimentele) Cardiologie/Elektrofysiologie, UMC Utrecht, Marie-Jose (voor alle vriendelijke en onvoorwaardelijke steun, vooral voor het aanleren van de CPC isolatietechniek), Steven, Joost, Tycho, Roberto, Peter (voor je ondersteuning bij het experimentele werk en je grote aandeel in het AV blok review), Fred, Harry, Giovanni.

Mijn dank aan de collega's van afdeling Anatomie, Embryologie en Fysiologie, AMC Amsterdam, Antoon (voor je enthousiasme en steun), Vincent (reeds 'eeuwen geleden' mocht ik als fellow-kindercardioloog in het AMC met jou op je werkkamer bij een kop koffie, de embryologie van het hart doornemen), Alexander, Gert, Jaco en alle ICT support staf (voor alle hulp bij het maken van de 3D reconstructies), Corrie (voor je hulp bij de ISH).

Mijn dank aan Arnold Wenink, anatoom (in ruste) te Leiden, die mij ooit de AV knoop aanwees.

Mijn dank aan de collega's van de veterinaire geneeskunde, Bart en Niels (voor jullie support van het 'iPS-idee'), Andrea, Viktor, Hilda, Alain.

Mijn dank aan de collega's van de afdeling Pathologie, Roel, Joyce (je bent een ware 'PCR Queen'), Domenico (voor je 'Italiaans' enthousiasme), Petra, Sabine, Erica (voor je les microdissectie) en alle andere collega's.

Mijn dank aan de collega's van de Inspanningsfysiologie, Bart, Erik, Marcel (jullie zijn enthousiast, betrokken en toppers in jullie vak).

Menno, ik ben je enorm dankbaar voor het maken van de lay-out. Het resultaat ziet er fantastisch uit!

Als laatste, maar belangrijkste, gaat mijn dank uit naar de constanten in mijn leven:
Aan mijn collega's van het mooiste (en beste ☺) kinderziekenhuis van Nederland, vooral mijn collega's kindercardiologen met wie ik ontelbare uren overdag en 's nachts heb doorgebracht en met wie ik gedurende tien jaar 'lief en leed' heb gedeeld. Een beter team had ik mij niet kunnen wensen: Jan, Matthias, Henriëtte, Gabrielle, Mirella, Hans, Gregor, Folkert, Jetske en Martijn.
Alle medewerkers van het Kinderhartcentrum en het WKZ die hierboven nog niet zijn genoemd, maar wel grote of kleine bijdragen aan dit proefschrift of mijn arbeidsvreugde leverden: hartelijk dank hiervoor.

Aan mijn familie en vrienden, Mutti und Vati, ihr seid mein Ursprung. Viele eurer Charaktereigenschaften leben in mir fort; vieles von eurer Art das Leben und die Welt zu sehen und zu interpretieren hat mich beeinflusst; ich danke euch für eure Liebe und eure immerwährende Unterstützung!

Schwesterherz, liebe Chrissie, unser Geschwister-Band war schon immer gut und stark; vielen Dank für alle schwesterliche Liebe und Vertrauen, die du deinem großen Bruder entgegenbringst! Sophie, deine Anwesenheit hat uns alle reicher gemacht!

Pa Schoordijk, Hilda, jullie zijn er helaas niet meer om de verdediging van dit proefschrift mee te mogen maken. Hoezeer had ik jullie trotse gezichten in het Academiegebouw willen aanschouwen! Jullie houden voor altijd een speciale plek in mijn hart!
Joke, Ad, Noa en David, jullie zijn de beste schoonfamilie die ik mij kan wensen: trouw, liefdevol en betrokken. Hartelijk dank voor dit alles.
Jessica, ook jij bent er helaas niet meer bij. Aan jou dank ik mijn voortvarende start in Nederland.
David, in mijn ogen ben je de ideale professor. Ik hoop ooit oud te worden op de manier die jij voorleeft; dank voor je advies en steun bij dit proefschrift.
Rob en Else: Rob, mijn vriend vanaf de Nederlandse collegebanken (mijn boek van Herman Hesse trok toen je aandacht) en begeleider van life-events (getuige bij mijn huwelijk en nu mijn paranimf); dank voor je hulp bij het afronden van dit proefschrift.
David en Antoinette: David, sinds onze gezamenlijke start in het 'Emma' (jij arts-assistent in opleiding, ik co-assistent) waren en zijn je diepzinnige gesprekken over kunst en cultuur een verrijking. Ik verheug mij alweer op de volgende Matthäus samen met jou en Antoinette.
Holm, du bist mein 'ältester' Studienfreund, auch sehen wir uns nicht mehr häufig, freue ich mich schon auf den nächsten Besuch bei dir, Antje, Patenkind Bruno und Klara!
Saskia en Juriaan: Sas, je behoort naast Rob tot de oude kern van oude studievrienden. Ook al zien wij jullie jaren niet, het voelt het nog steeds vertrouwd als het dan eindelijk lukt met elkaar af te spreken.
Dirk: in goede en slechte tijden. Hopelijk zien we elkaar weer spoedig.
Eszter: we met more than 25 years ago, as the wind of change blew through our countries; everything changed, but not our friendship.
Jan Caldeway: in de afgelopen jaren leerde je mij viola da gamba te spelen. Helaas moest ik de lessen in de laatste fase van mijn promotie laten vallen; ik hoop ze binnenkort weer bij jou te kunnen hervatten!

"Gelukkig is degene wiens reis eindigt in een veilige thuishaven"

Mijn thuishaven is mijn dierbare gezin: **Anita, Sebastiaan en Lucas**
Lieve Anita, je bent de liefde van mijn leven. Wat voel ik mij gezegend met jou! Jouw liefde, begrip en steun voor mij zijn onvoorwaardelijk; dat is een unieke gift waarvoor ik je niet genoeg kan bedanken.
Sebastiaan en Lucas, mijn grote 'mannen': ik ben erg trots op jullie en ben dankbaar jullie vader te zijn.

Curriculum Vitae

Curriculum Vitae

Andreas Christian Blank was born on February 5, 1968 in Potsdam-Babelsberg, Germany. He attended high school in Königs Wusterhausen, Germany, where he graduated with Abitur in 1986. After finishing a nurse training at the Military Medical Academy, Bad Saarow, Germany, he started studying Military Medicine at the University of Greifswald, Germany, in 1987. In 1989 he left the army, to study Medicine at the Universities of Greifswald and Rostock, Germany. In 1991 he moved to Amsterdam, the Netherlands, where he obtained his registration as medical doctor from the University of Amsterdam in 1996. From 1998-2002 he followed a training in Pediatrics at the Emma Children's Hospital | Academic Medical Center Amsterdam (Prof. dr. H.S.A. Heijmans). From 2002-2005 he followed a subspeciality training in Pediatric Cardiology at the Center of Congenital Heart Disease Amsterdam-Leiden (CAHAL; Prof. dr. J. Ottenkamp). Since 2005, he works as a Pediatric cardiologist at the Wilhelmina Children's Hospital | University Medical Center Utrecht, the Netherlands. He is married to Anita Schoordijk, together they have two sons, Sebastiaan and Lucas. His non-medical interests include literature, music (playing viola da gamba) and sports (recreational running).

Publicaties

Publicaties

International or national peer-reviewed journals

1. den Dekker MHT, Slieker MG, **Blank AC**, Haas F, Freund MW. Comparability of Z-score equations of cardiac structures in hypoplastic left heart complex. J Am Soc Echocardiogr 2013; 26: 1314–1321.
2. **Blank AC**, Hakim S, Strengers JL, Tanke RB, van Veen TA, Vos MA, Takken T. Exercise capacity in children with isolated congenital complete atrioventricular block: does pacing make a difference? Pediatr Cardiol 2012; 33:576–585.
3. van Geldorp IE, Delhaas T, Gebauer RA, Frias P, Tomaske M, Friedberg MK, [...] , **Blank AC**, Gabbarini F. Impact of the permanent ventricular pacing site on left ventricular function in children: a retrospective multicentre survey. Heart 2011; 97: 2051-2055.
4. Bongers BC, Hulzebos HJ, **Blank AC**, van Brussel M, Takken T. The oxygen uptake efficiency slope in children with congenital heart disease: construct and group validity. Eur J Cardiovasc Prev Rehabil 2011; 18: 384-392.
5. Takken T, **Blank AC**, Hulzebos EH, van Brussel M, Groen WG, Helders PJ. Cardiopulmonary exercise testing in congenital heart disease: equipment and test protocols. Neth Heart J 2009; 17, 339-344.
6. Takken T, **Blank AC**, Hulzebos EH, van Brussel M, Groen WG, Helders PJ. Cardiopulmonary exercise testing in congenital heart disease:(contra) indications and interpretation. Neth Heart J 2009; 17: 385-392.
7. **Blank AC**, van Veen TAB, Jonsson MKB, Zelen JSJ, Strengers JL, de Boer TP, van der Heyden MAG. Rewiring the heart: stem cell therapy to restore normal cardiac excitability and conduction. Curr Stem Cell Res Ther 2009; 4: 23-33.
8. Takken T, Hulzebos HJ, **Blank AC**, Tacken MHP, Helders PJM, Strengers J LM. Exercise prescription for patients with a Fontan circulation: current evidence and future directions. Neth Heart J 2007; 15: 142-147.
9. Takken T, Tacken MHP, **Blank AC**, Hulzebos EH, Strengers JLM, Helders PJM. Exercise limitation in patients with Fontan circulation: a review. J Cardiovasc Med 2007; 8: 775.

Books, or contribution to books

10. **Blank AC**, Loh P, Vos MA. Atrioventricular Block. In D. P. Zipes, J. Jalife, editors: Cardiac Eelectrophysiology: From Cell to Bedside, ed 6, Philadelphia, 2013, Saunders Elsevier.
11. **Blank AC**. Pacemakers. In: Brink vd GTWJ, Tol TNC, Vught van EM editors. Title: Leerboek intensive-care-verpleegkunde kinderen. Marssen: Elsevier Gezondheidszorg, 2008.
12. **Blank AC**, T. Takken. Cardio Pulmonary Exercise Testing in Children with Congenital Heart Disease. In: Congenital Heart Defects: Etiology, Diagnosis, and Treatment. Nova Science Publishers 2008.

Abstracts

13. De Klerk JCA, Clur SA, Delhaas T, **Blank AC**, Blom NA, De Kezel CCA, [...], Wilde AAM. Use of betablockade in patients with catecholaminergic polymorphic ventricular tachycardia. Cardiol Young 2008; 18: Supplement 1, 58.
14. De Klerk JCA, Clur SA, Delhaas T, **Blank AC**, Blom NA, De Kezel CCA, [...], Wilde AAM. Use of betablockade in patients with long QT syndrome. Cardiol Young 2008; 18: Supplement 1, 59.